



universität
wien

DISSERTATION

Titel der Dissertation

„Petrographic and geochemical analysis of distal
impact ejecta from large Proterozoic impacts“

Verfasser

Matthew Stephen Huber MSc

angestrebter akademischer Grad

Doktor der Naturwissenschaften (Dr. rer. nat.)

Wien, 2013

Studienkennzahl lt. Studienblatt:	A 791 426
Dissertationsgebiet lt. Studienblatt:	Erdwissenschaften/Geologie
Betreuerin / Betreuer:	Univ.-Prof. Dr. Christian Koeberl

PREFACE

This thesis represents three years of work at the University of Vienna Department of Lithospheric Research. The thesis focuses on ejecta from large meteorite impact events. In particular, in this work I am exploring how impact spherules, located in drill cores in Karelia, Russia, formed and how they may be related to the Vredefort impact structure in South Africa (Chapter 3); the petrography and geochemistry of impact ejecta from the Sudbury impact structure (Chapter 4); and finally, as part of these investigations, an algorithm designed to index data on planar deformation features, which form as during shock metamorphism (Chapter 5). Results of these studies have been submitted to peer-reviewed journals (*Geology* and *Meteoritics & Planetary Science*).

In addition to these chapters, this work also contains a brief introduction to the impact cratering process (Chapter 1) and a detailed description of the methods used to generate data in these studies (Chapter 2). Finally, a co-authored paper is included (Chapter 7) concerning a statistical model of impactors that could collide with earth. A Curriculum Vitae of the author is attached to the end of the thesis.

ACKNOWLEDGEMENTS

The author wishes to thank the many people who helped make this work possible:

- Aivo Lepland
- Akos Bazko
- Alenka Crne
- Ania Losiak
- Bevan French
- Boris Ivanov
- Bruce Simonson
- David King
- David Kring
- Dieter Mader
- Elizaveta Kovaleva
- Eugen Libowitzky
- Franz Brandstätter
- Franz Kiraly
- Gordon Osinski
- Iain McDonald
- Jüri Plado
- Kairi Poldsaar

- Klaus Schulz
- Lidia Pittarello
- Ludovic Ferriere
- Lutz Hecht
- Mattia Galliazzo
- Michael Poelchau
- Natasha Artemieva
- Rudolf Dvorak
- Steven Goderis
- Tamara Goldin
- Toni Schulz
- Uwe Reimold
- Victor Melezhik
- Wenke Wegner
- William Addison
- William Cannon
- My advisor, Christian Koeberl
- My loving parents, Ann and Steve Huber

Thanks also to the University of Vienna doctoral school IK-1045 and the Austrian Science Foundation grant P21821-N19 for funding this project, and also to the Barringer Family Fund for providing

me with a research grant. Travel grants were awarded by the Meteoritical Society, and the European Geoscience Union helped me to attend the EGU conference in Vienna.

ABSTRACT

Hypervelocity meteorite impacts generate a variety of shocked and melted products that are ejected from the impact crater. These products vary with distance from the crater. Distal ejecta is poorly understood. In this study, impact spherules from a large meteorite impact have been studied from the Fennoscandian Arctic Russia-Drilling Early Earth Project (FAR-DEEP) drill cores. These mm-diameter spherules are likely formed by a large meteorite impact event, with supporting evidence from the petrographic characteristics of the spherules being similar to previously investigated spherule layers from other parts of the world and the platinum group element (PGE) concentrations having distinct ratios and greater abundances from any local volcanic source could provide. It is likely that the Karelian spherule layer was formed from melted material of the Vredefort impact crater, based on the age of the formation being constrained to 1980-2050 Ma, similar to the 2020 Ma age of the Vredefort structure.

Closer to an impact crater, thicker deposits of debris can be found. Between ~5 crater radii and ~10 crater radii, discontinuously deposited distal ejecta can be found as brecciated clasts of target material mixed with melted, vesicular material and shocked grains. In the case of the Sudbury crater in Ontario, Canada, the ejecta has been found in Michigan, and Minnesota, USA, and western Ontario, Canada (particularly near the city of Thunder Bay). This work presents petrographic and geochemical data of ejecta from these locations, with samples taken from various distances from the impact crater to determine the variation with distance from the crater that ejecta deposition undergoes. Nearest the crater (ca. 500 km), the deposits are dominated by lithic clasts that are unshocked and unmelted. Farther away from the crater (ca. 700 km), the ejecta deposits are dominated by melt

droplets that are deposited thickly. In both of these cases, the deposits are capped by accretionary lapilli. The most distal ejecta studied (ca. 900 km) consists almost entirely of melt spherules.

To properly understand impact deposits, it is necessary to study shocked quartz. Shocked quartz is the most abundant and readily identifiable and quantifiable petrographic indicator of a hypervelocity impact event on Earth. However, the process of measuring the individual planar deformation features in a single grain and indexing them to the c-axis to determine the crystallographic orientation of the shock planes is a time consuming task, largely because, prior to this work, it was required that all samples be indexed by hand. This work presents a computer algorithm that facilitates the indexing of shocked quartz grains to greatly enhance the ability of researchers to rapidly and accurately process data gathered from U-stage measurements of planar deformation features in quartz grains.

ZUSAMMENFASSUNG

Hochgeschwindigkeits-Meteoriteneinschläge erzeugen eine Vielzahl an geschockten und geschmolzenen Produkten aus dem Einschlagskrater bei seiner Bildung ausgeworfen werden. Diese Produkte variieren mit der Distanz vom Krater. Distales Auswurfmaterial ist noch wenig verstanden. In dieser Studie wurden Impaktsphärülen eines großen Meteoriteneinschlags von Bohrkernen des Fennoskandisch-Arktisch-Russischen Früherden Bohrprojekts (FAR-DEEP) untersucht. Diese mm-großen Sphärülen wurden vermutlich durch ein großes Meteoriteneinschlagsereignis gebildet, belegt durch die petrographischen Charakteristiken der Sphärülen, welche den zuvor erforschten Sphärülenlagen in anderen Gegenden weltweit ähneln. Belegt wird dies auch durch die Platingruppenelement(PGE)-Konzentrationen, die sich durch höhere Häufigkeiten und unterschiedlichen Verhältnissen von jeglicher vulkanischer Quelle unterscheiden. Wahrscheinlich wurde die untersuchte Karelische Sphärülenlage durch geschmolzenes Material des Vredeforteinschlagkraters gebildet, basierend auf das angenommenen Alter der Lage (zwischen 1980-2050 Ma), in das das Alter der Vredefortstruktur (2020 Ma) fällt.

Nahe eines Impaktkraters kommt eine größere Häufigkeit an Auswurfmassen vor. Zwischen ~5 und ~10 Krateradien kann diskontinuierlich abgelagertes distales Auswurfmaterial, wie Brekzien gemischt mit geschmolzenem, vesikularem Material und geschockten Mineralen, gefunden werden. Im Falle des Sudbury Kraters in Ontario, Kanada, wurden Auswurfmassen in Michigan und Minnesota (USA) sowie in West-Ontario (Kanada, im Besonderen nahe der Stadt Thunder Bay) gefunden. Diese Arbeit präsentiert petrographische und geochemische Daten von Auswurfmaterial aus diesen Gegenden. Die Proben wurden dabei in unterschiedlichen Distanzen vom Impaktkrater

entnommen um die Variationen der Ablagerungen des Auswurfmaterials mit der Distanz zum Krater zu bestimmen. Näher zum Krater (ca. 500 km) werden die Ablagerungen von lithischen, ungeschockten und ungeschmolzenen Klasten dominiert. Etwas weiter vom Krater entfernt (ca. 700 km) werden die dicken Auswurfsablagerungen von Schmelztropfen dominiert. In beiden Fällen werden die Auswurfsablagerungen von akkretionierten Lapilli bedeckt. Die am entferntesten gelegenen untersuchten Auswurfsmassen (ca. 900 km) bestehen fast vollständig aus Schmelz-Sphäruhlen.

Um Impaktablagerungen ausreichend zu verstehen ist es notwendig geschockte Quarze zu untersuchen. Geschockter Quarz ist der häufigste, einfach identifizierbare und quantifizierbare petrographische Indikator eines Hochgeschwindigkeits-Impaktereignisses auf der Erde. Der Prozess des Messens der individuellen planaren Deformationsmerkmale in einem einzigen Mineralkorn und die Indizierung dieser zur C-Achse, um die kristallographische Orientierung der Schockebenen zu erfassen, ist jedoch zeitaufwändig, großteils, weil, es bisher notwendig war alle Proben manuell zu indizieren. Diese Arbeit präsentiert nun einen Computeralgorithmus der das Indizieren geschockter Quarzkörner erleichtert und somit die Fähigkeit des Forschers erweitert, schnell und genau Daten von U-Tisch-Messungen planarer Deformationsstrukturen in Quarzkörnern zu erhalten.

TABLE OF CONTENTS

Contents

Preface	iii
Acknowledgements	v
Abstract	viii
Zusammenfassung	x
Table of Contents	xii
1.0 Introduction	1
1.1 Mechanics of impact crater formation	4
1.2 Ejecta	7
1.3 Identification of impact structures on Earth	13
References:	19
2.0 Methods	26
2.1. Samples	26
2.2. Analytical Methods	28
2.2.2 Scanning electron microscope	29
References	38
3. Impact spherules from Karelia, Russia: possible ejecta from the 2.02 Ga Vredefort impact event.	40
Abstract	40

3.1 Introduction.....	41
3.2 Geological Setting	41
3.3 Description of Drill Cores	42
3.4 Methodology	43
3.5 Petrography.....	44
3.6 Geochemistry	45
3.7 Platinum Group Elements.....	46
3.8 Discussion.....	47
Acknowledgements	51
3.9 References Cited	51
4. Petrography and geochemistry of ejecta from the Sudbury impact event.....	67
Abstract	67
4.1 Introduction.....	68
4.2 Samples and Methods.....	72
4.3 Field observations	74
4.4. Results	76
4.5. Discussion.....	84
4.6. Summary and Conclusions	94
Acknowledgments:.....	96
4.7. References.....	96
4.8. Appendix.....	105

5. ANIE: A mathematical algorithm for automated indexing of planar deformation features in quartz grains	122
Abstract:	122
5.1. Introduction.....	123
5.2. Mathematical method for determining crystallographic orientations of PDFs.....	125
5.3. Description of the Automated Numerical Index Executor (ANIE) program	128
5.4. Comparison of mathematical method and graphical method for indexing PDFs.....	130
5.5. Conclusions and recommendations	132
Acknowledgments:.....	133
5.6. References.....	134
6. Recapitulation	142
7. Appendix	143
8. Curriculum Vitae	152 148

1.0 INTRODUCTION

Observations from telescopes and satellite missions to rocky planets, moons, and asteroids have revealed that impact craters are among the most common surface features in the Solar System. Impact craters are found on all rocky bodies (Fig. 1-1) (e.g., Melosh, 1989). The distribution of the impact craters, however, is not always even across the various planetary bodies. Bodies large enough to sustain surface modification processes tend to have a smaller number of visible impact craters. For example, an atmosphere (as in the case of Venus), liquids at the surface (as in the case of Titan), or ice tectonics (as in the case of Europa) can destroy impact craters after they have formed (e.g., de Pater and Lissauer, 2010). On Earth, the presence of an atmosphere, a large amount of liquid water at the surface, and plate tectonics serve to resurface the planet, limiting the number of visible impact craters. Only 184 impact craters are currently (mid-2013) confirmed on the surface of the Earth (Fig. 1-2) (Earth Impact Database; <http://www.passc.net/EarthImpactDatabase/index.html>), and many of those have no surface expression at all. This is in contrast to the millions of craters on the Moon, which, having essentially the same distance from the Sun as Earth throughout its history, should have encountered a similar number of impacting bodies (de Pater and Lissauer, 2010).

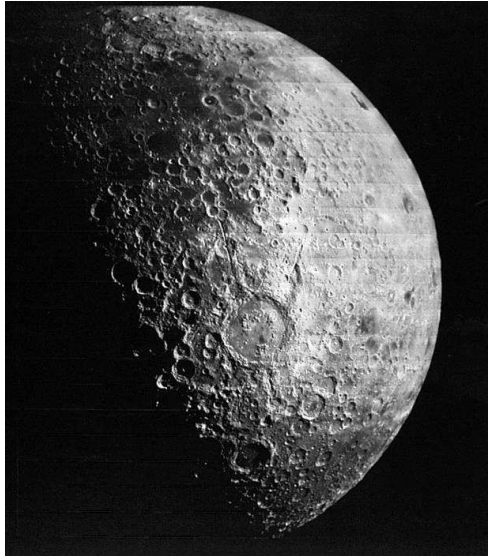


Figure 1-1: *Craters on the far side of the Moon. Photo mosaic prepared from the Lunar Orbiter program. From http://www.lpi.usra.edu/resources/lunar_orbiter/images/moon.jpg*

Craters have been extensively studied on Earth, with a full branch of geology being devoted to their study. Many cores have been drilled into impact craters, including the Chicxulub impact crater in Yucatan, Mexico (e.g., Dressler et al., 2004), the Bosumtwi crater in Ghana (e.g., Koeberl et al., 2007a), the El'gygytgyn crater in Russia (e.g., Melles et al., 2011); the Chesapeake Bay impact crater in Virginia, USA (Gohn et al., 2008), amongst others. From these studies, the internal morphologies of craters have been established. By combining these studies with observations of craters on other planets and with observations of nuclear explosion craters, an overall picture of impact cratering as a planetary process has been developed (Fig. 1-3).

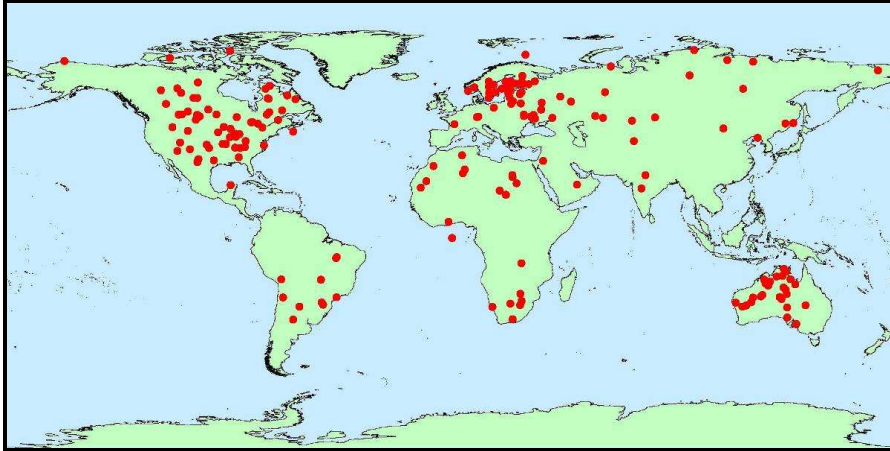


Figure 1-2: *Locations of the 184 meteorite impact craters on Earth. Data: Earth Impact Database.*



Figure 1-3: *Meteor Crater, Arizona, USA, is one of the first impact craters to have been identified as such on the Earth, and also one of the best studied, which has been instrumental as a pristine example of an impact crater that has greatly advanced the scientific for understanding of impact processes. Photo by author.*

1.1 Mechanics of impact crater formation

In order to form an impact crater, the impacting body must be moving with hypervelocity. The Earth orbits the Sun at a velocity of approximately 29.8 km/s. If a potential impacting body is travelling exactly in the same direction as Earth with the same distance from the Sun, it will have a relative velocity of 0 m/s. If the body is allowed to free-fall to the surface, it will obtain a minimum velocity of 11 km/s upon impact (the same velocity that would be required to escape from Earth's gravity). Earth's escape velocity from the Sun is 42.1 km/s, and any object at similar distance from the gravitational center of the Sun has the same escape velocity.. Therefore, an object with an elliptical orbit that has its perihelion at 1 AU and its aphelion at the edge of the Sun's gravitational influence could collide with Earth at a maximum velocity of $29.8 + 42.1$ km/s, resulting in a maximum impact velocity of 71.9 km/s. Thus, the velocity of extraterrestrial bodies impacting the Earth is constrained between ca. 11 and 72 km/s. Experiments and observations have shown that the most common meteorite impact velocities on Earth are approximately 20-30 km/s (e.g., Johnson and Melosh, 2012).

The effects of impact events are partially controlled by the angle of the impact. Craters will be circular for impacts arriving between approximately 15° and 90° (Melosh, 1989). Lower than 15° , craters can become elongate or have irregular morphologies. The angle of impact of any given bolide is random, which results in the average bolide striking the surface at 45° . While it is not simple to discriminate between impacts of differing angles, there is evidence that some minor morphological differences occur within craters striking at lower angles. The most visible effect of varying angle of impact is the effect on ejecta from the impact (i.e., Oberbeck, 1975; see below).

Impacts occurring at hypervelocities release enormous amounts of energy, following the physical law $KE = \frac{1}{2} m \cdot v^2$ (KE = kinetic energy; m = mass; v = velocity). Even an object of small mass can release a large amount of energy if it has a high velocity. A recent poignant example of the power of impacts on Earth was given by the Chelyabinsk meteorite fall. The meteor was observed in the early morning hours of February 15, 2013, over Chelyabinsk, Russia, and left an enormous fireball in the sky (Nazarov, 2013). A few seconds after the light from the fireball was visible, the shock wave arrived, shattering windows, blowing down doors, and eventually causing injuries to over 1000 people in the region. However, the bolide itself was only 10-15 m in diameter. It caused such damage because it was traveling at 18 km/s (Yeomans and Chodas, 2013).

When bolides impact the Earth at hypervelocity, the bolide will penetrate the ground to a depth roughly equal to the projectile's diameter (Melosh, 1989). The shock wave generated by the contact between the surface of the Earth and the projectile will propagate through the projectile, and upon reaching the opposite side of the projectile, will reflect, forming the rarefaction wave. As the rarefaction wave propagates, the projectile spalls apart, and eventually is completely vaporized. Meanwhile, the shock wave travels through the target materials, creating zones of high pressure with varying expressions. The initial shock wave can have pressures exceeding 100 GPa (French, 1998). The zone around the impact point will be completely vaporized. Further from the impact point, rocks will be completely melted, and farther still, minerals will experience shock effects. Rocks in a wide area around the impact point will be brecciated, faulted, and fractured (e.g., Robertson et al., 1977).

The shock wave propagates downward into the rock, eventually excavating a bowl-shaped hole called the transient cavity (Fig. 1-4). The transient cavity quickly collapses, whereupon the floor of the crater is uplifted and the diameter of the crater increases. The crater rim will also be up-

lifted at this point. The size of the impactor affects what will occur at this stage (Melosh, 1989). If the impactor is small, the target will rebound into a bowl-shaped cavity known as a simple crater. A sufficiently large impact event (depending on the target materials and gravity of the target body) will result in the floor of the transient cavity rebounding beyond its original depth, leaving behind an uplifted bump (the central peak) in the middle of the crater. This is a complex crater. Much larger impact events can result in concentric rings forming around the crater. Such multi-ring basins are known mainly from other planets, although some authors have argued for the Vredefort, Sudbury, and Chicxulub impact craters on Earth to be considered multi-ring basins (e.g., Grieve et al, 1999).

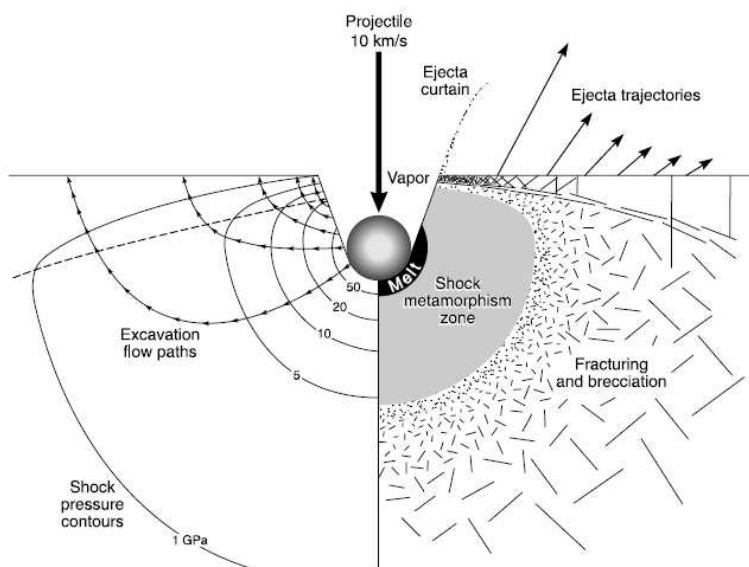


Figure 1-4: Shock wave and effects from hypervelocity meteorite impacts. From French (1998).

The upper surface of the target material is only in contact with the atmosphere, and thus creates a free surface that cannot propagate the shock wave (most of the wave is rebounded off of the

surface back into the rock). The effect of interference between the outward propagating waves and the rarefaction wave that can occur near the surface leads to some material being spalled off of the surface, which can generate secondary craters and potentially move large chunks of unshocked materials from the target to space (Ong and Melosh, 2012). Spallation has important implications for the study of other bodies in the solar system: it is the process by which pieces of the surface of Mars are ejected from the planet to eventually arrive at Earth with little shock damage (Melosh, 1984).

After the crater is formed, it undergoes the modification stage, wherein several processes occur to give the crater its final morphology (Melosh, 1989). The crater is filled by breccias formed from the shattered target rocks; large slump blocks from the newly uplifted, structurally unstable crater rim fall back into the crater along massive listric faults; and the rocks in the crater may experience hydrothermal alteration as the melt infill cools. These processes can take anywhere from a few minutes in the case of slumping and infill up to millions of years for the melt rocks in the crater to cool (e.g., Ivanov and Artemieva, 2002).

1.2 Ejecta

Approximately one third of the upper portion of the target material affected by the impact event will be removed from the crater as ejecta (Vickery, 1987). The vast majority of the ejecta is deposited in the continuous ejecta blanket. Most particles that are excavated by the impact travel out of the crater at approximately a 45° angle or higher (Anderson et al., 2004), and ejecta are deposited with inverse stratigraphy: the uppermost layer of the target material is the first layer deposited in the ejecta, and the lowest layer of the target material is the final layer deposited. The uppermost layers

of the target are usually found in the ejecta not only at the bottom of the stratigraphy of the ejecta blanket, but also in greater relative abundance closer to the impact crater than farther out from it. The overturned stratigraphy is characteristic of well-preserved impact craters (e.g., Carlson and Roberts, 1963).

The distribution of ejecta can be divided into proximal and distal ejecta (Stöffler and Grieve, 2007). Closest to the impact crater (up to 5 crater radii from the crater rim), the bulk of the ejecta are deposited as proximal ejecta (Simonson and Glass, 2004). This is contained within a continuous ejecta blanket, which is a region around a crater where there are no gaps in deposition between areas where breccias, melt rocks, shocked and unshocked materials from the crater are deposited. Farther from the impact, the discontinuous ejecta blanket is deposited, which has many of the same characteristics of the continuous ejecta blanket, but with gaps between individual deposits where little to no ejecta are deposited (Stöffler and Grieve, 2007).

1.2.1. Proximal ejecta

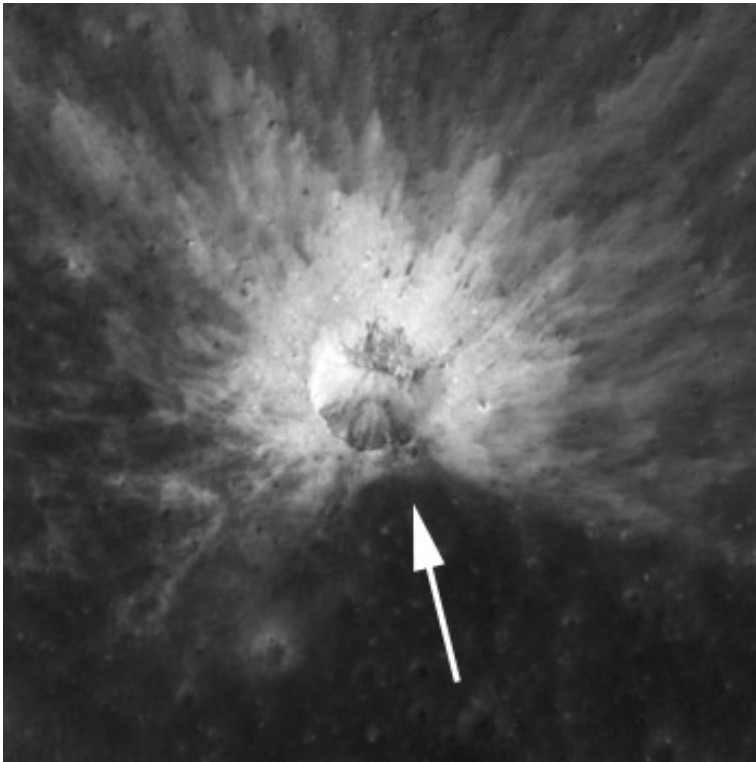


Figure 1-5: *The bright ejecta blanket of a lunar crater formed from a low-angle impact event. Arrow shows the approximate direction the impactor was traveling. Crater diameter is ~220 m. LROC image M1104509842L (NASA).*

The continuous ejecta blanket is found up to 5 crater radii away from the edge of the crater (though this is highly variable and depends on the planetary body being struck). Outside of the continuous ejecta blanket is the discontinuous ejecta blanket. The discontinuous ejecta blanket can be

found up to 10 crater radii from the impact crater, but it is highly variable (Melosh, 1989). The shape of the ejecta blanket is modified by a number of factors. The degree of asymmetry of the ejecta blanket can be affected by the angle of impact. Ejecta blankets from impacts at 90° will have circular symmetry, but impacts at low angles (i.e., $< 30^\circ$ from horizontal) will result in asymmetry of the ejecta blanket perpendicular to the direction of travel of the bolide (Wulf et al., 2012; Fig. 1-5). More ejecta will be deposited downrange of the crater with lower angle impacts. Low angle impacts also develop a “zone of exclusion” in the ejecta blanket downrange of the impact crater, which forms because of interference by the bolide during the ejection process. The ejecta blanket will also be affected by the composition of the target rocks. More competent materials will generate much different deposits than materials that are easily disaggregated or that are volatile-rich (Hoerth et al., 2013). The underlying structure of the target can also have an effect on the deposition of ejecta, as can a severe slope or topographic discontinuity that falls within the area affected by the impact. The presence and density of an atmosphere can have a major effect on the ejecta by causing particles to fall along pathways that are not strictly ballistic by slowing them in the atmosphere (e.g., Stöffler et al., 2002).

There are three main categories of breccias formed from through impact: monomict breccia (monomict = single clast lithology), polymict melt-free breccia (polymict = multiple clast lithologies), and polymict melt-bearing breccia (Stöffler et al., 2002). Deposits from the Ries crater offer a poignant and well studied example of how these are deposited. Monomict breccia is found in discrete layers deep within the crater filling material and also at the base of ejecta deposits. The polymict melt-free breccia is found overlying the monomict breccia. The polymict melt-bearing breccia, also known as suevite, is deposited at the top of the crater fill deposits and overlies the melt-free

breccias outside of the crater (Fig. 1-6). A sharp contact is found between the melt-free breccia (known at the Ries as Bunte Breccia) and the suevite, and a thermal alteration zone is found at the boundary between the two (Osinski, 2011).



Figure 1-6: *Bunte breccia from the Gundelsheim quarry at the Ries impact crater with particularly large clasts. Christian Koeberl for scale. Photo by author.*

1.2.2 Distal Ejecta

Outside of the discontinuous ejecta blanket, distal ejecta are deposited. Distal ejecta tends to form thin layers, with thicknesses of only a few cm in many cases (Simonson and Glass, 2004), with

most of the mass of ejecta already being deposited at close distances to the impact. Distal ejecta are defined to begin 10 crater radii from the edge of a crater. Distal ejecta can be composed of several components, including mostly sand-sized grains of solid and melted target material (Stöffler and Grieve, 2007). Very large impact events can generate global layers of ejecta. The Chicxulub impact crater, for example, is connected to a global ejecta layer that is a few cm thick at the K-Pg boundary (e.g., Claeys et al., 2002).

Very early after the initial contact of the bolide, melting and ejection of a small fraction of the target material known as tektites will occur (Fiske, 1996). Tektites are glasses formed from surface material (Serefiddin et al., 2007). A few tektites contain inclusions of other grains that are most likely the remnant unmelted grains of the target material (e.g., Glass and Barlow, 1979; Deloule et al., 2001). There are four well-known tektite strewn fields: The European strewn field, the Ivory Coast strewn field, the North American strewn field, and the Australasian strewn field (Koeberl, 2007). The European tektites were sourced from the Ries impact crater, the Ivory Coast tektites came from the Bosumtwi impact crater, and the North American tektites are related to the Chesapeake Bay impact crater, but the source crater of the Australasian strewn field is still unknown (e.g., Koeberl, 2007). Tektites are deposited downrange from an impact crater, which allows the direction of the indicated impacts to be determined with a high degree of certainty (e.g., Stöffler et al., 2002).

Some percentage of distal ejecta will leave the atmosphere. For an ejection angle of 45°, any ejecta that is ejected with sufficient velocity to travel at least 200 km must travel above the 100 km definition of the atmosphere. Ejecta with velocity above escape velocity (11 km/s) will leave the planet, but slower ejecta will fall back to Earth. The re-entry of ejecta will generate significant friction through interaction with the atmosphere (Goldin, 2010). This heat can cause a pulse of energy

to be released that can potentially have an effect on life. After an impact occurs, a plume of superheated vaporized rock will form over the impact crater (Johnson and Melosh, 2012). The plume is typically rapidly dispersed, and has a very low density. However, large impacts can form condensation spherules, which tend to be greatly enriched in material from the impacting body. These impact spherules can be found in global deposits and were useful in first identifying the Chicxulub impact crater as being responsible for K-Pg extinction event (Alvarez, 1980).

1.3 Identification of impact structures on Earth

Because Earth is a geologically active planet, there are a number of features that can form with grossly similar morphologies to impact craters. Therefore, to confirm that structures are impact-generated on Earth, there are only a few methods that are accepted: 1) Observed falls or strewn fields; 2) Shocked minerals; 3) Shatter cones; 4) Geochemical indicators of impact.

1.3.1 Observed falls and strewn fields

Observed falls present little difficulty in confirming, but only one crater is known to have formed from an observed fall in recent history, namely the Carancas crater in Peru, which was formed on September 15, 2007, near the village of Carancas, Peru (Brown et al., 2008). The crater was originally 4.5 m deep and 13.7 m in diameter. Because the impact was observed, including by a villager who was approximately 100 m from the impact site, there was no doubt about the impact origin of the structure. No large impact craters have been observed to form in recent human history.

Small pitted craters that are surrounded by strewn fields of meteorite fragments are usually accepted as impact-generated features. One such example is the Kaali craters in Estonia (Fig. 1-7), which are a set of 9 impact craters associated with an iron meteorite field that probably impacted within the last 10,000 years (Reinwald, 1937).



Figure 1-7: *Main crater of the Kaali craters. The craters are found associated with meteorite fragments, which is the only definitive evidence for impact origin of the craters. Image from wikipedia.org/wiki/Kaali_crater.*

1.3.2 Shocked minerals

Shocked minerals are formed by the passage of the shock wave through geological materials (Stöffler, 1992). Impacts result in a shock wave that can create pressures exceeding 100 GPa, which is unique in low temperature rocks on Earth. The most studied mineral in high pressure is quartz. Quartz experiences a number of high-pressure phase transitions that allow for identification of impact events. At pressures exceeding 100 GPa, quartz is completely vaporized (French, 1998). Above 60 GPa, quartz is transformed to glass. Small grains of the SiO₂ polymorph coesite are

formed from quartz above 30 GPa by compression of the crystal lattice. Similarly, quartz is altered to stishovite at pressures of 12-15 GPa. Planar deformation features (PDFs) form in quartz above 10 GPa, and planar fractures (PFs) form in quartz from 5-7 GPa (French, 1998).

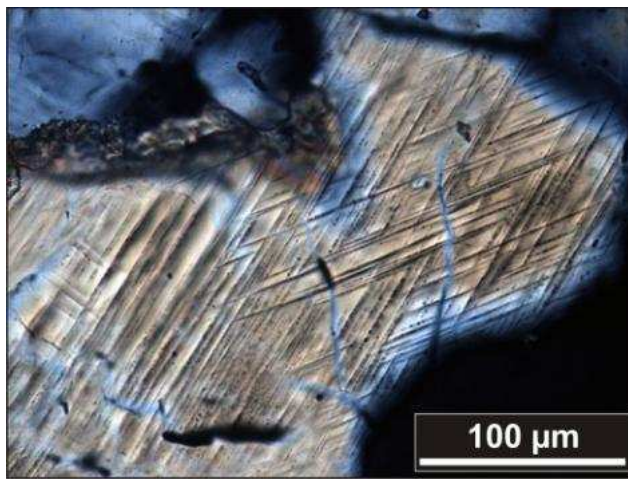


Figure 1-8: Shocked quartz grain from a quartzite clast in suevite in the Bosumtwi impact crater (core LB-07A, depth 240.36 m). Image by Ludovic Ferrière (Huber et al., 2011).

Shocked minerals form in all hypervelocity impacts, and identification of these mineral phase transitions are critical to determining if a structure is impact related (French and Koeberl, 2010). Quartz is ubiquitous on the surface of Earth and is geologically stable, and most impacts form in settings that allow PDFs to develop in quartz (Fig. 1-8). Planar deformation features are the most commonly used indicator of impact origin of a structure. While coesite can form in high-pressure geologic environments in tectonic settings (albeit with a clearly different provenance; e.g., Gillet et al., 1984), PDFs only form in impact settings, where a pulse of extremely high pressure occurs (Lan-

genhorst, 2002). PDFs are characterized by multiple sets of closed, extremely narrow, parallel planar regions in mineral grains, with a thickness of individual features of 2-3 μm and a spacing of 2-10 μm (Ferrière et al., 2009). PDFs are most commonly identified optically, although transmission electron microscope and electron backscatter diffraction images of quartz grains with PDFs can be used to confirm the amorphous planes of PDFs (Trepmann and Spray, 2005). One feature that makes PDFs ideal for identifying impact structures is that PDFs form along predictable crystallographic orientations (Ferrière et al., 2009). The orientation of PDFs can be determined optically by usage of the universal stage, which allows grains to be analyzed three-dimensionally in thin sections. Similar to PDFs, PFs form ubiquitously in quartz at even lower shock pressure. Planar fractures are parallel sets of multiple planar cracks or cleavages in the quartz grain that develop at the lowest shock pressures and are roughly 5-10 μm wide and are spaced at 15-20 μm (Goltrant et al., 1991).

1.3.3 Shatter Cones

The only macroscopic (hand-sample scale) features formed by impacts that are unique to impacts are shatter cones (Gash, 1971). Shatter cones are curved, striated fractures that typically form partial to complete cones and are generally found in rocks below the crater floor. Shatter cones are typically penetrative, such that breaking or eroding a rock with shatter cones at the surface will reveal similar internal features (Ferrière and Osinski, 2010). Shatter cones can develop in most rocks, but are best developed in fine-grained materials, such as limestone or quartzite. These features form very early in the impact process, as they can sometimes be found as clasts in crater-filling breccias. Shatter cones are unique to impacts, although similar percussion cones can be formed at

lower pressures during explosions, such as when blasting rock to make a road (e.g., Oh and Shin, 2005). Sedimentary features, such as cone-in-cone structures, are found in specific desert environments and bear a superficial similarity to shatter cones, but do not have the same penetrative quality of shatter cones. Slickensides can form tectonically, but do not have the same curved nature as shatter cones. Shatter cones tend to be widely distributed around an impact crater due to their formation at relatively low pressure (e.g., 5 GPa; Sagy et al., 2002).



Figure 1-9: Large shatter cone from the Sudbury impact crater located just east of the town of Sudbury, Ontario, Canada with hammer for scale. Photo by author.

1.3.4 Geochemical indicators of impact

When neither shocked minerals nor shatter cones can be found, the only reliable method of confirming an impact origin to a structure is through geochemical indicators. Platinum group elements (PGEs; Ru, Rh, Pd, Os, Ir, and Pt) are used as indicators of impact based on the relatively high abundance of elements such as Ir and Ru in chondrites and near absence of such elements on the surface of Earth (e.g., Koeberl 1998; Koeberl et al. 2012). Upon impact, the impactor is typically completely destroyed, with most of the impactor being vaporized and the remainder being mixed with rocks from the target. By measuring the PGE abundances in the melt rocks of the crater, a meteoritic signature can often be ascertained. This signature is most commonly very small (i.e., < 1%), but because of the high abundances of the PGEs in meteorites, the resulting mixture (e.g., melt rocks), and thus the PGE ratios, are dominated by the extraterrestrial signal. The ratios of PGEs and siderophile elements can be used to constrain the type of projectile forming impact craters, because different classes of meteorites have different elemental ratios (e.g., Palme et al., 1982). Any such analysis, though, must also include determination of the PGE contents of the target rocks, as some terrestrial rocks, such as komatiites, may have high abundances of PGEs that would confound this analysis (Fiorintini et al., 2011).

The same technique is especially powerful for studying ejecta deposits, which have usually undergone less of the reworking processes that happen within the crater itself, such as a differentiating melt sheet or hydrothermal activity. By examining the PGEs of the clays that mark the K-Pg layer, Alvarez et al. (1980) and Smit and Klaver (1981) were able to identify a spike in PGE abundances that indicated an impact origin, and provided the first definitive evidence that the end-

Cretaceous extinction was caused by asteroid impact. Similar studies have been carried out for anomalous spherule deposits found in the Australia and South Africa in Archean and Proterozoic layers (e.g., Lowe and Byerly, 2003). The layers almost never have shocked quartz associated with them. Investigations of PGEs have provided evidence that the spherule layers are impact related (Simonson and Glass, 2004).

The isotopic ratios of Cr have been used effectively to constrain the projectile type (Shukolyukov and Lugmair, 1998; Koeberl et al., 2007b). Achondrites are not enriched in siderophile elements, but they can have a significantly different ^{53}Cr abundance, which changes the ratio of ^{53}Cr to ^{52}Cr , and can thus be used to discriminate between projectile types. This powerful technique has successfully been used to determine the impactor type of numerous Precambrian ejecta layers (e.g., Koeberl, 2007; Simonson and Glass, 2004).

References:

- Anderson, J. L. B., Schulz, P. H., Heineck, J. T. 2004. Experimental ejection angles for oblique impacts: implications for the subsurface flow-field. *Meteoritics and Planetary Science*, 39:303-320.
- Alvarez, L.W., Alvarez, W., Asaro, F., and Michel, H.V., 1980. Extraterrestrial cause for the Cretaceous-Tertiary extinction. *Science*, 208:1095–1108.
- Brown, P., ReVelle, D.O., Silber, E.A., Edwards, W.N., Arrowsmith, S., Jackson Jr, L.E., Tancredi, G. and Eaton, D., 2008. Analysis of a crater-forming meteorite impact in Peru. *Journal of Geophysical Research*, 113:E09007, doi:10.1029/2008JE003105.

Carlson, R. H., and Roberts, W. A., 1963. Project Sedan mass distribution and throwout studies.

United States Atomic Energy Commission Report PNE-217F:146 pp.

Claeys, P., Kiessling, W., and Alvarez, W., 2002. Distribution of Chicxulub ejecta at the Cretaceous-Tertiary boundary. *in* Koeberl, C., and MacLeod, K.G., eds., *Catastrophic Events and Mass Extinctions: Impacts and Beyond*: Boulder, Colorado, Geological Society of America Special Paper 356:55–68.

de Pater, I., and Lissauer, J. J., 2010. *Planetary Sciences*. Cambridge University Press, 528 p.

Deloule, E., Chaussidon, M., Glass, B. P., and Koeberl, C., 2001. U-Pb isotopic study of relict zircon inclusions recovered from MuongNong-type tektites. *Geochimica et Cosmochimica Acta*, 65:1833-1838.

Dressler, B. O., Sharpton, V. L., Schwandt, C. S., and Ames, D., 2004. Impactites of the Yaxcopoil-1 drilling site, Chicxulub impact structure: Petrography, geochemistry, and depositional environment. *Meteoritics and Planetary Science*, 39:857-878.

Ferrière, L., and Osinski, G. 2010. Shatter cones and associated shock-induced microdeformations in minerals – New investigations and implications for their formation. *41st Lunar and Planetary Science Conference*, Abstract #1392.

Ferrière, L., Morrow, J.R., Amgaa, T., and Koeberl, C., 2009. Systematic study of universal-stage measurements of planar deformation features in shocked quartz: implications for statistical significance and representation of results: *Meteoritics and Planetary Science*, 44:925-940.

Fiske, P. S., 1996. Constraints on the formation of layered tektites from the excavation and analysis of layered tektites from northeast Thailand. *Meteoritics and Planetary Science*, 31:42-45.

-
- Fiorentini, M. L., Barnes, S. J., Maier, W. D., Burnham, O. M., and Heggie, G., 2011. Global variability in the platinum-group element contents of komatiites. *Journal of Petrology* 52: 83-112.
- French, B., 1998. Traces of Catastrophe. *Lunar and Planetary Institute Contribution No. 954*:120pp.
- French, B., and Koeberl, C., 2010. The convincing identification of terrestrial meteorite impact structures: What works, what doesn't, and why. *Earth-Science Reviews*, 98:123-170.
- Gash, P. J. S., 1971. Dynamic mechanism of the formation of shatter cones. *Nature Physical Science*, 230:32-35.
- Gillet, P., Ingrin, J. and Chopin, C., 1984. Coesite in subducted continental crust: *P-T* history deduced from an elastic model. *Earth and Planetary Science Letters*, 70:426-436.
- Glass, B. and Barlow, R. A., 1979. Mineral inclusions in Muong Nong-type indochinites: Implications concerning parent material and process of formation. *Meteoritics*, 14:55- 67.
- Goderis, S., Tagle, R., Belza, J., Smit, J., Montanari, A., Vanhaecke, F., Erzinger, J., and Claeys, P., 2013. Can siderophile element abundances and ratios across the K-Pg boundary be used to discriminate between possible types of projectiles? *Lunar and Planetary Science Conference XLIV*, Abstract #2167.
- Gohn, G. S., Koeberl, C., Miller, K. G., Reimold, W. U., Browning, J. V., Cockell, C. S., Horton Jr., J. W., Kenkmann, T., Kulpecz, A. A., Powars, D. S., Sanford, W., Voytek, M. A., 2008. Deep drilling into the Chesapeake Bay impact structure. *Science*, 320:1740-1745.
- Goldin, T. and Melosh, H. J., 2010. Self-shielding of thermal radiation by Chicxulub impact ejecta: Firestorm or fizzle? *Geology*, 37:1135-1138.

-
- Goltrant O., Cordier P., and Doukhan J. C., 1991. Planar deformation features in shocked quartz: A transmission electron microscopy investigation. *Earth and Planetary Science Letters*, 106:103–115.
- Grieve, R. A. F. and Therriault, A., 1999. Vredefort, Sudbury, Chicxulub: Three of a kind? *Annual Review of Earth and Planetary Sciences*, 28:305-338.
- Hoerth, T., Schäfer, F., Thoma, K., Kenkmann, T., Poelchau, M. H., Lexow, B. and Deutsch, A., 2013. Hypervelocity impacts on dry and wet sandstone: Observations of ejecta dynamics and crater growth. *Meteoritics and Planetary Science*, 48:23–32.
- Huber, M. S., Ferrière L., Losiak A., and Koeberl C., 2011. ANIE: A mathematical algorithm for automated indexing of planar deformation features in quartz grains. *Meteoritics and Planetary Science*, 46:1418–1424.
- Ivanov B. A. and Artemieva N. A. 2002. Numerical modeling of the formation of large impact craters. In Koeberl, C., and MacLeod, K. G. (Eds.), *Catastrophic events and mass extinctions: Impact and beyond*. Geological Society of America Special Paper 356:619–630.
- Johnson, B. C., and Melosh, H. J., 2012. Impact spherules as a record of an ancient heavy bombardment of Earth. *Nature*, 485:75-77.
- Koeberl, C. 1998. Identification of meteoritical components in impactites. In *Meteorites: Flux with Time and Impact Effects*; Grady, M. M., Hutchison, R., McCall, G. J. H., and Rothery, D. A., (Eds.), Geological Society of London, Special Publication 140:133-152.
- Koeberl, C. 2007. The geochemistry and cosmochemistry of impacts. In *Treatise of Geochemistry*, Vol. 1; Davis, A. (Ed.), Elsevier, p. 1.28.1 -1.28.52.

- Koeberl, C., Brandstätter, F., Glass, B. P., Hecht, L., Mader, D., and Reimold, W. U., 2007a. Uppermost impact fallback layer in the Bosumtwi Crater (Ghana): Mineralogy, geochemistry, and comparison with Ivory Coast tektites. *Meteoritics and Planetary Science*, 42:709-729.
- Koeberl C., Shukolyukov A., and Lugmair G. W., 2007b. Chromium isotopic studies of terrestrial impact craters: Identification of meteoritic components at Bosumtwi, Clearwater East, Lapajärvi, and Rochechouart. *Earth and Planetary Science Letters*, 256:534-546.
- Koeberl, C., Claeys, P., Hecht, L., and McDonald, I., 2012. Geochemistry of impactites. *Elements*, 8:37-42.
- Langenhorst, F., 2002. Shock metamorphism of some minerals: Basic introduction and microstructural observations. *Bulletin of Geosciences*, 77:265-282.
- Lowe, D.R., and Byerly, G.R., 2003. Field Guide to the Geology of the 3.5-3.2 Ga Barberton Greenstone Belt, South Africa. Guidebook prepared for Field Conference, Archean Surface Processes, June 23-July 2, 2003, 184 p.
- Melosh, H. J., 1984. Impact ejection, spallation, and the origin of meteorites. *Icarus*, 59:234-260.
- Melosh, H. J., 1989. Impact cratering: A geologic process. Oxford University Press, 245 p.
- Nazarov, M. A., 2013. Chelyabinsk. Meteoritical Bulletin Database MB 102.
- Oberbeck, V. R., 1975. The role of ballistic erosion and sedimentation in lunar stratigraphy. *Reviews of Geophysics*, 13:337-362.
- Oh, S. Y., and Shin, H. S. 2005. Effect of particle impact velocity on cone crack shape in ceramic material. *Key Engineering Materials*, 297-300:1321-1326.

- Ong, L., and Melosh, H. J., 2012. Nonlinear shock interactions produce high velocity, low pressure spall. *Lunar and Planetary Science Conference XLIV*, Abstract #2031.
- Osinski G. R., 2003. Impact glasses in fallout suevites from the Ries impact structure, Germany: An analytical SEM study. *Meteoritics and Planetary Science*, 38:1641–1668.
- Palme, H., Spettel, B., and Wlotzka, F., 1982. Fractionation of refractory metals in Ca Al-rich inclusions from carbonaceous chondrite. *Meteoritics*, 17:267.
- Reinwald, I., 1937. Kaali järve meteoorkraatrite väli. *Loodusvaatleja*, 4:97-102. (in Estonian)
- Robertson, P. B., Dence, M. R., and Vos, M. A., 1977. Deformation in Rock forming minerals from Canadian craters. In *Impact and Explosion Cratering*, D. J. Roddy, R. O. Pepin, and R. B. Merrill (eds.) *Impact and Explosion Cratering*, Pergamon Press, 433-452.
- Sagy, A., Reches, Z., and Fineberg, J., 2002. Dynamic fracture by large extraterrestrial impacts as the origin of shatter cones. *Nature*, 418:310–313.
- Serefiddin, F., Herzog, G. F., and Koeberl C., 2007. Beryllium-10 concentrations of tektites from the Ivory Coast and from Central Europe: Evidence for near-surface residence of precursor materials. *Geochimica et Cosmochimica Acta*, 71:1574-1582.
- Shukolyukov, A., and Lugmair, G.W., 1998. Isotopic evidence for the Cretaceous-Tertiary impactor and its type. *Science*, 282:927–929.
- Simonson, B. and Glass, B., 2004. Spherule Layers—Records of Ancient Impacts. *Annual Review of Earth and Planetary Sciences*, 32:329-361.
- Smit, J., and Klaver, G. 1981. Sanidine spherules at the Cretaceous-Tertiary boundary indicate a large impact event. *Nature*, 292:47-49.

- Stöffler, D. and Grieve, R. A. F., 2007. Impactites, Chapter 2.11. *in* Fettes, D. and Desmons, J. (eds.) *Metamorphic Rocks: A Classification and Glossary of Terms, Recommendations of the International Union of Geological Sciences*, Cambridge University Press, Cambridge, UK, 82-92, 111-125, and 126-242.
- Stöffler, D. Artemieva, N. A., and Pierazzo, E., 2002. Modeling the Ries-Steinheim impact event and the formation of the moldavite strewn field. *Meteoritics and Planetary Science*, 37:1893-1907.
- Treppmann, C. A., Spray, J. G., 2005. Planar microstructures and Dauphiné twins in shocked quartz from the Charlevoix impact structure, Canada. *in* Large Meteorite Impacts III, T. Kenkmann, F. Hörz, A. Deutsch, (Eds.) Geological Society of America Special Paper, 384:315-328.
- Vickery, A. 1987. Effect of an impact-generated gas cloud on the acceleration of solid ejecta. *Journal of Geophysical Research: Solid Earth*, 91:14139-14160.
- Wulf, G., Poelchau, M. H., and Kenkmann, T., 2012. Structural asymmetry in martian impact craters as an indicator for an impact trajectory. *Icarus*, 220:194-204.
- Yeomans, D., and Chodas, P., 2013. Additional details on the large fireball event over Russia on Feb. 15, 2013. NASA Near Earth Object Program report 130301.

2.0 METHODS

Many methods were employed in the analysis of rocks for this work. The samples were collected from drill cores and outcrops for analysis by various quantitative and qualitative methods. Approximately 100 thin sections were studied as part of this work, by optical microscopy, scanning electron microscope analysis, and electron microprobe analysis. Additionally, powders of the samples were used to measure the bulk chemical composition of the samples by X-ray fluorescence, instrumental neutron activation analysis, and inductively coupled plasma mass spectrometry.

2.1. Samples

Samples for these projects were selected from two distinct regions. The samples for the Karelina spherule project were selected from ICDP FAR-DEEP drill cores, with samples taken from cores 12A and 13A. In core 12A, samples were taken from 4.07 m to 4.29 m. In core 13A, samples were taken from 26.51 to 27.40 m, from 66.83 to 67.38 m, and from 71.10 m depth. Quarter-core samples were taken, with a diameter of approximately 2 cm.



Figure 2-1: FAR-DEEP 12A core box with sample locations marked by red stickers. The FAR-DEEP project was drilled near Lake Onega in Karelia, Russia.

Samples for the Sudbury ejecta project were obtained during a field season in August, 2010. The field excursion involved visiting a large number of sites that contain ejecta from the Sudbury impact event, and samples from these sites were returned to the University of Vienna. Three sites were selected, based on their preservation and distance from the Sudbury structure. The sites are the Connors Creek site, the Pine River site, and the Coleraine site. The Connors Creek site (GPS) was visited in the field and samples were collected directly from outcrops. The Pine River site (GPS) was sampled by a single exploratory diamond drill core that was recovered in 2004 by Falconbridge Limited. The core was obtained by Bill Addison, who subsequently sold a half-core split to the University of Vienna. Samples from the Coleraine site were obtained from four closely spaced drill cores that are housed by the Minnesota Department of Natural Resources core repository (MDNR) in Minnesota (USA). The MDNR facility was visited as a part of the field season, and cores DL 20009, DL 20018, DL 20021, and DL 20030 were sampled based on recovery in the drill cores.

Sample locations for the sites are as follows: The two Connors Creek sites are located at N 46° 37' 46.33", W 87° 50' 50.84" and N 46° 37' 48.50", W 87° 50' 50.36". The Pine River drill core was drilled at N 48° 03' 24", W 89° 30' 48". At Coleraine, there are four drill cores: DL 20009 located at 47° 18' 59.68" N, 93° 20' 09.68" W; DL 20018 located at 47° 19' 06.10" N, 93° 20' 46.17" W; DL 20021 located at 47° 19' 17.13" N, 93° 20' 12.37" W; and DL 20030 located at 47° 18' 49.70" N, 93° 21' 25.47" W. The Pine River core was sampled from a depth of 695.86 m to 691.4 m. Core DL 20009 was sampled from 116.9 m to 117.5 m depth; DL 20018 was sampled from 70.6

m to 70.7 m depth; DL 20021 was sampled from 66.3 m to 66.4 m depth; DL 20030 was sampled from 114.2 m to 114.8 m depth.

2.2. Analytical Methods

A wide variety of analytical methods were used for the study of samples in this study. For these analyses, powders of material or thin sections were required prior to the analysis taking place. Bulk powders were prepared by first crushing samples in a ceramic jaw crusher, then reducing the sample fragments to powders in an agate mill. Specific powders, particularly for analysis of accretionary lapilli and impact spherules, were drilled from areas of interest using a Nouvag NM 300 dental drill with a silicon carbide head. Thin sections were made at the University of Vienna.

2.2.1 Optical microscopy

Thin sections from each project were examined by transmitted light optical microscopy. The universal stage (U-stage) was used for analysis of shocked quartz grains; however, due to the low number of such grains, the U-stage was not used often. The U-stage (see Reinhard, 1931; Emmons, 1943; or Fèrriere et al., 2009 for details on usage) allows for samples to be studied by rotating thin sections to any desired inclination under the microscope. Because shock deformation features (PDFs and PFs) are planes within quartz grains along particular crystallographic axes, the determination of the particular orientation of the shock planes is a frequently used technique to differentiate shock features from other features in quartz grains. For this technique, the orientation of the c-axis and

each of the shock planes in the grain must be measured. The relative angle between the c-axis and PDF sets, combined with the angle between the various PDF sets in the grain, can be used to approximate which crystallographic axis the PDF sets occupy (Huber et al., 2011; Chapter 5. Once the orientations are measured, the data can be indexed to the crystallographic axis using either a Wulff stereonet (Ferriere et al., 2009) or a mathematical algorithm (Huber et al., 2011).

2.2.2 Scanning electron microscope and electron microprobe

The routine technique of scanning electron microscopy (SEM) allows high-magnification images to be acquired, as either secondary electron (SE) or backscattered electron (BSE) images. The SEM functions by firing electrons from an electron gun, which are then focused in the electron column. The electrons then bombard a sample in the specimen chamber, and then the resultant X-rays are captured in an X-ray analyzer. The mode of the SEM determines which X-rays are used to form an image. The X-ray analyzer can be used to perform semi-quantitative chemical analysis of samples. The SEM can be used to achieve magnification up to about 50,000 times. Further information can be found in Potts (1987), Gill (1997), Watt (1997), and Goldstein et al. (2003).

The electron source is most commonly tungsten, which can emit electrons at energy most often from 5-30 keV. The electrons emitted from the anode are focused by condenser lenses, which then pass through deflection coils. The electron beam then passes through the objective lens, which focuses the electrons into the sample. Once the electrons interact with the sample, they interact with a teardrop-shaped area of the sample, known as the interaction volume. The size of the interaction volume depends on the energy of the beam, the density of the sample, and the atomic number of the

elements in the sample. Electrons will reflect from the sample by elastic and inelastic scattering, and some electrons are absorbed by the sample, producing various forms of radiation; for this study, the most significant are secondary electrons and backscattered electrons.

Secondary electrons are emitted from the K-orbitals of atoms by inelastic scattering of incident electrons. These are low-energy electrons (< 50 eV) that are generated near the sample's surface, making them ideal for imaging the surface of a sample in detail.

Backscattered electrons are high-energy electrons from the electron beam that are reflected from the interaction volume by inelastic scattering. Because high-atomic number atoms more efficiently reflect electrons, BSE images can be used to estimate the composition of samples. In such images, brighter regions correspond to higher mean atomic number and darker areas correspond to relatively low atomic number.

The sample will also emit X-rays with specific wavelength and energy depending on the element that emitted the X-ray. Such radiation can be measured by an X-ray analyzer to estimate the chemical composition of a sample. The X-ray analyzers are most commonly either energy dispersive X-ray spectrometers (EDS) or wavelength dispersive spectrometers (WDS). The EDS uses a solid state semiconductor to measure X-ray energies. It is used effectively for qualitative analysis because it can analyze a large number of elements simultaneously, although it is less sensitive than WDS and is thus less capable of quantitative analysis. The WDS uses Bragg diffraction to discriminate the X-ray wavelengths, such that only the desired X-ray wavelengths reach the detector. This results in much higher accuracy of measurement than EDS, although only a single element may be analyzed by the detector during any measurement. The WDS is preferred for quantitative analysis for this reason.

To be electrically conductive, samples must be coated with a thin layer of a conductive material, most commonly carbon for geological materials. For this study, samples were carbon coated and then studied using a JEOL JSM 6400 SEM at the Natural History Museum of Vienna and a JEOL JXA 8500A electron microprobe at the Natural History Museum of Berlin. Each of these machines is equipped with an EDS. Samples were measured primarily in BSE mode to differentiate various mineral phases. Qualitative chemical measurements were used to estimate the compositions of various phases and to prepare targets for quantitative analysis. The operating conditions were 15 keV voltage and 1.2 nA beam current. The interaction volume was approximately 2 μm diameter. The relative error of EDS is <5 % with a theoretical detection limit of about 0.1 wt. %, WDS has a relative error of <1 % for major elements, and has a theoretical detection limit of 0.01 wt. % (Goldstein et al., 2003).

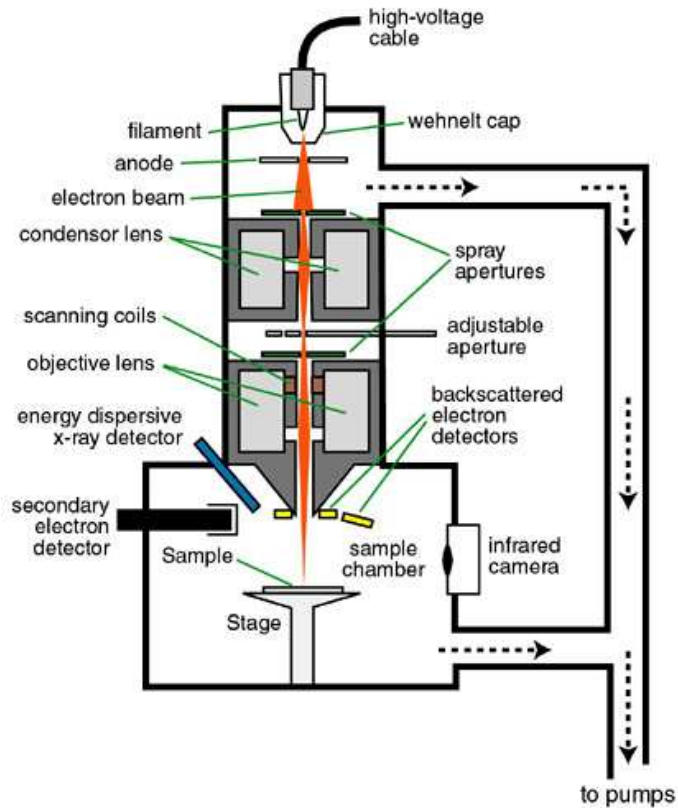


Figure 2-2. Schematic diagram of a typical scanning electron microscope. After Goldstein *et al.* (2003).

2.2.3 X-ray fluorescence

X-ray fluorescence (XRF) spectrometry is a commonly used method for bulk chemical analysis of geological samples. The technique is highly accurate and precise, and requires only small amounts of sample. The XRF system can be used to determine a wide range of elements. The XRF

generates X-rays from an X-ray tube (the primary radiation source), a sample holder, a primary collimator (to orient photons), an analyzing crystal, a secondary collimator, and a detector. The sample is irradiated with high-energy X-rays from the X-ray tube, which liberate electrons from the lowest energy orbitals of atoms. Electrons from the outer orbitals then fill the newly opened space, which simultaneously releases secondary X-rays (fluorescence). Each element produces a unique fluorescent X-ray signature that is determined by the difference between the two binding energies of the corresponding shells. The fluorescent X-rays are collimated and spectrally divided with an analyzing crystal to form a spectrum; these diffracted X-rays are again collimated so that a parallel beam of X-rays arrives at the detector. This process can be customized by adjusting the position of the secondary collimator, the analyzing crystal, and the detector, so that only X-rays of the desired element will arrive at the detector. The intensities of the X-rays arriving at the detector are quantified by comparing them with reference standards. For details on XRF spectrometry, see Potts (1987) and Gill (1997).

For this study, XRF analysis was performed at the University of Vienna for determining major element oxides (SiO_2 , TiO_2 , Al_2O_3 , Fe_2O_3 , MnO , MgO , CaO , Na_2O , K_2O , and P_2O_5) and trace element abundances (V, Cr, Co, Ni, Cu, Zn, Rb, Sr, Y, Zr, Nb, and Ba). For major elements, powders were made into fused glass beads by combining them with lithium metaborate. The trace elements were measured on pressed powder discs. The samples were measured using a Philips PW 1400 XRF spectrometer.

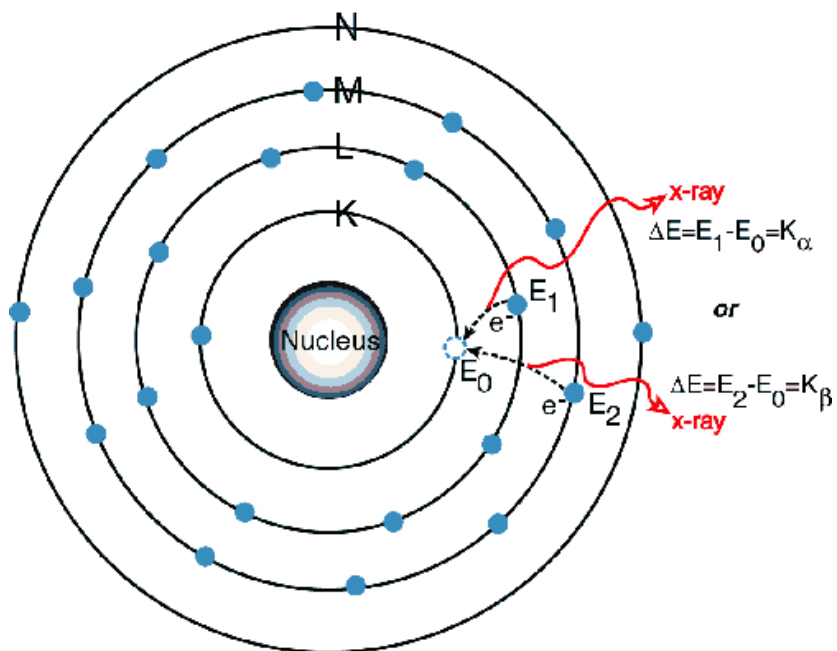


Figure 2-3. Emission of X-rays from the lower electron shell of an atom, which is the fundamental principle of X-ray fluorescence. X-rays are fired towards a sample, where they cause an electron from the lower shell of an atom. The newly vacant electron (in the K-shell) is then replaced by an electron that had been occupying a higher energy state (i.e., the L-shell). As the electron moves to a lower energy state, X-rays are emitted from the atom. The X-rays emitted are unique to each atom. Image from <http://www.amptek.com/xrf.html>.

2.2.4 Inductively coupled plasma mass spectrometry

Mass spectroscopy is a method by which a large number of elements can be measured with a high degree of accuracy. For studies in this volume, the method was used to determine the precise

concentrations of platinum group elements (PGEs; Ir, Ru, Pt, Pd, Rh, and Au) in samples that were concentrated using the nickel sulphide fire assay concentration procedure (as described in Huber et al., 2001). The inductively coupled plasma mass spectrometry technique (ICP-MS) functions by first ionizing a sample and then using a mass spectrometer to quantify the ions. Inductively coupled plasma is formed by transforming a sample to plasma by first preparing liquid solutions, then introducing the solutions to inductive heat sources to form plasma. The ionized gas is then introduced to a mass spectrometer,

Within the mass spectrometer (Fig. 2-4), the gas is accelerated by a high voltage field in a vacuum. The isotopes move past a magnetic source that deflects ions based on their mass to charge ratio, which is distinct for most isotopes (although isobars, isotopes with the same mass number, cannot be separated by this technique, and extra controls must be introduced prior to introduction to the mass spectrometer to distinguish between them). The now separated ions eventually arrive at a detector, which consists of either a Faraday cup or an electron multiplier detector. The detector can function by measuring either the charge or the current induced by the ions striking the collector. A fully detailed description of the process can be found in Potts (1987), Gill (1997) or de Groot (2004).

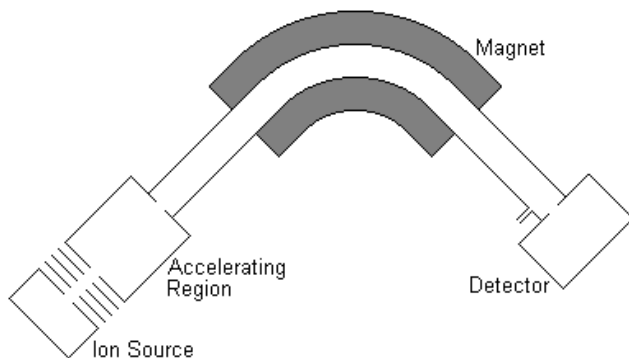


Figure 2-4. *Schematic diagram of a mass spectrometer. After*

http://www.succeedingwithscience.com/labmouse/chemistry_as/1001.php

For measurement of PGEs, samples were prepared using the nickel sulfide fire assay preconcentration and tellurium coprecipitation procedure. Fifteen grams of powdered samples were mixed with a flux, then melted in a furnace to generate a concentrated metal sulfide bead. After cooling, the bead was powdered and added to a solution of aquamara to prepare for ICP-MS analysis. Full details can be found in McDonald and Viljoen (2006).

2.2.5 Instrumental neutron activation analysis

Instrumental neutron activation analysis (INAA) allows for precise determination of up to 40 elements without chemical treatment. For INAA, small amounts of powder are necessary (usually 75-150 μg). Samples are irradiated by neutrons in a nuclear reactor, whereby a stable isotope undergoes a neutron capture reaction to generate a short-lived radioactive isotope that will then undergo decay (mostly beta decay), releasing an X-ray or gamma ray. Isotopes can be identified from the emitted gamma rays, which are unique to each isotope. During the decay process, the spectrum changes over time due to the half-life of the isotopes, so that various nuclides are producing the highest intensity gamma rays at different times. Therefore, multiple measurement cycles are performed to maximize the accuracy and breadth of the technique. When the measurements are completed, the data is quantified by comparison of the measured samples to reference materials. For more detailed information on the technique as performed at the University of Vienna, see Mader and

Koeberl (2009), and for more information on the INAA method, see Ehmann and Vance (1991), Koeberl (1993), Koeberl (1995), and Gill (1997).

To prepare the samples for analysis, 90-150 mg of each sample powder and approximately 90 mg of powder from standards were used. Three standards were used: The AC-E granite (Centre de Recherche Petrographique et Geochimique, Nancy, France; Govindaraju, 1994); the Allende carbonaceous chondrite (ALL; Smithsonian Institute, Washington D.C., USA; Jarosewich et al., 1987); and Devonian Ohio Shale (SDO1; United States Geological Survey; Govindaraju, 1989). Powders were weighed, then sealed into water-tight polyethylene capsules. Samples were then irradiated, then allowed to cool for a period of 4 days. After this period, gamma ray flux was measured at the University of Vienna, Department of Lithospheric Research. Four high-purity germanium detectors with efficiencies between 12 and 45% and energy resolutions between 1.76 and 1.85 keV were used for the measurements, which were performed at three separate times to account for the different half-lives of nuclides. The initial measurement took place four days after irradiation, with a counting time of one hour for each sample; the second measurement began 10 days after irradiation, with a counting time of 3 hours; and finally, the third counting period began one month after irradiation and each sample was counted for 12-24 hours. In all cases, additional time was given for samples with lower activity to provide better accuracy. The once all measurements are completed, data is processed by the automated software PNAA v1.1, and then the results of the analysis were compared to XRF analysis where overlap for both elements existed.

References

- de Groot, P. A. 2004. Handbook of stable isotope analytical techniques, Vol. 2. Belgium: Elsevier. 1323 p.
- Ehmann, W. D. and Vance, D. E., 1991. *Radiochemistry and nuclear methods of analysis*. New York: John Wiley and Sons. 531 p.
- Emmons R. C., 1943. The universal stage (with five axes of rotation). *Geological Society of America Memoir* 8, 205 p.
- Ferriere L., Morrow, J. R., Amgaa, T., and Koeberl., C., 2009. Systematic study of universal-stage measurements of planar deformation features in shocked quartz: Implications for statistical significance and representation of results. *Meteoritics & Planetary Science* 44:925–940.
- Gill, R., 1997. *Modern analytical geochemistry: an introduction to quantitative chemical analysis techniques for earth, environmental and materials scientists*. Longman: Harlow. 329 p.
- Goldstein, J., Newbury, D., Joy, D., Lyman, C., Echlin, P., Lifshin, E., Sawyer, L., and Michael, J., 2003. Scanning electron microscopy and X-ray microanalysis. New York:Springer 690 p.
- Govindaraju, K. 1989. Compilation of working values and sample description for 272 geostandards. *Geostandards Newsletter, The Journal of Geostandards and Geoanalysis* 13:1-113.
- Govindaraju, K., 1994. 1994 compilation of working values and sample description for 383 geostandards. *Geostandards Newsletter* 18:1–158.
- Huber, M. S., Ferrière L., Losiak A., and Koeberl K., 2011. ANIE: A mathematical algorithm for automated indexing of planar deformation features in quartz grains. *Meteoritics and Planetary Science* 46:1418–1424.

- Jarosewich, E., Clarke, R. S. J., and Barrows, J. N., 1987. The Allende meteorite reference sample. *Smithsonian Contributions to the Earth Sciences* 27:1–49.
- Koeberl, C., 1993. Instrumental neutron activation analysis of geochemical and cosmochemical samples: a fast and reliable method for small sample analysis. *Journal of Radioanalytical and Nuclear Chemistry* 168:47–60.
- Koeberl, C., 1995. Neutron activation analysis. In *Methods and instrumentations: results and recent developments*, Advanced mineralogy, Vol 2, Marfunin A. S. Berlin (ed.), Heidelberg, New York:Springer-Verlag. 322–329 p.
- Mader, D., and Koeberl, C., 2009. Using Instrumental Neutron Activation Analysis for geochemical analyses of terrestrial impact structures: Current analytical procedures at the University of Vienna Geochemistry Activation Analysis Laboratory. *Applied Radiation and Isotopes*, 67:2100-2103.
- McDonald, I., and Viljoen, K. S. 2006. Platinum-group element geochemistry of mantle eclogites: a reconnaissance study of xenoliths from the Orapa kimberlite, Botswana. *Applied Earth Science (Transactions of the Institution of Mining and Metallurgy Section B)*, 115:81-93.
- Potts P. J. 1987. *A handbook of silicate rock analysis*. Glasgow: Blackie. 622 p.
- Reinhard M. 1931. *Universaldrehtischmethoden*. Basel, Switzerland: Birkhäuser. 118 p.
- Watt I. M. 1997. *The principles and practice of electron microscopy*, 2nd ed. Cambridge: Cambridge University Press. 484 p.

3. IMPACT SPHERULES FROM KARELIA, RUSSIA: POSSIBLE EJECTA FROM THE 2.02 GA VREDEFORT IMPACT EVENT.

Matthew S. Huber¹, Alenka E. Crne², Aivo Lepland², Iain McDonald³, Lutz Hecht⁴, Victor A. Melezhik² and Christian Koeberl^{1,5}

¹*Department of Lithospheric Research, University of Vienna, Althanstrasse 14, 1090 Vienna, Austria*

²*Geological Survey of Norway, Postboks 6315 Sluppen, N-7491 Trondheim, Norway*

³*Cardiff University School of Earth and Ocean Sciences, Cardiff CF10 3AT, United Kingdom*

⁴*Museum für Naturkunde, Invalidenstraße 43, 10115 Berlin, Germany*

⁵*Natural History Museum, Burgring 7, 1010 Vienna, Austria*

Article submitted to Geology; currently under review

Abstract

Spherule beds of possible impact origin have been discovered in two drill cores in the Paleoproterozoic Zaonega Formation, Karelia, NW Russia. Platinum group element contents of the spherule beds indicate mixing of target rocks with a small meteoritic component. The age of the Zaonega Formation is constrained between 1.980 ± 0.027 Ga and 2.050 ± 0.020 Ga, which brackets the age of the 2020 Ma Vredefort impact structure in South Africa, and suggests that the spherule beds could represent ejecta from that event. If the link is confirmed, the size of the spherules and thickness of

the beds necessitating that the distance from the impact site be <2500 km, thereby constraining the paleogeographic distance between the Fennoscandian Shield and Kaapvaal Craton during the late Paleoproterozoic, and providing evidence that the Vredefort impact event was caused by an impactor of chondritic composition.

3.1 Introduction

The terrestrial impact cratering record includes impact structures and ejecta layers (Glass and Simonson, 2012). The oldest confirmed terrestrial impact crater is the 2.02 Ga old, originally ca. 300-km-diameter Vredefort structure (Kamo et al., 1996; Gibson et al., 1997). Early Archean impact ejecta were found in supracrustal sequences on the Kaapvaal and Pilbara cratons (Lowe et al., 1989, Simonson and Glass, 2004).

The only possible occurrence of Vredefort ejecta that has been described is the Graenescio spherule layer in Greenland (Chadwick et al., 2001), but the age constraint on that layer is poor (2.130-1.848 Ga), the spherules were reported from a single sample, and no unambiguous evidence of impact origin was found. Herein we present petrographic and geochemical data on sedimentary rocks of the Paleoproterozoic Zaonega Formation that host possible impact ejecta of the Vredefort impact event.

3.2 Geological Setting

The Fennoscandian Shield contains well-preserved Paleoproterozoic supracrustal successions in Karelia, Russia. One such succession, the Zaonega Formation of the Onega Paleobasin, is

represented by basaltic lavas and organic-matter rich siliciclastic and carbonate sedimentary rocks deposited in a deep marine basin mainly from turbidity currents (Črne et al., 2013a, b). The minimum age of ca. 1.98 ± 0.02 Ga is constrained by Sm-Nd and Pb-Pb isochrons on a mafic-ultramafic sill overlying the Zaonega Formation (Puchtel et al., 1998) and an upper age constraint of ca. 2.05 ± 0.02 Ga was obtained on the basis of Re-Os isochron on organic matter from the uppermost part of the Zaonega Formation (Hannah et al., 2008). Rocks of the Zaonega Formation have been affected by contact metamorphism, hydrothermal fluid alteration, and petroleum migration, triggered initially by emplacement and heating effects of basalts and co-magmatic gabbro sills during deposition and subsequently by regional metamorphism up to greenschist facies during the 1980-1790 Ma Svecofennian Orogeny (e.g., Volodichev, 1987; Strauss et al., 2013).

In 2007, the Fennoscandia Arctic Russia-Drilling Early Earth Project (FAR-DEEP) was initiated within the International Continental Drilling Program (ICDP). Within FAR-DEEP, 15 holes intersecting Paleoproterozoic rocks were drilled in Russian Karelia region and Kola Peninsula. Two of the Karelian cores, core 12A (N 62° 29' 41", W 35° 17' 20") and core 13A (N 62° 35' 21", W 34° 55' 38"), drilled at the northern shore of the Lake Onega intersected the upper part of the Zaonega Formation, and included intervals that were found to contain spherulitic particles.

3.3 Description of Drill Cores

Given the metamorphic alteration of rocks, lithologies are reported herein as meta-lithologies. The lower part of core 12A contains basalts (or a possible diabase intrusion) overlain by a 20-m-thick interval of massive organic-rich rocks and bedded mudstones and sandy limestones. The base of interbedded dolostones and cherts at 9 m marks a major facies change (Črne et al.,

2013a). Core 13A, drilled 20 km northwest of core 12A (Fig. 1), contains comparable lithologies and the same major facies change as observed in core 12A: in 13A, bedded mudstones are overlain by dolostones and cherts at a depth of 76.6 m (Črnek et al., 2013b). Within core 13A, however, the lower part of dolostones and cherts (49-76.6 m) has been brecciated by pyrobitumen veining resulting in monomict breccias composed of either dolostone or chert clasts and a pyrobitumen matrix (Črnek et al., 2013b). The upper interval of dolostones and cherts (26-49 m) is also fractured, but contains fewer breccias than the lower interval (Črnek et al., 2013b). The major facies change represented by the first dolostones and cherts can be used for correlating the boundary at 9.3 m in core 12A with the same boundary at 76.6 m in core 13A (Črnek et al., 2013b). The correlation between the cores is sustained by similar organic matter $\delta^{13}\text{C}$ trends (Supplementary materials Fig. A1). In core 12A, spherules were found between 4.03 and 4.28 m. In core 13A, there is an upper interval with spherules from 26.51 to 27.69 m and a lower interval from 66.83 to 67.33 m, with a small number of individual spherules found in a few cm-sized dolostone clasts within a breccia at 71.10 m. The spherules in all intervals are petrographically remarkably similar to each other.

3.4 Methodology

Twelve bulk samples were studied by X-Ray fluorescence, 6 samples with spherules were examined by electron microprobe and scanning electron microscope, and 16 bulk samples were analyzed for platinum group elements (See supplemental information for details), including samples from the spherule-rich intervals beds, magmatic rocks in the core, and the Vredefort granophyre.

3.5 Petrography

Most spherules are perfectly round, but approximately 5% have dumbbell or teardrop shapes (Fig. 2A). Spherules span the size range from 200-1500 μm , with an average size of 800 μm . The spherules are observed to have a distinct outer zone and interior zone (Fig. 2B) that are both texturally and geochemically distinct. Typically, the outer zone makes up approximately 20-30% of the radius of each individual spherule. In both spherule-rich intervals, the spherules have been significantly altered to phyllosilicates (usually varieties of biotite). Calcite replacement, sometimes complete, is recognizable in most spherules (Fig. 2C). Although most spherules have a simple inner and outer zone, some of the spherules show complex internal structures, often including internal partitions with the same mineralogical characteristics as the outer zone (Fig. 2D).

The outer zone most commonly consists of closely spaced microcrystalline ($<5 \mu\text{m}$) phyllosilicates, noticeably smaller than in the inner zone. In some cases, the textures show inward-radiating crystals (Fig. 2B). Most commonly, the border between the zones is demarcated by an irregular botryoidal line. The distinction between the two zones indicates their distinct genetic history. In addition to phyllosilicates and calcite, the outer zone of most spherules also contains 50-100- μm -sized crystals of rutile and anatase and rare 10- μm -sized monazite and zirconalite crystals.

The inner zone contains larger elongate phyllosilicate crystals with random orientations. These phyllosilicates are more loosely packed in comparison to than the outer zone, often with bituminous material filling the pore spaces. This is observed both in cases where the phyllosilicates are

preserved and in cases where calcite alteration has completely replaced the spherules. Accessory minerals are not observed in the inner zones.

Spherules often have an outer rim of pyrite. In some cases pyrite has overgrown the minerals within the spherules. Some of the pyrite is Ni-rich, and some gersdorffite (AsNiS) is observed inter-fingering with the pyrite rims. Additionally, some spherules have thin (<20 μm) apatite rims, but no phosphates are observed within spherules.

3.6 Geochemistry

The bulk composition of the spherule-rich intervals dominantly reflects the carbonate matrix, with approximately 28-29 wt. % CaO, 14.4-17.2 wt. % MgO, 7-11 wt. % SiO₂, 2.4-3.5 wt. % Fe₂O₃, 2.8-3.8 wt.% Al₂O₃, and 1.0-1.8 wt. % K₂O. The spherule-rich intervals have elevated Ni (190-230 ppm) and Cr (75-110 ppm) concentrations relative to portions of the core that contain no spherules (typically 35-90 ppm and 40-60 ppm for volcanic rocks in the Zaonega Formation, respectively).

Although the compositions are similar, the outer zone of spherules tends to be relatively enriched in Al, K, and Si relative to the inner zone, and the inner zone tends to be relatively enriched in Mg and Fe. The outer zone contains an average of 50 wt. % SiO₂, 11 wt. % MgO, 23 wt. % Al₂O₃, 0.9 wt. % FeO, and 9.1 wt. % K₂O. The inner zone contains an average of 48 wt. % SiO₂, 16 wt.% MgO, 20 wt. % Al₂O₃, 1.2 wt. % FeO, and 8.5 wt. % K₂O (Supplemental materials Table A1).

The concentrations of Al, Mg, and Si were mapped (Supplemental materials Fig. A2), showing the locations of dolomite, calcite, and two compositionally distinct phyllosilicates (Si-rich and

Si-poor). The inner and outer zones are easily distinguished on the basis of their petrographical and geochemical characteristics.

3.7 Platinum Group Elements

To test the hypothesis that the spherules are impact generated rather than volcanic-related, platinum group element (PGE) concentrations were measured in samples from the spherule-rich intervals. The contents of siderophile elements, including the PGEs, are much higher in most meteorites compared to contents in the upper terrestrial crust (e.g., Rudnick and Gao, 2003); such enrichments have been used for identifying meteoritic components in impact melt rocks, breccias, and ejecta (see, e.g., Koeberl et al., 2012). The iridium concentration in the lower spherule-rich intervals was found to be elevated up to 0.75 ppb above a background of 0.04 ppb found in the magmatic rocks of the core (Table 1; Fig. 3). The upper interval has a much more modest enrichment of 0.14 ppb Ir. The Ru/Ir ratio in spherule-rich intervals was found to have an average value of 2.0, compared to an average background value of 4.7 (where the Ru/Ir ratio of CI chondrites is approximately 1.5 and the upper crust is 10 (Rudnick and Gau, 2003)) (Supplemental materials Fig. A3). The Ru/Ir ratio of the magmatic rocks is dissimilar to the spherule-rich samples (Fig. 3). The abundances of Rh, Pt, Pd, and Au in the spherules are similar to those of the magmatic samples, but the higher abundances of Ir and Ru in the spherule-rich intervals result in significantly different elemental ratios (Supplemental materials Fig. A4). Iridium and Ru in both the upper and lower spherule-rich intervals are strongly correlated, but in the magmatic samples, which have very low abundances of both elements, there is not a correlation between these two elements. The ratios of Ir to Pt

and Pd in the spherule-rich samples do not correspond to those in the magmatic samples (Fig. 3). The absolute concentrations of the PGEs are low, but the ratios of the elements are consistent with a small contribution from a chondritic source.

The samples of Vredefort granophyre have PGE abundances comparable to the spherule-bearing samples. The Ir abundances are 0.11 and 0.20 ppb, and the ratios of the PGEs are largely similar to the ratios observed in the spherule-rich samples (Supplementary materials Fig. A4).

3.8 Discussion

The typical indicators of meteorite impact structures or ejecta are the presence of shocked minerals or a meteoritic component, which can be verified by elevated abundances of siderophile elements, especially the PGEs, or by the isotopic compositions of Cr and Os (e.g., Simonson and Glass, 2004, French and Koeberl, 2010, Koeberl et al., 1996, 2012). In Precambrian spherule layers, shocked minerals are almost completely absent and identification relies heavily on PGE abundance and Cr or Os isotope data (e.g., Simonson et al., 2009, Koeberl et al., 2012).

The textures of the Karelian spherules are similar to those of known impact spherules (Glass and Simonson, 2012). The teardrop and dumbbell shapes are typical of melt droplets, with distinct inner and outer zones, which have been observed in a number of impact spherule layers (Walkden et al., 2002; Simonson and Glass, 2004), but similar morphologies are observed in the products of volcanic fire-fountaining events (Rutherford and Papale, 2009). Emplacement of basalts and co-magmatic gabbro sills, coeval with sedimentation, is characteristic of the Zaonega Formation in the region where cores 12A and 13A were drilled (Galdobina, 1987; Qu et al., 2012; Crne et al.,

2013a,b). However, the PGE ratios of the magmatic samples are significantly different from those of the spherule-rich intervals (Fig. 2), and, therefore, a volcanic source is considered highly unlikely for these melt droplets. Moreover, the Ru/Ir ratios of the volcanic rocks are in the terrestrial range, averaging about 5, and are clearly distinct from the much lower Ru/Ir ratios of about 2 found in all intervals containing spherules.

Correlative spherule-rich intervals in cores 12A and 13A show that the spherules were distributed over an area extending at least 20 km, which is expected for impact ejecta from a large impact and not typical of the distribution of fire fountaining, which is contained in areas less than a few square km (Rutherford and Papale, 2009).

In addition to the solitary clast at 71.10 m depth containing a few spherules within pyrobitumen breccia, there are two intervals with abundant spherules in core 13A. Both intervals of spherules have similar textures, compositions, spherule sizes, and accessory minerals and appear to have impact related origin. While it cannot be excluded that two large impact events are recorded in the drill core, this is considered statistically unlikely. Although the time interval represented by the 40 m stratigraphic difference is uncertain, the recurrence interval of Vredefort-sized impact events is approximately 0.15Ga (French, 1998), which is much longer than the time represented by deposition of the entire Zaonega Formation (a smaller impact would not be capable of producing such deposits, as it would generate smaller melt droplets, a thinner deposit, or contain many other components at nearer distances to the impact; e.g., Johnson and Melosh, 2012).

The two layers of phyllosilicates found in the spherules are taken to represent originally hollow melt spherules based on the chemical and textural distinction between the two layers. The outer layer is chemically distinct and houses the accessory minerals that are found in the spherules. The

density of phyllosilicates is much greater in the outer layer. Hollowness is a typical feature of distal impact spherules (Walkden et al., 2002), and inner edge of hollow spherules is commonly botryoidal (cf., Bohor et al., 1987).

PGE abundances in Chicxulub impact ejecta are most elevated in the fine-grained material that settled above the impact layer after condensing from the impact plume (Claeys et al., 2002); this layer is also the most susceptible to erosion and does not form deposits nearly as thick as ballistically emplaced ejecta. However, in Precambrian spherule layers, PGEs are significantly enriched in ballistically emplaced beds (e.g., Simonson et al., 2009). The PGEs of the Karelian spherules show evidence of contribution from a chondritic source, but do not have the >100 ppb Ir abundances observed for Archean spherule layers (Kyte et al., 1992; Simonson et al., 2009). Similar modest enrichment of PGEs (i.e., <1.5 ppb Ir) is observed in ejecta from the similar-scale Sudbury impact event (Pufahl et al., 2007). The ratios of PGEs are not sufficiently well constrained to distinguish a particular chondritic group, which is unsurprising given the low absolute PGE abundances.

The size of spherules based on the diameter of the impacting body is (Johnson and Melosh, 2012):

$$D_m \sim 0.9 (R_{\text{imp}}/V_{\text{ej}})^{2/3} (1)$$

where D_m is the diameter of the spherule, R_{imp} is the radius of the impactor, and V_{ej} is the velocity of the ejecta leaving the impact crater. For velocities of ejecta likely to result from a hypervelocity impact (i.e., 2-5 km/s; Johnson and Melosh, 2012) and using an average diameter of spherules of 850 μm , an 8-16 km impactor diameter can be suggested. While there is significant uncertainty in the calculation, the clear implication is that impact spherules of the diameter found in Karelia must result from a large impact. Additionally, the total thickness of the spherule-rich intervals (excluding

the matrix) is ca. 10 cm. A bed of this approximate thickness generated from a 20-km-diameter impactor should be <2500 km from the site of the impact (Artemieva and Morgan, 2011).

The Vredefort granophyre has similar Ru and Ir abundances and ratios to the spherule-rich intervals (Fig. 3). The other elemental ratios (Fig. 3) found in the granophyre do not exclude a link between the spherules and melts in the Vredefort crater. However, it is unclear how directly these two melts can be compared, as the granophyre likely formed well below the surface of the Vredefort structure (Koeberl et al., 1996), while impact spherules should form from the upper portions of the transient crater. Koeberl et al. (1996) found that the granophyre contained an extraterrestrial component equivalent to about 0.2% chondrite. The granophyre may compare well to the spherules because of a similar amount of chondritic contribution, although the process by which enrichment took place is vastly different.

The age of the spherule beds in the Karelian drill cores is constrained between 1.980 ± 0.027 Ga and 2.050 ± 0.020 Ga, which brackets the 2.020 ± 0.001 Ga Vredefort impact event. The Karelian spherules thus represent either ejecta from Vredefort or a previously unknown large-scale impact event occurring at about the same time. If one or both of the investigated spherule-rich intervals is, in fact, ejecta from the Vredefort impact event, then the distance between the paleogeographic locations of the Fennoscandian Shield at Lake Onega and the Kaapvaal Craton at the site of the Vredefort structure is constrained to <2500 km during the late Paleoproterozoic. This agrees with the interpretation of Koeberl et al. (1996) that the Vredefort impact structure was formed by a chondritic impactor.

Acknowledgements

The authors wish to thank the many people who assisted with analysis and understanding the data, including Uwe Reimold (Museum für Naturkunde, Berlin), Bruce Simonson (Oberlin College), Steven Goderis (Vrije Universiteit Brussel), Ludovic Ferrière (Natural History Museum Vienna), and Natalia Artemieva (Planetary Science Institute). Funding is provided by the University of Vienna doctoral school IK-1045 and Austrian Science Foundation grant P21821-N19.

3.9 References Cited

- Artemieva, N., and Morgan, J., 2009, Modeling the formation of the K-Pg boundary layer: *Icarus*, v. 201, p. 768-780.
- Bohor, B. F., Triplehorn, D. M., Nichols, D. J., and Millard, H. T., 1987, Dinosaurs, spherules, and the magic layer – a new K-T boundary clay site in Wyoming: *Geology*, v. 15, p. 896-899
- Chadwick, B., Claeys, P., and Simonson, B., 2001, New evidence for a large Palaeoproterozoic impact: spherules in a dolomite layer in the Ketilidian orogen, South Greenland: *Journal of the Geological Society*, v. 158, p. 331-340.
- Claeys, P., Kiessling, W., and Alvarez, W., 2002, Distribution of Chicxulubejecta at the Cretaceous-Tertiary boundary: *in* Koeberl, C., and MacLeod, K.G., eds., *Catastrophic Events and Mass Extinctions: Impacts and Beyond*: Geological Society of America Special Paper 356, p. 55-68.

- Črne, A.E., Melezhik, V.A., Prave, A.R., Lepland, A., Romashkin, A.E., Rychanchik, D.V., Hanski, E.J., and Lueo, Z., 2013a, Zaonega Formation: FAR-DEEP holes 12A and 12B, and neighboring quarries: *in* Melezhik, V.A., ed., Reading the archive of Earth's oxygenation, Volume 3: Heidelberg, Springer p. 946-1007.
- Črne, A.E., Melezhik, V.A., Prave, A.R., Lepland, A., Romashkin, A.E., Rychanchik, D.V., Hanski, E.J., and Luo, Z., 2013b, Zaonega Formation: FAR-DEEP hole 13A: *in* Melezhik, V.A., ed., Reading the archive of Earth's oxygenation, Volume 3: Heidelberg, Springer p. 1008-1046.
- French, B.M., 1998, Traces of catastrophe: Houston, TX, LPI Contribution No. 954, Lunar and Planetary Institute, 120 p.
- French, B.M., and Koeberl, C., 2010, The convincing identification of terrestrial meteorite impact structures: What works, what doesn't, and why: *Earth-Science Reviews*, v. 98, p. 123-170.
- Galdobina, L.P. 1987, The Ludicovian super-horizon. In: Sokolov, V.A. ed., *Geology of Karelia*. Nauka (Science), Leningrad, p. 59–67 (in Russian)
- Gibson, R.L., Armstrong, R.A., and Reimold, W.U., 1997, The age and thermal evolution of the Vredefort impact structure: A single-grain U-Pb zircon study: *Geochimica et Cosmochimica Acta*, v. 61, p. 1531-1540.
- Glass, B.P., and Simonson, B.M., 2012, Distal impact ejecta layers: Spherules and more: *Elements*, v. 8 p. 43-48.
- Hannah, J. L., Stein, H. J., Zimmerman, A., Yang, G., Melezhik, V.A., Filippov, M.M., Turgeon, S.C., and Creaser, R.A., 2008. Re-Os geochronology of shungite: A 2.05 Ga fossil oil field in Karelia (Abstract). *Geochimica et Cosmochimica Acta*, v. 72, p. A351.

- Johnson, B., and Melosh, J., 2012, Formation of spherules in impact produced vapor plumes: *Icarus*, v. 217, p. 416-430.
- Kamo, S., Reimold, W.U., Krogh, T.E., and Colliston, W.P., 1996, A 2.023 Ga age for the Vredefort impact event and a first report of shock metamorphosed zircons in pseudotachylitic breccias and granophyre: *Earth and Planetary Science Letters*, v. 144, p. 369-387.
- Koeberl, C., Reimold, W.U., and Shirey, S.B., 1996, A Re-Os isotope and geochemical study of the Vredefort granophyre: clues to the origin of the Vredefort Structure, South Africa: *Geology* v. 24 p. 913-916.
- Koeberl, C., Claeys, P., and Hecht L., and McDonald I., 2012, Geochemistry of impactites: *Elements*, v. 8, p. 37-42.
- Koistinen, T., Stephens, M.B., Bogatchev, V., Nordgulen, Ø., Wenneström, M., and Korhonen, J., 2001, Geological Map of the Fennoscandian Shield, Scale 1:2 000 000, Geological Surveys of Finland, Norway and Sweden and the North-West Department of Natural Resources of Russia.
- Kyte, F. T., Lei, Z., and Lowe, D. R., 1992, Noble-metal abundances in an early Archean impact deposit: *Geochimica et Cosmochimica Acta*, v. 56 p. 1365-1372.
- Lowe, D., Byerly, G., Asaro, F., and Kyte, F., 1989, Geological and geochemical record of 3400-million-year-old terrestrial meteorite impacts: *Science*, v. 245, p. 959-962.
- Puchtel, L.S., Arndt, N.T., Hofmann, A.W., Haase, K.M., Kröner, A., Kulikov, V.S., Garbe-Schönberg, C.D., and Nemchin, A.A., 1998, Petrology of mafic lavas within the Onega pla-

teau, central Karelia: Evidence for 2.0 Ga plume-related continental crustal growth in the Baltic Shield: *Contributions to Mineralogy and Petrology*, v. 130, p. 134-153.

Pufahl, P. K., Hiatt, E. E., Stanley, C. R., Morrow, J. R., Nelson, G. J., and Edwards, C. T., 2007, Physical and chemical evidence of the 1850 Ma Sudbury impact event in the Baraga Group, Michigan: *Geology* v. 35 p. 827-830.

Qu, Y., Črne, A.E., Lepland, A., and van Zuilen, M., 2012. Methanotrophy in a Paleoproterozoic oil field ecosystem, Zaonega Formation, Karelia, Russia. *Geobiology*, 10, 467–478.

Rudnick, R.L. and Gao, S., 2003 The composition of the continental crust, *in* Holland, H. D., and Turekian, K. K., eds. *Treatise on Geochemistry Volume 3*: Oxford, Elsevier-Pergamon, p. 1-64.

Rutherford, M.J., and Papale, P., 2009, Origin of basalt fire-fountain eruptions on Earth versus the Moon: *Geology*, v. 37, p. 219-222.

Simonson, B., and Glass, B., 2004, Spherule layers – Records of ancient impacts: *Annual Review of Earth and Planetary Science*, v. 32, p. 329-261.

Simonson B.M., McDonald I., Shukolyukov A., Koeberl C., Reimold W.U., and Lugmair G., 2009, Geochemistry of 2.63–2.49 Ga impact spherule layers and implications for stratigraphic correlations and impact processes. *Precambrian Research* v. 175, 51-76.

Strauss, H., Melezhik, V.A., Lepland, A., Fallick, A.E., Hanski, E.J., Filippov, M.M., Deines, Y.E., Illing, C.J., Črne, A.E., and Brasier, A.T., 2013. 7.6 Enhanced Accumulation of Organic Matter: The Shunga Event. In: Melezhik, V.A., Kump, L.R., Fallick, A.E., Strauss, H., Hanski,

E., Prave, A.R., and Lepland, A., (Eds.): Reading the Archive of Earth's Oxygenation, vol. III, Springer, p. 1195–1273.

Volodichev, O.I., 1987. Metamorphism. In: Sokolov, V.A. (Ed.) Geology of Karelia, Nauka, Leningrad, p.152–175. (in Russian)

Walkden, G., Parker, J., and Kelly, S., 2002, A late Triassic impact ejecta layer in Southwestern Britain: Science, v. 298, p. 2185-2188.

Figures

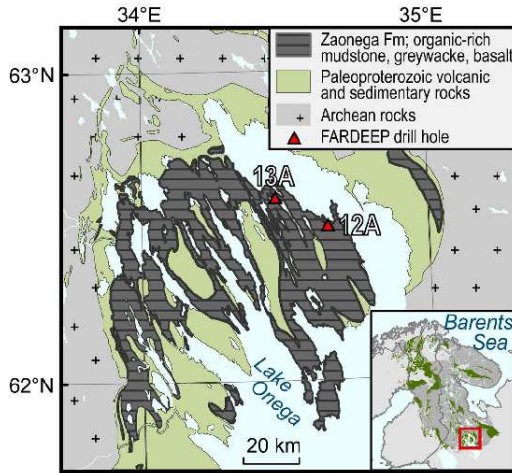


Figure 1. Simplified geological and geographical map of the Lake Onega region in the Fennoscandian Shield (modified after Koistinen et al. 2001) showing locations of the drill cores 12A and 13A.

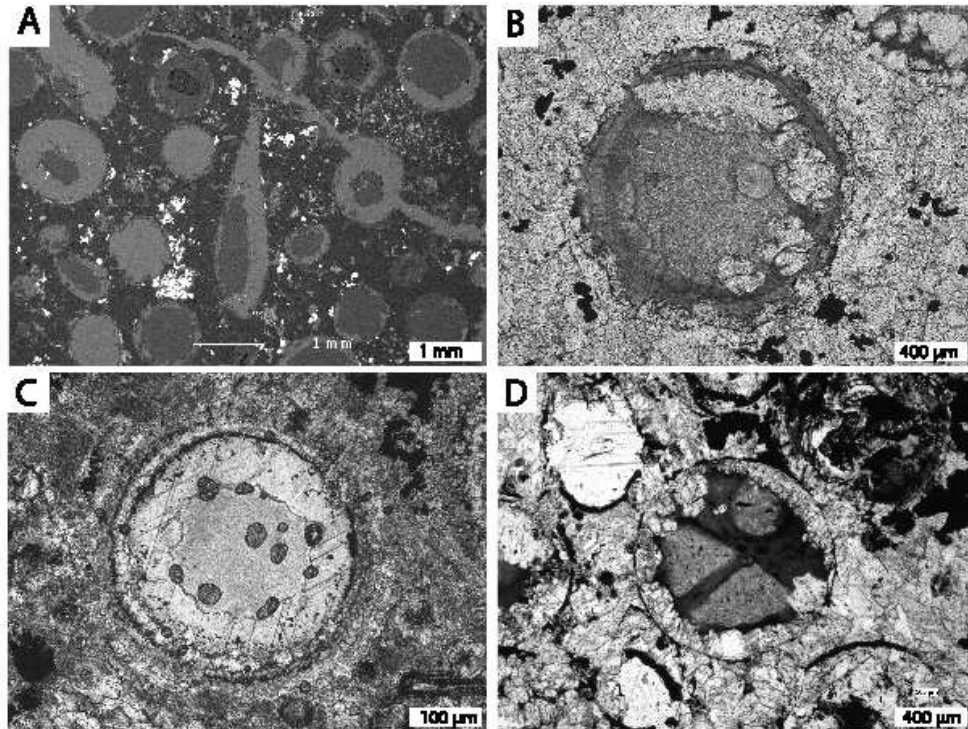


Figure 2. Images of spherules from core 13A. A) BSE-SEM image of spherules from 27.10 m. A large teardrop-shaped spherule is present in the center of the image, and a dumbbell shaped spherule is partially visible in the upper left corner. Most spherules are circular in cross-section. B) Photomicrograph (plane polarized light - PPL) of a spherule from 27.00 m clearly showing the inner and outer zones of the spherule. The outer zone has fibrous crystals of phlogopite-biotite with an outward radial pattern. Calcite has partially replaced the upper right portion of the outer zone. C) Photomicrograph (PPL) of a spherule from 67.21 m. The spherule is completely replaced by calcite, but the two zones within the spherule are still clearly visible. D) Photomicrograph (PPL) of a spherule from 26.90 m showing distinct chambers within the spherule.

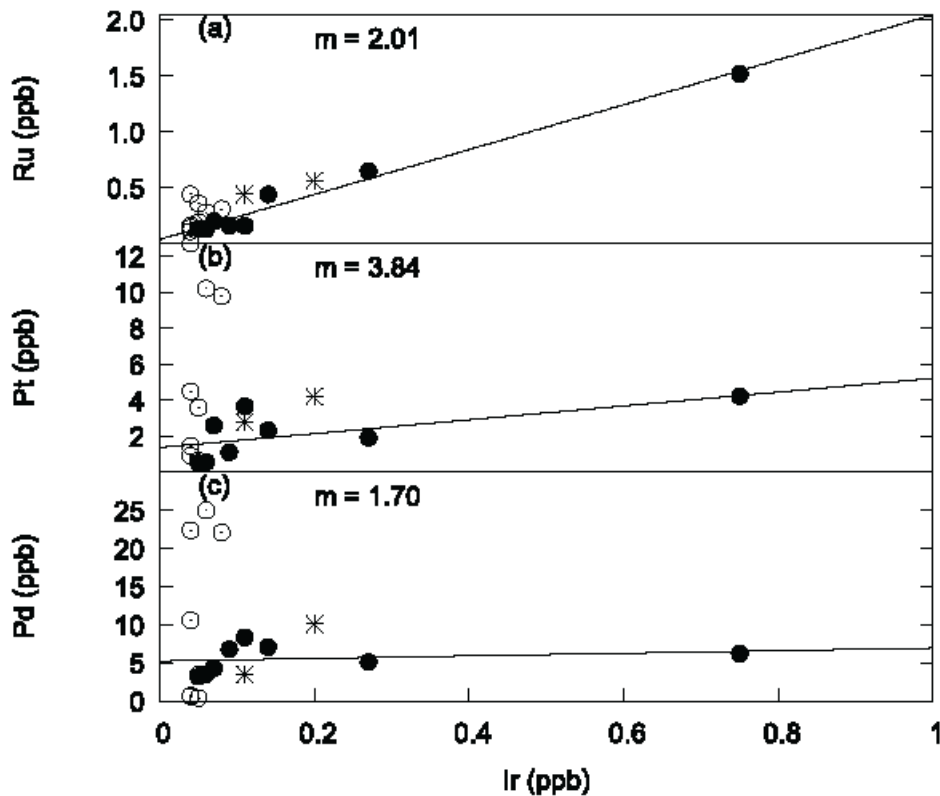


Figure 3. PGE abundances of measured samples. Filled circles represent measured spherule-bearing samples, open circles represent magmatic samples, and stars represent Vredefort granophyre. The linear regression of the spherule-bearing samples is plotted and the slope of the line (m = slope of linear regression) is indicated. The ratios of PGEs in the spherules are clearly distinct from the magmatic samples for all examples. Note that Ru/Ir for the spherules is quite similar to the Vredefort granophyre.

TABLE 1. RESULTS OF PLATINUM GROUP ELEMENT ANALYSES IN FAR-DEEP CORE

Depth (m)	Lithology	Ir (ppb)	Ru (ppb)	Rh (ppb)	Pt (ppb)	Pd (ppb)	Au (ppb)
12A							
4.03	Spherule-bearing dolostone	0.07	0.2	0.48	2.6	4.31	3.88
67.46	Diabase/Basalt	0.05	0.36	0.36	3.59	3.45	2.29
83.75	Diabase/Basalt	0.04	0.16	0.52	4.5	10.6	9.47
13A							
26.92	Spherule-bearing dolostone	0.11	0.16	1.11	3.67	8.36	1.36
27	Spherule-bearing dolostone	0.05	0.13	0.16	0.53	3.22	1.87
27	Spherule-bearing dolostone	0.06	0.13	0.21	0.57	3.55	2.1
27.28	Spherule-bearing dolostone	0.09	0.16	0.78	1.12	6.77	4.17
27.36	Spherule-bearing dolostone	0.14	0.44	1.25	2.33	7.08	7.76
67.12	Spherule-bearing dolostone	0.75	1.52	1.88	4.23	6.24	1.87
67.12	Spherule-bearing dolostone	0.27	0.65	0.89	1.92	5.13	1.62
94.17	Basalt	0.05	0.19	0.05	0.65	0.44	1.2
109.06	Peperite	0.04	0.11	0.06	1.47	0.62	1.39
122.18	Diabase	0.04	0.14	0.07	0.92	0.72	0.96
203.64	Diabase/Basalt	0.06	0.28	0.64	10.2	25	8.61
203.64	Diabase/Basalt	0.08	0.31	0.54	9.77	22.1	8.96
236	Diabase/Basalt	0.04	0.44	0.83	12.7	22.4	4.07
BG-9	Vredefort granophyre	0.2	0.56	0.43	4.2	10.1	2.41
BG-168	Vredefort granophyre	0.11	0.44	0.38	2.8	3.5	2.3
	Upper Crust	0.02	0.21	0.38	0.51	0.52	1

Note: Samples with same depth indicated are duplicate analyses of a single powder. Crustal values from Rudnick and Gau (2003).

Supplemental Information

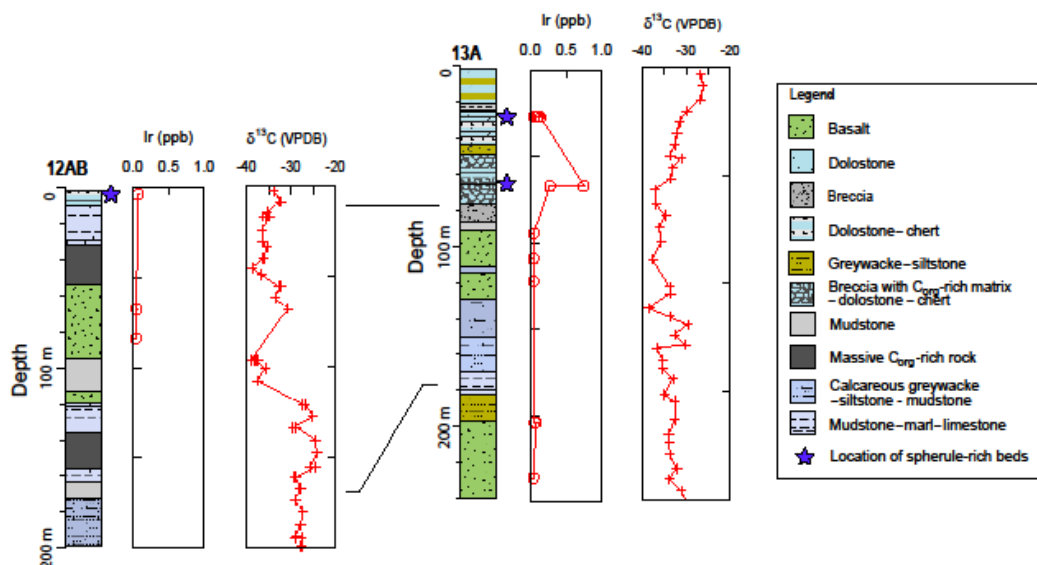


Figure A1. Lithostratigraphy, organic matter $\delta^{13}\text{C}$ profiles, and Ir abundances for the upper parts of cores 12A and 13A and the positions of spherule-rich beds. Correlation between the cores is based on lithology (Črne *et al.*, 2013a,b) and corroborated by the stratigraphic trends of $\delta^{13}\text{C}$ of organic matter ($\delta^{13}\text{C}$ data within core 12A are from Kump *et al.*, 2011; $\delta^{13}\text{C}$ data for core 13A from Lee Kump, accessed via the internal FAR-DEEP website, far-deep.icdp-online.org). The Ir anomaly of the upper and lower spherule-rich layers in core 13A is indicated; note that no samples were analyzed between the two spherule-rich layers. Lithologies are meta-lithologies.

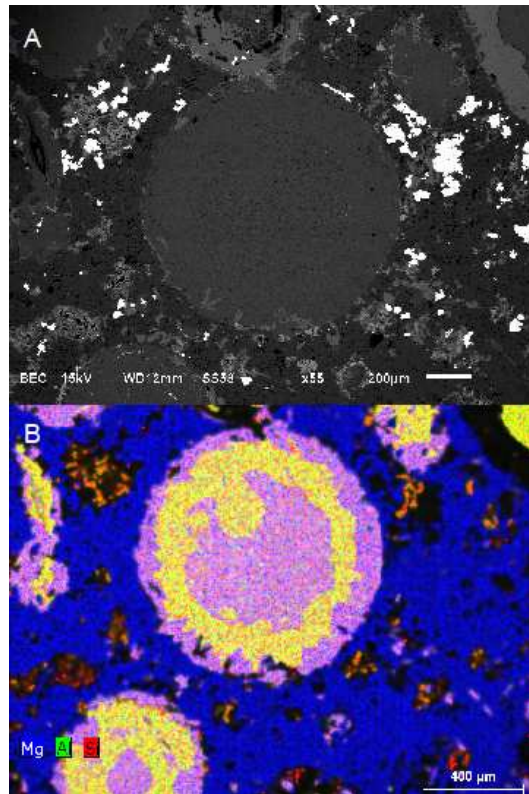


Figure A2. A) BSE_SEM image of a spherule from core 13A at 27.0 m depth with distinct inner and outer phyllosilicate layers; The electron density of the phyllosilicates is similar, obscuring the compositional difference. B) EDX map of the same spherule, showing a clear separation of inner and outer zone, with the inner zone composed of the same Si-enriched phyllosilicates found in the matrix. This pattern is reflected in most examined spherules. The pattern is likely the result of originally hollow spherules being later infilled by phyllosilicates. The pink and yellow colors on the map are the result of overlap of Al and Si, with the pink area being relatively enriched in Si and yellow relatively enriched in Al.

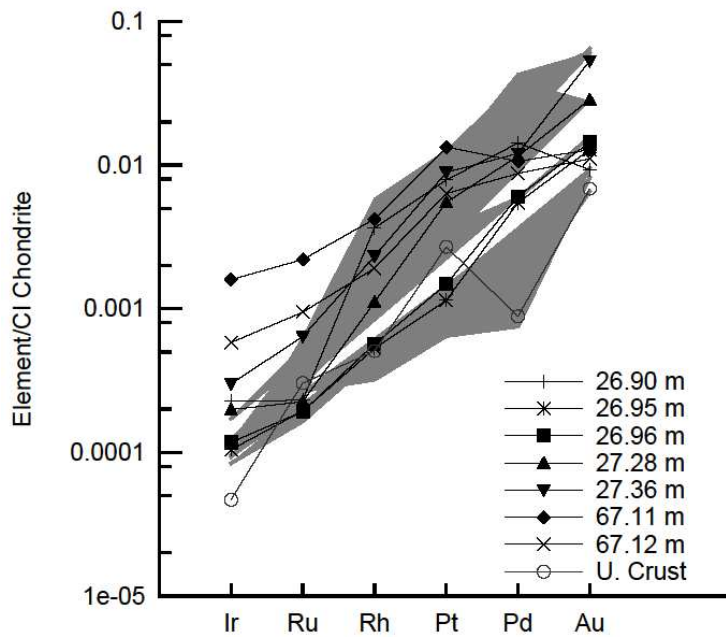


Figure A3. Chondrite normalized (after McDonough and Sun, 1995) platinum group element chemistry of the spherule intervals in core 13A and the PGE concentrations in volcanic rocks (grey fields). Iridium and Ru abundances are clearly elevated in the spherule-rich layer relative to both the volcanic deposits in the core and relative to upper crustal values. U.Crust = upper crust. Crustal values from Rudnick and Gau (2003).

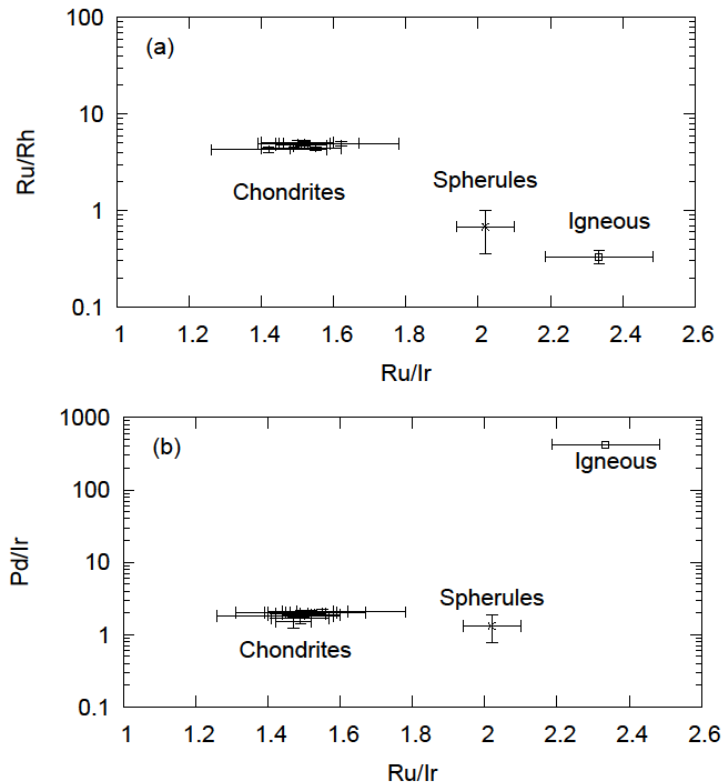


Figure A4. Comparison of ratios between elements in spherules and magmatic samples from core samples. Individual samples are not plotted; values are determined from a linear regression of all analyses (see Figure 6), and error bars represent the 95% confidence interval. A) Ru/Rh vs Ru/Ir for spherules, magmatic samples, and various chondrite groups. B) Pd/Ir vs Ru/Ir for spherules, magmatic samples, and chondritic groups. The spherules are clearly distinct from the magmatic samples and have an apparent chondritic source of PGEs. Likely due to the low abundances of the PGEs in these samples, the particular chondritic source cannot be identified. Data for chondrites from Tagle and Hecht (2006).

Methodology

Whole-rock X-ray fluorescence analysis of major and trace elements of 12 samples was carried out at the Geological Survey of Norway using a PANalytical Axios at 4 kW. The precision (1σ) is typically around 2 rel. %.

The major element composition of the phyllosilicates within spherules of six samples was determined at the Museum für Naturkunde (MfN) in Berlin using a JEOL JXA 8500A electron microprobe with a field emission cathode and five wavelength-dispersive spectrometers. Measurements were made at 15 kV acceleration voltage and 30 nA beam current. The sample spot size (surface) was approximately 1 μm . Back-scattered electron images and element mappings were also done with a JEOL JSM-6610LV scanning electron microscope equipped with a Bruker AXS Quantax 800 EDX system at MfN.

Iridium, Ru, Pt, Rh, Pd, and Au abundances were measured in Cardiff by inductively coupled plasma mass spectrometry after being concentrated from 15 g powders by NiS fire assay (see Huber et al, 2001 and McDonald and Viljoen, 2006 for details on the method). Eight samples containing spherules were analyzed and eight samples of basalt, diabase, and pepperite from other depths in the same drill core were measured for background values (see Table 1). In addition, PGEs from two samples of Vredefort granophyre were measured for comparison. The samples BG-9, a spherulitic granophyre, and BG-168, a granular granophyre, were previously used in the study of Koeberl et al. (1996).

References

- Črne, A.E., Melezhik, V.A., Prave, A.R., Lepland, A., Romashkin, A.E., Rychanchik, D.V., Hanski, E.J., and Lueo, Z., 2013a, Zaonega Formation: FAR-DEEP holes 12A and 12B, and neighboring quarries: *in* Melezhik, V.A., ed., Reading the archive of Earth's oxygenation, Volume 3: Heidelberg, Springer p. 946-1007.
- Črne, A.E., Melezhik, V.A., Prave, A.R., Lepland, A., Romashkin, A.E., Rychanchik, D.V., Hanski, E.J., and Luo, Z., 2013b, Zaonega Formation: FAR-DEEP hole 13A: *in* Melezhik, V.A., ed., Reading the archive of Earth's oxygenation, Volume 3: Heidelberg, Springer p. 1008-1046.
- Koeberl, C., Reimold, W.U., and Shirey, S.B., 1996, A Re-Os isotope and geochemical study of the Vredefort granophyre: clues to the origin of the Vredefort Structure, South Africa: *Geology* v. 24 p. 913-916.
- Kump, L.R., Junium, C., Arthur, M.A., Brasier, A.T., Fallick, A.E., Melezhik, V.A., Lepland, A., Črne, A.E., and Luo, G., 2011. Isotopic evidence for massive oxidation of organic matter following the great oxidation event: *Science* v. 334, p. 1694–1696.
- Huber H., Koeberl C., McDonald I., and Reimold W.U., 2001, Geochemistry and petrology of Witwatersrand and Dwyka diamictites from South Africa: search for an extraterrestrial component. *Geochimica et Cosmochimica Acta*, v.65, 2007-2016.
- McDonald, I., and Viljoen, K. S., 2006, Platinum-group element geochemistry of mantle eclogites: a reconnaissance study of xenoliths from the Orapa kimberlite, Botswana: *Applied Earth Sciences*, v. 115, p. 81-93.

Rudnick, R.L. and Gao, S., 2003 The composition of the continental crust, *in* Holland, H. D., and Turekian, K. K., eds. Treatise on Geochemistry Volume 3: Oxford, Elsevier-Pergamon, p. 1-64.

Tagle, R., and Hecht, L., 2006. Geochemical identification of projectiles in impact rocks: Meteoritics and Planetary Science, v. 41 p. 1721-1735.

4. PETROGRAPHY AND GEOCHEMISTRY OF EJECTA FROM THE SUDBURY IMPACT EVENT

Matthew Huber^{1*}, Iain McDonald², and Christian Koeberl^{1,3}

¹*Department of Lithospheric Research, University of Vienna, Althanstrasse 14,
A-1090 Vienna, Austria*

²*School of Earth and Oceanic Sciences, Cardiff University, Cardiff CF10 3AT, United Kingdom*

³*Natural History Museum, Burgring 7, A-1010 Vienna, Austria*

**corresponding author: matthew.huber@univie.ac.at*

Submitted to: Meteoritics and Planetary Science, 17 May, 2013

Abstract

To better understand the nature of the Sudbury impact event, ejecta from the Connors Creek site in Michigan (500 km from the Sudbury Igneous Complex [SIC]), the Pine River site in Western Ontario (650 km from the SIC), and the Coleraine site in Minnesota (980 km from the SIC) were sampled for petrographic and geochemical analysis. The Connors Creek site was found to have approximately 2 m of ejecta, including shocked quartz, melt droplets, and accretionary lapilli; the Pine River site has similar deposits with about 1 m of thickness, although with smaller lapilli; the Coleraine site contains only impact spherules in a 20-cm thick layer. The ejecta transition from a chaotic deposit of massively bedded impactoclastic material intermixed with locally derived detritus at the Connors Creek site to a deposit with apparently very little detrital material that is made up primarily

of impact melt droplets at the Pine River site to a deposit that is almost entirely composed of impact spherules at the Coleraine site. The major and trace element compositions of the ejecta were measured, confirming the previously observed similarity of the ejecta deposits to the Onaping Formation in the SIC. Platinum group element (PGE) concentrations from each of the sites were also measured, revealing significantly elevated PGE contents compared to background values. PGE abundances in samples from the Pine River site can be reproduced by addition of approximately 0.2% CI chondrite to the background composition of the underlying sediments in the core. These results provide evidence that, although the contribution of the impactor to the ejecta deposits is too low to pinpoint the exact type of the impactor, PGE interelement ratios indicate that the Sudbury impact event was likely caused by a chondritic impactor.

4.1 Introduction

4.1.1 Sudbury Structure

The 1.85 Ga Sudbury impact structure (Davis 2008), preserved near Sudbury, Ontario (Canada), is the remnant of one of the largest impact craters currently known on Earth. Its original diameter is thought to have been approximately 200-250 km (e.g., Dickin et al. 1996; Mungall et al. 2004). The most prominent feature of the current structure is the Sudbury igneous complex (SIC), which was deformed into a 30 by 18 km truncated oval by the Penokean orogeny at approximately 1.85 Ga and the Yavapai orogeny at approximately 1.75 Ga (Piercey et al. 2007) and later by the Grenville orogeny (Szabo and Halls 2006). There are numerous shock indicators in and around the SIC, including shatter cones, impact breccias, pseudotachylitic breccia, and planar deformation features

(PDFs) in quartz, coesite, and impact diamonds (e.g., French 1970; Rousell et al. 2003). Shatter cones occur around the SIC on all sides, being well-developed in the fine-grained sediments of the target material, and apparently more abundant on the southern edge of the structure, including in the city of Sudbury (e.g., Bray 1966). The SIC is cut by a complex series of large-scale faults that are related to both original emplacement and later deformation, and include the economically important offset dikes. The impact struck metasedimentary rocks of the Huronian supergroup, including quartzites, shales, and also carbonates, in addition to the Archean crystalline basement (e.g., Fedorowich et al. 1999), locally intruded by granitic plutons and the East Bull Lake suite, which included noritic dikes and layered intrusions (e.g., Vogel et al. 1998).

The SIC is divided into the granophyre and norite layers (Dressler 1984). The SIC is overlain by the Onaping Formation, which is divided into the Sandcherry and Dowling members. The two members have been interpreted to be the result of two different formation mechanisms (Grieve et al. 2010). The Sandcherry member is thought to have formed through direct fallback of ejecta, while the Dowling member is thought to have formed through phreatomagmatic interaction between the melt sheet and water as it filled the structure. The Sandcherry member experienced thermal and hydrothermal alteration as a result of overlying the still-molten melt sheet, and the Dowling member was formed through explosive interactions, such that only clasts-within-clasts remain of the original ejecta deposits (Grieve et al. 2010). As such, neither member represents unaltered ejecta.

Investigations into the nature of the impactor that formed the Sudbury impact structure have been more successful at determining the mechanics of the impact than the composition of the impactor (e.g., Pope et al. 2004; Deutsch et al. 1995; Grieve et al. 1991; Mungall et al. 2004). While a few authors argue for a cometary impactor (i.e., Darling et al. 2010), most models of the impact involve

an approximately 10 km diameter body impacting at asteroidal velocities of about 20 km/s (i.e., Ivanov 2005). The models typically use a dunitic impactor, although models involving an icy comet have been attempted (Darling et al. 2010). The composition of the impactor has not been positively identified owing to the high concentrations of platinum group elements (PGEs) from the host rocks that obscure the meteoritic signature in melt rocks (i.e., Cohen et al. 2000). The large amount of PGE in the SIC is likely due to melting of the entire crust (probably including intrusions of the East Bull Lake suite containing PGE mineralization; e.g. Peck et al 2001) during the impact event (Kring 1995; Pope et al. 2004). Attempts to use isotopic systems to identify the impactor have been inconclusive (Morgan et al. 2002; Koeberl and Shirey 1997). Morgan et al. (2002) found low concentrations of meteoritic Os in their analysis of PGEs in ores from the SIC, which they argued suggests that the impactor may have been a IIB iron meteorite.

4.1.2 Ejecta deposits

Distal ejecta from the Sudbury impact have been described from locations with distances from the center of the SIC ranging from 450 to 980 km in Michigan, Minnesota, and Ontario (Figure 1). Direct evidence of distal ejecta from the Sudbury impact was first described by Addison et al. (2005). The sites described by Addison et al. (2005) and those subsequently described by Pufahl et al. (2007), Cannon et al. (2010), and Addison et al. (2010) are shown in Figure 1. The most extensive study of the Sudbury ejecta, by Cannon et al. (2010), characterized the stratigraphy and petrography of ten sites, and measured the major element, trace element, and rare earth element (REE) geochemistry of ejecta materials at five sites. The paper by Addison et al. (2005) included the pe-

trography and stratigraphy of samples from four other sites that were not examined by Cannon et al. (2010), along with zircon U/Pb data demonstrating the age correlation between the ejecta layer and the Sudbury impact event (constraining the layer to an age of 1836-1878 Ma). To date, only one attempt has been made to determine the PGE chemistry of the ejecta deposits (Pufahl et al. 2007), which indicated that ejecta-bearing samples from two cores drilled near Marquette, MI, have PGE anomalies, with Ir abundances up to 0.74 ppb. The work did not attempt to constrain the impactor composition. Finally, Addison et al. (2010) described the petrography and stratigraphy of an additional eight sites, but did not present geochemical data.

The stratigraphy of most of these sites indicates deposition into shallow water settings, although some of the sites from Ontario may have been deposited in a subaerial setting (Addison et al. 2010). The sites south of Lake Superior, in the USA, were almost certainly deposited in a foreland basin (Cannon et al. 2010; Schulz and Cannon 2007). Ejecta overlie various rock types, depending on the location, but most commonly it is found overlying shale, chert, or banded iron formations. Each site where ejecta have been found is distinct in terms of the exact nature of the ejecta, thickness of various units, geochemistry, etc., but only a few components are present in the various ejecta deposits. These components are: 1) altered melt droplets, 2) shocked quartz grains, 3) unshocked quartz and chert, and 4) accretionary lapilli (Addison et al. 2005; Pufahl et al. 2007; Cannon et al. 2010; Addison et al. 2010). These components frequently overlie locally brecciated rocks. A few sites also include megabreccias, with single clasts up to 6 m in diameter (Addison et al. 2010). In this study we revisit three sites to more fully characterize the abundances of the major and trace elements, including the REEs and the PGEs, of the various ejecta components in order to better understand the Sudbury impact event. The Connors Creek, Pine River, and Coleraine sites have been

selected because of pristine preservation of ejecta, limited geochemical alteration, similar depositional environment (all three are quiet water shelf deposits), and at a range of distances from the impact (with distances of 500, 650, and 980 km from the SIC, respectively; Figure 1).

4.2 Samples and Methods

Field work and visits to core repositories by M. H. in August, 2010, resulted in the collection of samples of ejecta from the Connors Creek, Pine River, and Coleraine sites, which were then petrographically and geochemically investigated. The Connors Creek site is accessible at an outcrop (see below), but the Pine River and Coleraine sites are known only from drill cores. The Pine River samples were obtained from a single exploratory diamond drill core that was recovered in 2004 by Falconbridge Limited. Samples from the Coleraine site were obtained from four closely spaced drill cores that are housed by the Minnesota Department of Natural Resources core repository (MDNR) in Minnesota (USA). Six bulk samples were selected from the Connors Creek site across the entire stratigraphy, while the drill cores from the other two locations allowed for samples to be obtained along the entire ejecta-bearing section. The Pine River site was sampled at intervals of 4-5 cm, starting from the breccia, just below the accretionary lapilli, up to just above the lapilli. Samples from Coleraine were selected depending on sample recovery from the drill cores. Location details for the samples can be found in the appendix.

A set of 30 thin sections were prepared for petrographic investigation. Samples were crushed using a ceramic jaw crusher, and powders of 15 g were prepared with an agate mortar for major and trace element analysis by X-ray fluorescence (XRF). XRF analyses were performed at the University of Vienna using a Philips PW2400 after 1.2 g fused beads were generated using a Philips Perl X3

automatic bead machine in a Pt-Au crucible and mold. Trace element contents were determined after 10 g pressed powder pellets were homogenized with 0.5 ml of polyvinyl alcohol. Measurements were made in the Philips PW2400 while a 3 kW Rh-anode X-ray tube generated X-rays (see Schmid et al., 2000, for details on precision).

Powders for samples from each site were irradiated for 6-8 h in the 250 kW Triga Mark II reactor at the Atomic Institute of the Austrian Universities at a thermal flux of $1.7 \times 10^{12} \text{ ncm}^{-2}\text{s}^{-1}$ as preparation for measurement of short-lived nuclides by instrumental neutron activation analysis (INAA) at the University of Vienna (see Mader and Koeberl 2009, for details on instrumentation, methodology, analytical precision, and standards).

Approximately 15 g of powder was also used for PGE analysis; PGEs were concentrated into a bead using the fire assay method (see Huber et al 2001 and McDonald and Viljoen 2006 for more details on methodology), which was then powdered and measured by inductively coupled plasma mass spectrometry at Cardiff University.

In addition, Raman spectrometry was used to identify mineral species in thin sections. Spectra were obtained using an edge filter based confocal Renishaw RM1000 micro-Raman spectrometer, with a 632.8 nm HeNe laser source, at the University of Vienna.

Note on terminology: Although the term “lapilli” strictly refers to a size category of volcanic ejecta, the term “accretionary lapilli” has been frequently used in impact literature to describe a petrographically identical component of impact ejecta. In this paper, “lapilli” is used to describe accretionary clasts of impact origin.

4.3 Field observations

4.3.1. Connors Creek

The Connors Creek site was previously examined by Cannon et al. (2010). The site is approximately 500 km from the center of the SIC. The site has undergone minimal tectonic deformation. There are two outcrops at this site that contain evidence of being impact related. These outcrops have been exposed by recent glacial activity, with the outcrops being located in the centers of two glacially carved drumlins. A stratigraphic section of outcrop 1 shows approximately 1 m of black chert that represents the local host rock (Figure 2a). This unit is overlain by 21 cm of sand sized material that contains chert, quartz, phyllosilicates, and carbonates. Above this section is 27 cm of sand that contains large chert clasts (ca. 15 x 5 cm sized clasts), in some places mixed with accretionary lapilli. For 7 cm, no accretionary lapilli are mixed with the sand, followed by 15 cm of thinly interbedded accretionary lapilli and sand. This is then overlain by 1.50 m of sand mixed with chert cobbles, lapilli, and cm-scale altered glass fragments. The outcrop is eroded above this point. The second outcrop is approximately 100 m N from outcrop 1 and has very different characteristics, consisting of about 12 cm of black chert that is overlain by 2 m of apparently cross-bedded sand (although it is possible that the sand is not strictly cross-bedded, but deposited on a slope). The sand contains chert fragments and fragments of lapilli, but there are no bedded lapilli at this outcrop. The rock existing above the sand at this outcrop has been removed by erosion, but a nearby white bedded chert appears to overlie the sand. Cannon et al. (2010) interpreted the two outcrops to be continuous with one another, suggesting that the second outcrop directly overlies the first one; however, this is not the only possible interpretation, and an alternative interpretation would be that the outcrops are

not stratigraphically continuous, perhaps owing their different characteristics to the chaotic nature of ejecta deposition.

4.3.2. Pine River

Samples from the Pine River drill core were included as part of the study of Addison et al. (2005), but the drill core is not described in detail, nor is geochemical information presented. The core was drilled approximately 650 km from the center of the SIC. The samples obtained are well preserved, with only diagenetic alteration affecting the rocks in the core. The base of the sampled interval is located at 695.22 m depth (Figure 2b), where brecciated clasts of chert are visible in a sandy matrix. This extends for 13 cm, grading into a carbonate mudstone with gray coloration and some chert clast inclusions. Fifteen cm above the base, white carbonaceous sand is present and separated from the lower mud unit by stylolites. Alternating beds of grey and white mud with clasts of chert are present up to 40 cm above the base of the outcrop. From 40 to 62 cm above the base of the outcrop, greenish mud and sand are interlayered with some rounded cm-scale clasts that are incorporated into the mud. From 62 to 70 cm above the base, similar clasts occur but have angular shapes. Accretionary lapilli appear in a concentrated layer at 71 cm, and then become less concentrated until they totally disappear at 81 cm. A single chert pebble was seen incorporated into the lapilli layer. The lapilli are overlain by a green sand from 81 to 96 cm, then overlain by cross-bedded mud and sand up to 107 cm above the base, which is taken to be the end of the impactoclastic material; earlier studies by Addison et al. (2005) have shown that this interval contains shocked quartz grains within the sands. The original thickness of the layer is obscured by numerous stylolites.

4.3.3. Coleraine

Four drill cores in Northern Minnesota, approximately 980 km from the center of the SIC, contain ejecta from the Sudbury impact. These represent the most distal ejecta identified so far from the Sudbury impact event. The cores have similar thickness and petrographic characteristics. The ejecta layer is identified in the Biwabik Iron Formation in the transition zone between the Upper Cherty member and the overlying Virginia Formation graywackes. Each core contains a bedded layer up to 20 cm thick that consists primarily of melt droplets altered to (mainly) phyllosilicates. The friable nature of the ejecta layer resulted in only partial core recovery. The samples have only been compacted and undergone diagenetic alteration. The ejecta are preserved primarily as sub-mm melt spherules encased in a very fine-grained silicate matrix (except in the case of DL 20018, which has an Fe-rich matrix). The ejecta layers are bedded. In some cases, the bedding deforms around cm-sized clasts of chert, demonstrating their presence as part of the original deposit; in other cases, replacement of original phases by chert is apparent. Stylolites show that compaction has reduced the total thickness of the beds. Accretionary lapilli were not found at this location.

4.4. Results

4.4.1. Petrographic observations

4.4.1.1. Connors Creek site

The Connors Creek site is notable for having abundant accretionary lapilli in a m-thick, cross-bedded layer. The lapilli are approximately 1 to 3 cm in diameter, often with an up to 2:1 ratio of long to short axis (probably due to tectonic compression) (Figure 3a). The rims of the lapilli are somewhat distorted because of intrusions from surrounding grains and diagenetic activity. They are composed of very fine-grained silicates that are layered concentrically around a nucleus, which is most frequently an agglomeration of mm-sized grains bound together in an aphanitic groundmass (composed of phyllosilicates and some carbonates). While the groundmass is aphanitic, there are some phaneritic clasts contained in the lapilli, most of which are $<20\ \mu\text{m}$ in size. These clasts are mostly angular quartz and chert fragments. Up to 3% of the quartz grains are shocked (i.e., containing planar fractures [PFs] and/or planar deformation features [PDFs]), and frequently, the grains exhibit undulose extinction. Some lapilli include phyllosilicate clasts, although the phyllosilicates may represent diagenetic alteration. Phyllosilicate laths within lapilli are almost always smaller than the laths that occur in the matrix.

The lapilli are entrained as clasts in a sandy matrix that is indistinguishable from the underlying sand that does not contain lapilli, except in the frequency of phyllosilicates representing altered melt droplets. Quartz grains in the sand are usually $<200\text{-}\mu\text{m}$ -size and range from sub-rounded to well rounded. There are also chert clasts up to 3 mm in diameter. Some angular clasts of aphanitic material resemble broken lapilli. Significant carbonate alteration has obscured part of the original composition; some samples are entirely altered to carbonate, while the least altered samples still contain approximately 10 area % carbonate in thin section. The original texture is still visible in almost all cases, with flow textures and amygdales, which may represent infilled vesicles.

Where phyllosilicates are preserved, irregular blobs of material up to 1 cm diameter with flow textures and entrained quartz grains are present, with vesicles in the shape of either preserved spheres or collapsed ovoids (Figure 3b). Some vesicles retain shapes and textures reminiscent of microtektites or microkrystites. Rutile grains tend to outline the edges of vesicles and also appear occasionally in the interior of the melt droplets. Where quartz grains are entrained, they often have rims and flow textures around them composed of the phyllosilicate groundmass, and are very well rounded. These grains sometimes show undulose extinction, but no shocked quartz grains have been observed within melt droplets. Melt droplets contain a significant amount of carbonates in the form of calcite and dolomite. Some samples have clasts that appear to be primary calcite inclusions, although some euhedral crystals of calcite are clearly secondary. It is unclear what percentage of the carbonate is actually secondary. Samples CC 3-6 appear to have a much higher percentage of secondary carbonate.

4.4.1.2. Pine River site

Samples from the Pine River drill core are very well preserved. Ejecta at this location are finely bedded. The impact sand consists almost entirely of altered melt droplets, which now consist of various phyllosilicates (mostly chlorite and biotite) that have been deformed by diagenetic compaction. There are abundant shocked quartz grains, making up as much as 5 area % of some thin sections. Unshocked quartz and chert are also common, but the vast majority of the grains are altered melt droplets. There is not a significant petrographic difference in the sand above and below the accretionary lapilli. At various places in the core, carbonate alteration obscures the original petrographic characteristics. The samples show evidence of compaction, but the original textures seem

to be preserved. Fine-scale zonations within melt particles are visible, with different phyllosilicates being present in different melt droplets. These are finely interwoven, with some retaining the appearance of devitrification. The melt droplets are presently aligned perpendicular to the direction of compaction, so that the shape of the melt droplets is difficult to ascertain. The droplets are up to 1 cm long, though it is difficult to be certain if this represents the original morphology. Grains of quartz and chert are present as subrounded to angular mm scale clasts in a matrix of melt droplets. Some of the quartz grains have well-preserved PDFs (up to three sets per grain as seen under the optical microscope; Figure 4a), and toasted quartz (e.g., Ferrière et al., 2009) is also present. There are some samples where carbonate replacement has been significant, especially samples PR 11A, B, and C.

While the Pine River core does contain accretionary lapilli, they are petrographically different from those found at the Connors Creek site. The lapilli tend to be much smaller in size, with the largest being only 1 cm, and rarely show evidence of multiple zonation as at the Connors Creek site. However, the mineralogy is similar, with subangular quartz grains and phyllosilicates. The lapilli here appear to be similar to the agglomerated nuclei of the Connors Creek lapilli.

4.4.1.3. Coleraine site

The material from the drill cores at Coleraine is similar in many respects to the material from Pine River, in that the ejecta deposits are bedded and contain mostly ejected melt material rather than the abundant detrital grains observed at the Connors Creek site. The fragments of glass have been replaced by phyllosilicates, chert, and carbonate. Within the beds, occasional rounded chert clasts appear to have deformed the bedded ejecta, and thus would seem to be present prior to diage-

nesis. PDFs in quartz are exceptionally rare at this location; only a single, 70 μm grain of shocked quartz has been confirmed (Figure 4b). The abundant subrounded to angular quartz grains show undulose extinction and in some cases toasting, although these features are not considered diagnostic of impact (French and Koeberl 2010). As at the Pine River site, quartz is a much less significant constituent than the melt droplets (now altered to phyllosilicates). Alternating with beds of melt droplets are mm to cm thick beds of aphanitic material, which in some cases pinch out within the thin section scale, although most seem to be more extensive. This aphanitic material contains some fine-grained quartz grains, and has a general appearance similar to that observed as the matrix of lapilli at the Connors Creek and Pine River sites.

Very well preserved impact spherules are observed at this location. The spherules are observed in the upper portions of the cores, where they are present as 1-2 mm spheroids (Figure 3d). The spherules have complex internal morphologies, with vesicles, quartz inclusions, and layers of different phyllosilicates preserving the original structure of the spherules. Many of the spherules have an outer rim composed of microcrystalline rutile or anatase. Most commonly, the cores of the spherules are finer grained material than the outer edges. It is possible that some of the structures indicate that the spherules originally were hollow.

The melt droplets at Coleraine are more spherical and contained vesicles that are distributed differently than vesicles in melt droplets nearer to the impact site. Closer to the impact structure, at Connors Creek and Pine River, melt droplets tend to be larger and irregularly shaped, and vesicles are distributed randomly in the melt droplets. Vesicles in these glasses tend to be smaller. At the Coleraine site, vesicles tend to be localized in the center of spherical glass droplets.

4.4.2. Major and Trace Element Composition

Major and trace element data are summarized in Table 1; stratigraphic positions of samples are given in Fig. 2. Samples analyzed from Connors Creek fall into the category of either carbonate-poor or carbonate-rich, depending on the amount of calcite present in the samples. The carbonate-poor samples have, on average, 73.8 wt. % SiO_2 , 12.7 wt. % Al_2O_3 , 3.75 wt. % K_2O , 3.65 wt. % Fe_2O_3 (total), 1.93 wt. % MgO , 0.81 wt. % CaO and 0.43 wt. % TiO_2 , and LOI of 2.5 wt. %. This is consistent with petrographic observations, which show that the majority of the unaltered samples are made of sandy quartz with phyllosilicates. There is almost no Na_2O in any of the Connors Creek samples. The carbonate-rich samples from Connors Creek (CC-3, 4, 5, and 6) were found to have, on average, 24.8 wt. % SiO_2 , 8.98 wt. % Al_2O_3 , 2.43 wt. % K_2O , 6.68 wt. % Fe_2O_3 (total), 8.78 wt. % MgO , 20.3 wt. % CaO , and 0.27 wt. % TiO_2 . Notably, these samples had 27.4 wt. % LOI (about 20% calcite). This is also consistent with the petrographic analysis that showed a major amount of carbonate alteration. Carbonate alteration in this case has diluted silica to approximately 1/3 of the abundance observed in other samples. Samples from Pine River have fairly consistent major element chemistry. Through the ejecta layer, there is an average of 47.0 wt. % SiO_2 , 21.1 wt. % Al_2O_3 , 7.49 wt. % K_2O , 4.71 wt. % CaO , 4.13 wt. % MgO , 4.40 wt. % Fe_2O_3 , and 0.90 wt. % TiO_2 . The lesser amount of detrital quartz observed in these samples accounts for the much lower SiO_2 values in these samples as compared to the Connors Creek site. Coleraine samples are slightly different than other sites, with much higher Fe_2O_3 . The average composition is 43.0 wt. % SiO_2 , 26.0 wt. % Fe_2O_3 , 14.6 wt. % Al_2O_3 , 3.80 wt. % K_2O , 3.33 wt. % MnO , and 0.55 wt. % TiO_2 . These samples

represent mostly melt spherules, but the spherules reside in a matrix that is similar in composition to the underlying shales.

Trace element compositions are summarized in Table 1. Ejecta from Connors Creek have Cr values up to 2850 ppm, Ni up to 304 ppm, and very little Co. Vanadium and Ba contents are elevated, although this is similar to samples in the underlying bedded chert formations. The Pine River site has Cr concentrations up to 301 ppm, Ni up to 56 ppm, and up to 11 ppm Co. Vanadium is highly enriched in these samples, with values up to 2280 ppm. Rubidium and Ba contents are also elevated in these samples. The Coleraine site has up to 173 ppm Cr and 172 ppm Ni, the only site measured where the Ni content exceeds that of Cr.

Rare earth elements (REEs) have similar patterns for all samples. The heavy REEs are elevated relative to the light REEs, and all samples seem to have a slightly negative Eu anomaly. The La/Yb ratio of the samples, ranges from 10 to 25 for measured samples, except for one sample from Coleraine, which has anomalously high La. The samples generally contain very little Th and U, although several samples contain > 10 ppm of these elements, with PR 4 having 12.5 ppm Th and 14.1 ppm U, and CR 9-2 having 8.7 ppm Th and 14.8 ppm U.

4.4.3. PGE chemistry

Platinum group element concentrations for each site are summarized in Table 2. The chondrite-normalized values of the PGEs are shown in Figure 5. At the Connors Creek site, PGE abundances are clearly diluted by the presence of a large amount of detrital material, including chert clasts, which carry no PGEs. The maximum Ir concentration measured is 0.33 ppb, with the mini-

mum being indistinguishable from a crustal value of 0.09 ppb. Ruthenium concentrations are also only slightly elevated relative to crustal values, ranging from 0.29 to 0.75 ppb. The Ru/Ir ratio of chondrites is 1.6, and the Ru/Ir ratio of the upper continental crust is 15.5 (Rudnick and Gau 2004). The Ru/Ir ratios of material at Connors Creek range from 1.8 to 4.4. All measured samples show a depression of Rh, with values of 0.04 to 0.37 ppb, which are in some cases below the crustal value of 0.06. The Pt content is much more variable, with the CC2 sample having 0.29 ppb Pt, though all other samples (excluding CC2) have more Pt, ranging from 1.32 to 3.91 ppb. As can be seen in Figure 6, the absolute abundances of the PGEs at the Connors Creek site are lower than either of the other sites. However, the ratios of the elements are clearly comparable to the other sites. The ratios of PGEs are closer to chondritic values than to the intrusive suites in the target rocks (Figure 7).

The Pine River samples show the most consistent elevation of PGEs of the measured ejecta samples, likely because the samples are composed almost entirely of ejected melt material with little locally derived material. Iridium concentrations range from 0.44 to 1.16 ppb in measured samples, and Ru concentrations range from 1.15 up to 2.68 ppb. The Ru/Ir ratio is consistently in the range of 2.2-2.6. All other PGEs are elevated relative to average crustal background (McDonough and Sun 1995), with the contents of Pt ranging from 2.27 ppb to 13.4 ppb and those of Rh ranging from 0.39 to 1.11 ppb. This is the site with the highest abundances of PGEs, and also the site with PGE ratios closest to chondritic.

Coleraine samples are somewhat variable in their PGE concentrations. Iridium values range from 0.19 ppb to 0.91 ppb in measured samples, and Ru concentrations range from 0.50 up to 3.09 ppb. The Ru/Ir ratio falls between 1.6 and 3.4. Platinum values are range between 1.91 and 3.42 ppb, whereas those of Rh values vary from 0.21 to 0.96 ppb.

4.5. Discussion

The Connors Creek, Pine River, and Coleraine sites have distinct characteristics, but these differences primarily reflect the variation in the nature of deposition with increasing distance from the impact. The depositional environment of each of the three sites was a shelf setting (Schulz and Cannon, 2007), and so the differences observed between the sites are taken to be close to representative of the differences that occur due to the change of nature of fallout with distance from the impact. The Chicxulub and Sudbury impact events are similar to each other; the Sudbury impact took place on a shallow marine shelf environment that included carbonates, and both impact structures were of similar size (Kring 1995; Pope et al. 2004). Thus, computational models used to explain emplacement of ejecta from Chicxulub are applicable to discuss ejecta thicknesses at 500, 650, and 980 km from the center of the Sudbury impact structure, where the thicknesses are approximately 2.3 m, 1.07 m, and 0.30 m, respectively. A model of ejecta thickness for the Chicxulub impact event was presented in Artemieva and Morgan (2009). This model shows that ballistic sedimentation alone is inadequate to explain the full thickness of ejecta at various distances from the site of the impact event. A combination of three mechanisms has been used to explain the observations of ejecta thickness from the Chicxulub impact: 1) ballistic emplacement, 2) turbulent motion within an expanding impact plume, and 3) atmospheric dispersal during re-entry of ejecta. In addition to these factors, post-depositional processes, such as reworking through wave activity and mass wasting provide mechanisms to explain the distribution of ejecta.

4.5.1. Comparison of petrography

Each site contains a significant component of melt droplets (less abundant at the Connors Creek site), which may originally have been in the form of microkrystites, microtektites, or possibly as disaggregated melt particles. They are now altered to phyllosilicates with original textures still visible in many cases. The melt droplets constitute an important component of the overall ejecta material at each location, although the Connors Creek site has abundant detrital material, whereas the Pine River and Coleraine sites are composed almost entirely of melt droplets. There are obvious petrographic similarities between the melts at each location: each site contains droplets with vesicles in the size range of 1-2 mm in diameter. The Connors Creek site also has > 1 m thick cross-beds of accretionary lapilli at the top of the deposit; much smaller-scale cross-beds (i.e., 1 cm amplitude) are observed at the Pine River site. Cross bedding is not observed in the Coleraine cores. The cross-bedding is suggestive of wave activity taking place soon after deposition of the ejecta. There has been some debate about the depth of water at the site of the Sudbury impact, with authors suggesting anywhere from a subaerial impact to an impact into deep ocean water (e.g., Cannon et al. 2010). The ejecta deposits are consistent with the impact event taking place in relatively shallow water, such as a shelf deposit. This could potentially generate wave activity akin to the well-studied Chesapeake Bay impact structure (Dypvik 2003), which has been shown to result in tsunamis along the shelf that would be sufficient to disturb the newly deposited beds (such activity would additionally depend on the geometry of the coastline relative to the impact site). Impact-generated tsunamis dampen more quickly than tectonic tsunamis (Van Dorn 1961), which is consistent with major wave activity observed at 500 km from the impact and greatly reduced wave activity observed 1000 km from the

impact (although this also depends on water depth, which is difficult to determine). Another possible explanation for the difference in reworking of material is that large blocks (observed up to 8 m in diameter at some ejecta locations; see Addison et al. 2010), which were likely ballistically emplaced, may have generated additional wave activity near the Connors Creek site, while these blocks are largely absent at greater distances from the impact.

Few shocked quartz grains were found in any of the sites observed in this study. The Connors Creek site has shocked quartz within accretionary lapilli. Most of the quartz grains at the Connors Creek site were probably derived locally. The Pine River site has a comparatively high percentage of shocked quartz mixed with the melt droplets. Only one shocked quartz grain was observed at the Coleraine site. The reason for this variation is likely explained by the mechanisms of deposition (see below).

The model of Artemieva and Morgan (2009) predicts that downrange ballistic emplacement will result in about 1 m of ejecta at 500 km, about 20 cm of ejecta at 650 km, and about 10 cm of ejecta at 1000 km for the Chicxulub impact event, which can be taken as a minimum thickness for the somewhat larger Sudbury impact event (the two impact events have been considered by several authors to represent energy release of similar order of magnitude; e.g., Pope et al. 2004; Grieve and Therriault 2000). This model reasonably accounts, at least to an order of magnitude, for the observed thicknesses at Connors Creek and Coleraine, but does not predict the thickness of ejecta at the Pine River site. The present day thickness of the Pine River site is about 1 m, though this does not account for the compaction that generated stylolites in the section. The core does not show clear evidence of reworking, although this cannot be fully ruled out as a possibility. More likely is that other processes created a local maximum in ejecta thickness, due to the turbulent nature of re-entry

by ejecta that traveled above the atmosphere. It is important to note that the topography of the depositional environment was not likely to be smooth; rather, troughs and rises were undoubtedly present. Because of that, the depositional environment could differ significantly even along relatively short distances; e.g., the McLure site, located just 10 km from the Connors Creek site, is up to 40 m thick and lacks the clear stratification that is present at the Connors Creek site (Cannon et al. 2010).

4.5.2. Mineralogical and geochemical composition

The mineralogy of the melt droplets at various sites is fairly consistent, ranging from Si-rich phyllosilicates to Si-poor biotite and phlogopite, which likely reflects similar original compositions. Such phyllosilicates are typical of altered impact glass, and similar compositions have been found at Chicxulub (Koeberl 1993), in the Alamo Breccia (Morrow and Harris 2005), and in Archean spherules (Simonson et al. 2009; Hassler et al. 2011). Only the most refractory elements are expected to be immobile. The major element chemistry of the phyllosilicates is most likely entirely secondary, although it is suggestive of reducing conditions during diagenesis (Duchac and Hanor 1987). The Pine River site contains higher abundances of Al_2O_3 compared to the other sites (excepting the carbonate-altered PR 10, 11A, 11B, and 11C); this is probably a result of the high phyllosilicate abundance of the Pine River site (and sample CR 9-2). The depletion of Na_2O in samples is likely the result of mobilization after deposition.

The ubiquitous rutile and anatase observed in the melt droplets reveal the thermal history of the samples. Although several dozen Ti phases were examined by Raman spectrometry, all were found to be either anatase or rutile. The transition point between rutile and anatase at low pressures

is 500-600°C (Dachille et al. 1968), which is taken as a temperature of crystallization in this case, as there was insufficient Zr observed to use as a geothermometer. As rutile and anatase are observed at all of the ejecta sites and none of the sites experienced high peak metamorphic temperatures, it is likely that these phases formed as the melt droplets were cooling. It should be noted that Ti phases are always observed in the interior of the melt droplets and never in the groundmass or matrix, showing that the enrichment of Ti is from the impact melt rather than intrinsic to the host rock.

Using the classification system of Winchester and Floyd (1977), which was previously applied to the Onaping formation (Ames et al. 2002), the ejecta are shown to have compositions ranging from andesite to dacite to trachyandesite, with some samples having alkaline basaltic ratios on the Zr/TiO₂ versus Nb/Y plot (Figure 8). This compares favorably with the Onaping formation, and previously measured Sudbury ejecta (Cannon et al. 2010) which has andesitic and dacitic compositions. Similarly, the Zr/TiO₂ ratio can be reasonably explained as an average composition of the norites, mafic norites, and granophyres of the SIC (Figure 9).

4.5.3. PGE Chemistry

Previous attempts to determine the impactor composition at Sudbury have been unsuccessful (i.e., Morgan et al. 2002). The Sudbury structure itself contains elevated PGE contents because of fractionation of the impact melt sheet that concentrated both terrestrial and meteoritic PGEs in the SIC. The impact ejecta, however, experienced no such concentration of PGEs, and the strongest signal of PGE should be from the impactor. The previous attempt to determine the PGE content of

the ejecta (Pufahl et al. 2007) made no attempt to constrain the impactor type, except in concluding that the impactor was a meteorite rather than a comet.

This study finds that all sites have elevated Ir abundances and have elemental ratios much closer to chondritic values than to terrestrial ones. For example Ru/Ir ratios average ~2.5; closer to chondritic ratios that cluster between 1.4-1.6, rather than average crust which typically has Ru/Ir >10 (Figure 6). The highest ratios of Cr/Ni are observed in samples from the Pine River site. Figure 7 shows that Ru and Rh correlate most strongly with Ir. Although Pt and Pd correlate with Ir, there is a weaker correlation, probably indicating addition of these elements from the PGE-rich ores that were affected by the impact, such as the East Bull Lake Suite deposits (Vogel et al. 1998; James et al. 2002). The abundances of the PGEs are much lower in these samples than many other impact melts (i.e., McDonald et al. 2001; McDonald 2002; Tagle and Claeys 2005), which seriously complicates the task of identifying the impactor group. The ejecta appears to have a small chondritic component, as many of the elemental ratios involving PGE with high condensation temperatures and low crustal abundances are near to the chondritic values (Figure 7). Achondrites seem unlikely to generate such PGE enrichments, as they are typically Ir-depleted (i.e., Laul et al. 1972). However, distinguishing between an asteroid and a comet on the basis of PGEs is problematic, as the abundances of nonvolatile elements in comets is largely unknown (Tagle and Hecht 2006), and studies of grains of comet Wild 2 from the Stardust mission reveal that the Cr/Ni ratios of the comet are approximately chondritic (Lanzirotti et al., 2008). Although Pufahl et al. (2007) claimed that the “geochemical contrasts” found in the ejecta are sufficient to rule out a comet, the authors did not provide any details of how this conclusion was reached. The geochemical evidence favors a chondritic impactor, but does not unequivocally rule out a cometary impactor. However, the impact record on

Earth suggests that cometary impactors are significantly less common than asteroidal ones (Koeberl et al. 2012).

This study bears similar results to previous studies of ejecta from the Sudbury impact. The Cr/Ni ratio of the deposits is in line with analyses from Cannon et al. (2010) (Figure 10), although abundances of both elements are significantly higher in this study. The data are also consistent with previous measurements from the Onaping Fm (Mungall et al. 2004). In addition to the Cr/Ni ratios, the Ni/Ir ratios of the ejecta deposits are consistent with measurements from the Onaping Fm, although samples from Pine River and Coleraine may have a slightly higher contribution from the impactor than the Onaping Formation (Mungall et al. 2004) (Figure 11). The ejecta deposits at all sites appear to have less Ni than the Onaping Fm, which is likely associated with carbonate alteration (as reported in Pufahl et al., 2007).

To determine the contribution of the impactor to the ejecta composition, the HMX mixing model (Stöckelmann and Reimold 1989) was used to determine the contributions necessary from the Sudbury area mafic intrusions and the impactor. The background composition of the Rove shale that underlies the Sudbury ejecta in the Pine River drill core was used as minimum values, and sample PR 5 was used for model values. As an approximation of the original impactor, a CI chondritic composition (McDonough and Sun 1995) was used for the impactor source, while the Agnew intrusion, part of the East Bull Lake intrusions, was used as representative of the mafic composition, based on the presence of these intrusions in the impact basin and their relatively high concentration of PGEs (average of 0.2 ppb Ir, 0.5 ppb Ru, 17.9 ppb Pt, 19.2 ppb Pd, 1.46 ppb Au, 159.3 ppm Cr, 41.8 ppm Co, and 137.8 ppm Ni) (Vogel et al. 1998). The Agnew intrusion is located 70 km to the west of the SIC. In addition, upper crustal values (Rudnick and Gao 2004) were used.

The HMX model was attempted with contributions from the Rove shale, East Bull Lake intrusions, upper crustal values, and CI chondrite. The results were inconclusive, however, after multiple trials, a consistent contribution of approximately 0.2 wt. % CI chondrite closely was found to be necessary for the abundances of Ir, Ru and Rh in the ejecta (Figure 12). This is also consistent with algebraic mixing models, and a similar amount of CI contribution can be seen in Figure 11. Other chondritic groups, such as ordinary chondrites, produce similar results.

4.5.4. Interpretation of depositional mechanisms

Observations of continuous ejecta blankets from impact craters on planetary bodies show that they tend to extend approximately 1-2 crater radii from the crater rim (Melosh 1989). In the case of the Sudbury impact event, it is difficult to determine what distance this would actually correlate to because of the large disagreements between various researchers on 1) the size of the Sudbury event itself (e.g., Mungall et al. 2004); 2) the location of the SIC within the original Sudbury structure, with some authors arguing that the SIC represents the center of the structure, while other argue that it represents the rim of the structure (e.g., Grieve and Therriault 2000); and 3) continuous ejecta blankets from large impacts on Earth are only understood from a small number of impacts (e.g., Pope et al. 1999; Osinski et al. 2005). While previous authors have suggested that the continuous ejecta blanket from the Sudbury event may have been close to this distance (Pufahl et al. 2007), this is difficult to ascertain with certainty. If the center of the SIC is taken to represent approximately the location of the center of the Sudbury impact crater, and the crater had a diameter of 200 km, then the continuous ejecta blanket should extend about 500 km from the center of the SIC. This would mean

that the Connors Creek site would be just outside of the continuous ejecta blanket. If the SIC holds the location of the western edge of the original crater, however, then the site should be well outside of the continuous ejecta blanket. The thicknesses of the ejecta seem to correspond more closely to models of distal ejecta than to models of the continuous ejecta blanket (see below), which suggests that the sites can be considered to sample three distances within the discontinuous ejecta blanket.

The deposition of ejecta at the Connors Creek site, 500 km from the SIC, shows a complex depositional history. The melt droplets are mixed with large (at least 20 cm diameter) clasts of locally derived chert (or possibly other compositions that have altered to chert), and the sand bearing the melt droplets is mostly unshocked, suggesting that this material was locally derived. The same is true at the Sudbury ejecta sites that contain megabreccias, where the megaclasts were not derived from the impact crater (not documented in this paper, see Addison et al. 2010), but are locally derived. A base surge has been proposed to explain deposition of the Sudbury ejecta (Addison et al. 2010), though it is unclear exactly how such a process should operate. A somewhat similar process has been proposed to explain the Stac Fada ejecta deposit (Branney and Brown, 2011). In the Branney and Brown (2011) model, the impact generates a deposit identical to a volcanic pyroclastic density current (PDC), which propagates along the ground surface. In this model, the melt droplets mixed with the unshocked sands would represent the lowermost part of the base surge. This model also accounts for the late deposition of accretionary lapilli, which would not settle out of the plume until late in the depositional event. The alternative model for deposition of the Connors Creek ejecta is that it was ballistically emplaced and then reworked (Cannon et al. 2010). Because the accretionary lapilli observed at the Connors Creek site are not well mixed with the melt-bearing sands, the authors consider it unlikely that the entire package was reworked. However, the lapilli at the top of

the outcrop are cross-bedded, which almost certainly represents reworking due to late wave activity (which may or may not be directly related to impact effects).

Modeled ballistic emplacement of ejecta at the Pine River site, 650 km from the impact, accounts for only about 25% of the observed thickness of 80 cm. Of course, the numerical model does not predict fine-scale deposits, although a factor of 4-5 difference from the modeled value may require explanation. It is unlikely that the deposit has been completely reworked, since the accretionary lapilli only occur in a discrete layer, although like the Connors Creek site, there appears to have been wave activity forming channels in the sediments above the lapilli layer. Additionally, almost all of the material in the Pine River deposit is derived from the impact. The smaller accretionary lapilli found at this site as opposed to the ones observed at the Connors Creek site are likely due to the greater travel distance to the site allowing for heavier particles to already have been deposited before reaching this distance.

Finally, the thickness of ejecta at the Coleraine site can be accounted for entirely by ballistic emplacement of melt spherules. The thickness is approximately the same as predicted by ballistic emplacement. The lack of accretionary lapilli or any significant impact indicators can be accounted for by dispersal of the dense accumulations of particles that would result in the formation of accretionary clasts. The model of Artemieva and Morgan (2009) predicts a low ejection velocity of basement material, so that at 1000 km from the site of impact, materials are only emplaced ballistically. This could explain not only the greater proportion of melt spherules at this site, but also the dearth of observed shocked quartz grains, which would be less likely to travel to such distances.

Melt droplet properties change somewhat with distance from the impact location, with regard to the overall shape of the glasses and the vesicles within them. Ejecta deposited at the Coleraine

site, being farthest from the site of impact, would have had more time for vesicles to coalesce before being quenched, resulting in the single vesicle that they are observed to have. In contrast, ejecta at the nearer Connors Creek and Pine River sites would have had lower ejection velocity (for the same ejection angle) and thus vesicles would be less likely to coalesce due to shorter flight times before quenching. The trace element chemistry of the melts seems to be consistent between these sites. The ejecta reflect the composition of the target material at the Sudbury site, and they share many similarities with the Onaping formation in terms of the geochemical and petrographic similarity (Figures 8-11; Cannon et. al. 2010), with armored clasts in the Sandcherry member of the Onaping formation closely resembling the accretionary lapilli observed at the Connors Creek and Pine River sites.

Curiously, the thicknesses modeled by Artemieva and Morgan (2009) are for the downrange direction from the Chicxulub impact. In all other directions, ejecta thicknesses would be less. Ejecta have only been described in one vector from the Sudbury impact, but the ejecta thickness seems to be roughly (at least in an order-of-magnitude scale) in line with predictions of the model. Therefore, either the ejecta deposits that have been found are in the downrange direction from the impact (i.e., $<45^\circ$ from the path of the impactor), or the energy released during the Sudbury impact event was much larger than the Chicxulub impact event.

4.6. Summary and Conclusions

The Connors Creek (ca. 500 km from the SIC), Pine River (ca. 650 km from the SIC), and Coleraine (ca. 980 km from the SIC) sites, which each contain ejecta from the Sudbury impact, have been investigated to determine petrographic and geochemical properties. The Connors Creek site

consists of chert overlain by ejecta-bearing breccia with melt droplets, which is overlain by cross-bedded accretionary lapilli. The Pine River drill core records approximately 1 m of material deposited as a result of the Sudbury impact event, primarily consisting of mm-scale melt droplets, with a thin layer of small accretionary lapilli that is overlain by cross-bedded sediments that contain melt droplets. The Coleraine site contains approximately 20 cm of impact melt spherules with very little breccia or locally derived materials. The melt droplets at each of the sites have been altered to phyllosilicates. Each of the sites contains some amount of shocked quartz, although at the Connors Creek site the shocked quartz is only observed inside of accretionary lapilli. The Pine River site contains shocked quartz mixed with the melt droplets. The Coleraine site contains very little shocked quartz, with only one grain identified.

The PGE abundances of samples from each of the sites are elevated above the background abundances expected for typical upper continental crust. The maximum observed Ir abundance is 1.16 ppb Ir, which is the highest abundance yet observed in Sudbury ejecta. The Ru/Ir, Rh/Ru, and Pt/Ir ratios are consistent with contribution from a chondritic source, but the small extraterrestrial component does not allow for reliable identification of the impactor amongst the different potential chondritic groups. By modeling the PGE abundances in the Rove formation that hosts the ejecta as compared to the elevated PGEs in the ejecta deposits, a contribution of 0.2 wt. % chondritic impactor was found.

The ejecta deposits appear to have been deposited by primarily ballistic emplacement, with some atmospheric disturbances. Based on the thicknesses of the ejecta compared to previously performed models of ejecta thickness from a large impact event, the ejecta likely have been deposited in the downrange direction from the Sudbury impact event.

Acknowledgments:

The authors wish to acknowledge the great assistance offered by William Cannon (retired; USGS), Klaus Schulz (USGS), William Addison, Greg Brumpton, Mark Severson (Natural Resource Research Institution), David Kring (Lunar and Planetary Institute), Ludovic Ferriere (Natural History Museum, Vienna), Natasha Artemieva (Planetary Science Institute), and the many others who contributed to this project. Funding is provided by the University of Vienna doctoral school IK-1045 and Austrian Science Foundation grant P21821-N19.

4.7. References

- Addison, W.D., Brumpton, G. R., Vallini, D. A., McNaughton, N. J., Davis, D. W., Kissin, S. A., Fralick, P. W., and Hammond, A. L. 2005. Discovery of distal ejecta from the 1850 Ma Sudbury impact event. *Geology* 33:193-196.
- Addison, W. D. Brumpton, G. R., Davis, D. W., Fralick, P. W., and Kissin, S. A. 2010. Debrisites from the Sudbury impact event in Ontario, north of Lake Superior, and a new age constraint: Are they base-surge deposits or tsunami deposits? in Gibson, R. L. Reimold, W. U., *Large Meteorite Impacts and Planetary Evolution IV*, Geological Society of America Special Papers 465, 465:245-268.
- Ames, D. E., Golightly, J. P., Lightfoot, P. C., and Gibson, H. L. 2002. Vitric compositions in the Onaping Formation and their relationship to the Sudbury Igneous Complex, Sudbury Structure. *Economic Geology* 97:1541-1562.

-
- Artemieva, N., and Morgan, J. 2009. Modeling the formation of the K-Pg boundary layer. *Icarus* 201:768-780.
- Branney, M.J., and Brown, R.J. 2011. Impactoclastic density current emplacement of terrestrial meteorite-impact ejecta and the formation of dust pellets and accretionary lapilli: evidence from Stac Fada, Scotland. *Journal of Geology* 119:275-292.
- Bray, J.G., and Geological Staff. 1966. Shatter cones at Sudbury. *Journal of Geology* 74:243-245.
- Cannon, W. F., Schulz, K. J., Horton, J. W., Jr., and Kring, D. A. 2010. The Sudbury impact layer in the Paleoproterozoic Iron Ranges of Northern Michigan, USA. *Geological Society of America Bulletin* 122:50-75.
- Cohen, A. S., Burnham, O. M., Hawkesworth, C. J., and Lightfoot, P. C. 2000. Pre-emplacment Re-Os ages from ultramafic inclusions in the sublayer of the Sudbury Igneous Complex, Ontario. *Chemical Geology* 165:37-46.
- Dachille, F., Simons, P., and Roy, R. 1968. Pressure-temperature studies of anatase, brookite, rutile, and TiO₂-2. *American Mineralogist* 53:1929-1939.
- Darling, J. R., Hawkesworth, C. J., Storey, C. D., and Lightfoot, P. C. 2010. Shallow impact: Isotopic insights into crustal contributions to the Sudbury impact melt sheet. *Geochimica et Cosmochimica Acta* 74:5680-5696.
- Davis, D.W. 2008. Sub-million year age resolution of Precambrian igneous events by thermal extraction-thermal ionization mass spectrometer Pb dating of zircon: Application to crystallization of the Sudbury impact melt sheet. *Geology* 36:383-386.

- Deutsch, A., Grieve, R.A.F., Avermann, M., Bischoff, L., Brockmeyer, P., Buhl, D., Lakomy, R., Muller-Mohr, V., Ostermann, M., and Stoffler, D. 1995. The Sudbury structure (Ontario, Canada): A tectonically deformed multi-ring impact basin. *Geologische Rundschau* 84:697-709.
- Dickin, A. P., Artan M. A., and Crocket, J. H. 1996. Isotopic evidence for distinct crustal sources of North and South Range Ores, Sudbury Igneous Complex. *Geochimica et Cosmochimica Acta* 60:1605-1613.
- Djon, M. L. N. and Barnes, S. J. 2012. Changes in sulfides and platinum-group minerals with the degree of alteration in the Roby, Twilight, and High Grade Zones of the Lac des Iles Complex, Ontario, Canada. *Mineralium Deposita* 47:875-896.
- Dressler, B.O. 1984. General geology of the Sudbury area. In Pye, E.G., Naldrett, A.J., Giblin, P.E. (Eds.), *The Geology and Ore Deposits of the Sudbury Structure*. Ontario Geological Survey Special Vol. 1:57-82.
- Duchac, K., and Hanor, J. 1987. Origin and timing of the metasomatic silicification of an early Archean komatiite sequence, Barberton Mountain Land, South-Africa. *Precambrian Research* 37:125-146.
- Dypvik, H., and Jansa, L.F. 2003. Sedimentary signatures and processes during marine bolide impacts: a review. *Sedimentary Geology* 161:309-337.
- Fedorowich, J. S., Rousell, D. H., and Peredery, W. V. 1999. Sudbury breccia distribution and orientation in an embayment environment. in Dressler, B.O., and Sharpton, V.L., eds., *Large*

meteorite impacts and planetary evolution II, Geological Society of America Special Paper 339:305-315.

- Fèrriere, L., Morrow, J.R., Amgaa, T., and Koeberl, C. 2009. Systematic study of universal-stage measurements of planar deformation features in shocked quartz: Implications for statistical significance and representation of results. *Meteoritics and Planetary Science* 44:925-940.
- French, B. M. 1970. Possible relations between meteorite impact and igneous petrogenesis, as indicated by the Sudbury Structure, Ontario, Canada. *Bulletin Volcanologique* 34:446-517.
- French, B. M., and Koeberl, C. 2010. The convincing identification of terrestrial meteorite impact structures: What works, what doesn't, and why. *Earth-Science Reviews* 98:123-170.
- Govindaraju K. 1994. Compilation of working values and samples description for 383 geostandards. *Geostandards Newsletter*, 18: 1-158.
- Grieve, R. A. F., and Theriault, A. 2000. Vredefort, Sudbury, Chicxulub: Three of a kind? *Annual Review of Earth and Planetary Science* 28:305-338.
- Grieve, R. A. F., Stöffler, D., and Deutsch, A. 1991. The Sudbury Structure – controversial or misunderstood. *Journal of Geophysical Research – Planets* 96:22753-22764.
- Grieve, R. A. F., Ames, D. E., Morgan, J. V., and Artemieva, N. 2010. The evolution of the Onaping Formation at the Sudbury Impact Structure. *Meteoritics and Planetary Science* 45:759-782.
- Hassler, S.W., Simonson, B.M., Sumner, D.Y., and Bodin, L. 2011. Paraburdoo spherule layer (Hammersley Basin, Western Australia): Distal ejecta from a fourth large impact near the Archean-Proterozoic boundary. *Geology* 39:307-310.

-
- Huber H., Koeberl C., McDonald I., and Reimold W.U. 2001. Geochemistry and petrology of Witwatersrand and Dwyka diamictites from South Africa: search for an extraterrestrial component. *Geochimica et Cosmochimica Acta* 65: 2007-2016.
- Ivanov, B. A. 2005. Numerical modeling of the largest terrestrial meteorite craters. *Solar System Research* 39:381-409.
- Ivanov, B., and Deutsch, A. 1999. Sudbury impact event: Cratering mechanics and thermal history, in Dressler, B.O., and Sharpton, V.L., eds., *Large meteorite impacts and planetary evolution II*, Geological Society of America Special Paper 339:389-397.
- James, R. S., Easton, R. M., Peck, D. C. and Hrominchuk, J. L., 2002. The East Bull Lake Intrusive Suite: Remnants of a ~2.48 Ga Large Igneous and Metallogenic Province in the Sudbury Area of the Canadian Shield. *Economic Geology*, 97: 1577-1606.
- Koeberl, C. 1993. Chicxulub crater, Yucatan - Tektites, impact glasses, and the geochemistry of target rocks and breccias. *Geology* 21:211-214.
- Koeberl, C., and Shirey, S. B. 1997. Re-Os systematics as a diagnostic tool for the study of impact craters and distal ejecta. *Palaeogeography, Palaeoclimatology, Palaeoecology* 132:25-46.
- Kring, D. 1995. The dimensions of the Chicxulub impact crater and impact melt sheet, *Journal of Geophysical Research-Planets* 100:16979-16986.
- Lanzirotti, A., Sutton, S.R., Flynn, G.J., Newville, A., and Rao, W. 2008. Chemical composition and heterogeneity of Wild 2 cometary particles determined by synchrotron X-ray fluorescence. *Meteoritics and Planetary Science* 43:187-213.

- Laul, J.C., Keays, R.R., Ganapathy, R., Anders, E., and Morgan, J.W. 1972. Chemical fractionations in meteorites: V, volatile and siderophile elements in achondrites and ocean ridge basalts. *Geochimica et Cosmochimica Acta* 36:329-345.
- Mader, D., and Koeberl, C. 2009. Using instrumental neutron activation analysis for geochemical analyses of terrestrial impact structures: Current analytical procedures at the University of Vienna Geochemistry Activation Analysis Laboratory. *Applied Radiation and Isotopes* 67:2100-2103.
- McDonald, I., Andreoli, M.A.G., Hart, R.J., and Tredoux, M. 2001. Platinum-group elements in the Morokweng impact structure, South Africa: Evidence for the impact of a large ordinary chondrite projectile at the Jurassic-Cretaceous boundary. *Geochimica et Cosmochimica Acta* 65:299-309.
- McDonald I and Viljoen K.S. 2006. Platinum-group element geochemistry of mantle eclogites: a reconnaissance study of xenoliths from the Orapa kimberlite, Botswana. *Appl. Earth Science (Trans. Inst. Min. Metall. B)*, 115: B81-93.
- McDonald, I., Peucker-Ehrenbrink, B., Coney, L., Ferriere, L., Reimold, W. U., and Koeberl, C. 2007. Search for a meteoritic component in drill cores from the Bosumtwi impact structure, Ghana: Platinum group element contents and osmium isotopic characteristics. *Meteoritics and Planetary Science* 42:743-753.
- McDonough, W. and Sun, S. 1995. The composition of the Earth. *Chemical Geology* 120:223-253.

- Meisel T., and Moser J. 2004. Reference materials for geochemical PGE analysis: new analytical data for Ru, Rh, Pd, Os, Ir, Pt and Re by isotope dilution ICP-MS in 11 geological reference materials. *Chemical Geology*, 208: 319-338.
- Morgan, J. W., Walker, R. J., Horan, M. F., Beary, E. S., and Naldrett, A. J. 2002. Pt-190-Os-186 and Re-187-Os-187 systematics of the Sudbury Igneous Complex, Ontario. *Geochimica et Cosmochimica Acta* 66:273-290.
- Morrow, J. R., and Harris, A. G. 2005. Late Devonian Alamo Impact, southern Nevada, USA: Evidence of size, marine site, and widespread effects. *in* Kenkmann, T., Hörz, F., and Deutsch, A., eds., Large meteorite impacts III, Geological Society of America Special Paper 384:259-280.
- Mungall, J. E., Ames, D. E., and Hanley, J. J. 2004. Geochemical evidence from the Sudbury structure for crustal redistribution by large bolide impacts. *Nature* 429:546-548.
- Osinski, G. R., Spray, J. G., Lee, P. 2005. Impactites of the Houghton structure, Devon Island, Canadian High Arctic. *Meteoritics and Planetary Science* 40:1789-1812.
- Pearson D.G., and Woodland S.J. 2000. Solvent extraction/cation exchange separation and determination of PGEs (Os, Ir, Pt, Pd, Ru) and Re-Os isotopes in geological samples by isotope dilution ICP-MS. *Chemical Geology*, 165: 87-107.
- Peck, D. C., Keays, R. R., James, R. S., Chubb, P. T. and Reeves, S. J., 2001. Controls on the Formation of Contact-Type Platinum-Group Element Mineralization in the East Bull Lake Intrusion. *Economic Geology*, 96: 559-581.

-
- Piercey, P., Schneider, D. A., Holm, D. K. 2007. Geochronology of Proterozoic metamorphism in the deformed Southern Province, northern Lake Huron region, Canada. *Precambrian Research* 157:127-143.
- Pope, K. O., Ocampo, A. C., Fischer, A. G., Alvarez, W., Fouke, B. W., Webster, C. L., Vega, F. J., Smit, J., Fritsche, A. E., Claeys, P. 1999. Chicxulub impact ejecta from Albion Island, Belize. *Earth and Planetary Science Letters* 170:351-364.
- Pope, K. O., Kieffer, S. W., and Ames, D. E. 2004. Empirical and theoretical comparisons of the Chicxulub and Sudbury impact structures. *Meteoritics and Planetary Science* 39:97-116.
- Pufahl, P. K., Hiatt, E. E., Stanley, C. R., Morrow, J. R., Nelson, G. J., and Edwards, C. T. 2007. Physical and chemical evidence of the 1850 Ma Sudbury impact event in the Baraga Group, Michigan. *Geology* 35:827-830.
- Rousell, D.H., Fedorowich, J.S., and Dressler, B.O. 2003. Sudbury Breccia (Canada): a product of the 1850 Ma Sudbury event and host to footwall Cu-Ni-PGE deposits. *Earth-Science Reviews* 60:147-174.
- Schulz, J. K., and Cannon, W. F. 2007. The Penokean orogeny in the Lake Superior Region. *Precambrian Research* 157:4-25.
- Simonson B.M., McDonald I., Shukolyukov A., Koeberl C., Reimold U.W., and Lugmair G. 2009. Geochemistry of 2.63–2.49 Ga impact spherule layers and implications for stratigraphic correlations and impact processes. *Precambrian Research* 175: 51-76.

- Stöckelmann, D., and Reimold, W.U. The HMX Mixing Calculation Program. *Mathematical Geology* 21:853-861.
- Szabo, E., and Halls, H.C. 2006. Deformation of the Sudbury Structure: Paleomagnetic evidence from the Sudbury breccia. *Precambrian Research* 150:27-48.
- Tagle, R. and Hecht, L. 2006. Geochemical identification of projectiles in impact rocks. *Meteoritics and Planetary Science* 41:1721-1735
- Tredoux M., and McDonald I. 1996. Komatiite WITS-1, low concentration noble metal standard for the analysis of unmineralised samples. *Geostandards Newsletter*, 20: 267-276.
- Van Dorn, W.G. 1961. Some characteristics of surface gravity waves in the sea produced by nuclear explosions. *Journal of Geophysical Research* 66:3845-3862.
- Vogel, D. C., James, R. S. and Keays, R. R. 1998. The early tectono-magmatic evolution of the Southern Province: Implications from the Agnew Intrusion, Central Ontario, Canada. *Canadian Journal of Earth Sciences* 35:854-870.
- Winchester, J. and Floyd, P. 1977. Geochemical discrimination of different magma series and their differentiation products using immobile elements. *Chemical Geology* 20:325-343.

4.8. Appendix

Specific locations of samples:

The two Connors Creek sites are located at N 46° 37' 46.33", W 87° 50' 50.84" and N 46° 37' 48.50", W 87° 50' 50.36". The Pine River drill core was drilled at N 48° 03' 24", W 89° 30' 48". At Coleraine, there are four drill cores: DL 20009 located at 47° 18' 59.68" N, 93° 20' 09.68" W; DL 20018 located at 47° 19' 06.10" N, 93° 20' 46.17" W; DL 20021 located at 47° 19' 17.13" N, 93° 20' 12.37" W; and DL 20030 located at 47° 18' 49.70" N, 93° 21' 25.47" W. The Pine River core was sampled from a depth of 695.86 m to 691.4 m. Core DL 20009 was sampled from 116.9 m to 117.5 m depth; DL 20018 was sampled from 70.6 m to 70.7 m depth; DL 20021 was sampled from 66.3 m to 66.4 m depth; DL 20030 was sampled from 114.2 m to 114.8 m depth.

Figures

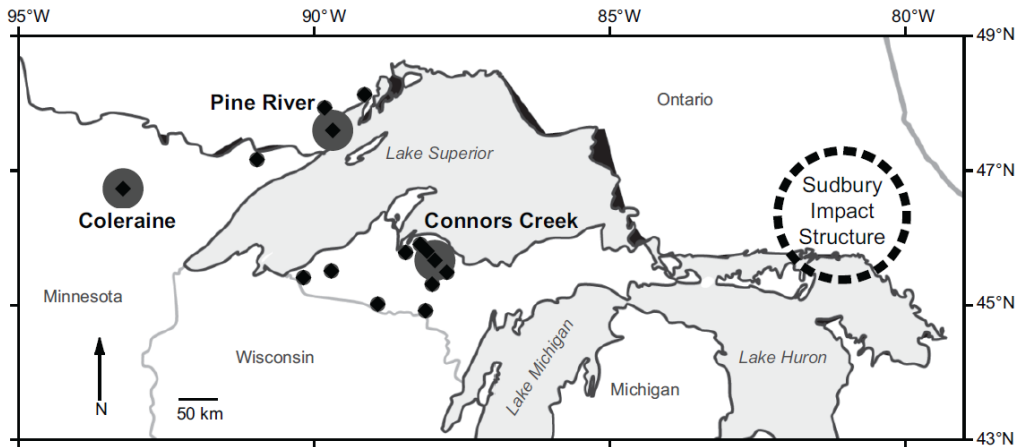


Figure 1. General map showing the locations of the three Sudbury ejecta sites that have been documented and investigated in this study (grey halos): the Connors Creek, Pine River, and Coleraine sites.

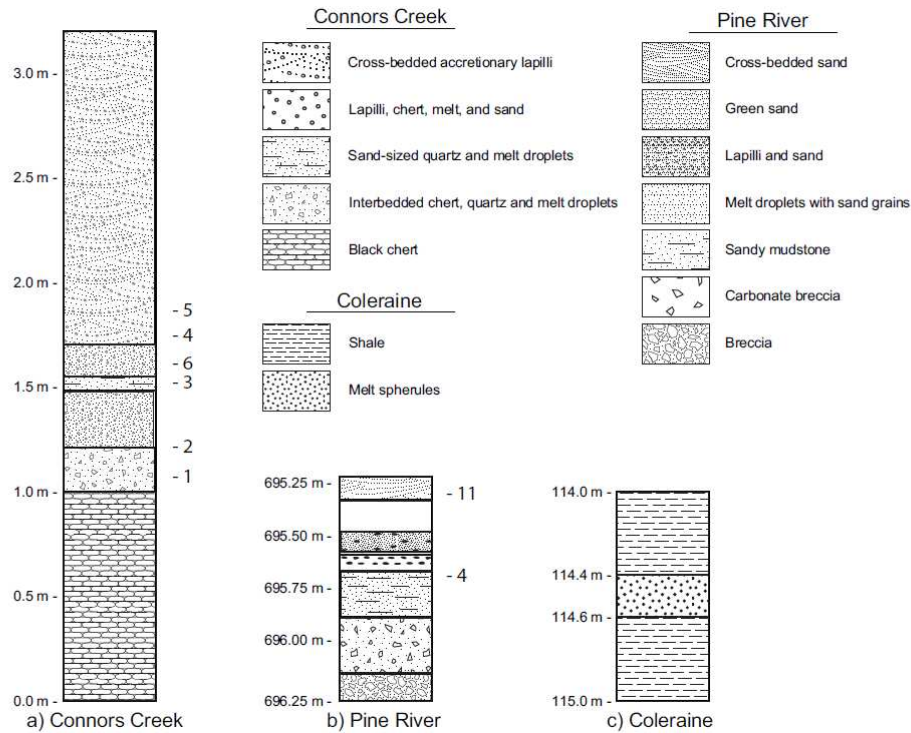


Figure 2. A) Stratigraphic column of the Connors creek site showing the visible outcrop at Site 1. Height above ground level is indicated. Approximate stratigraphic position of samples is indicated to the right of the column. B) Stratigraphic column of the Pine River drill core showing the ejecta-bearing interval. Depth in drill core indicated. Stratigraphic position of samples PR-4 and PR-11 are indicated; other samples are spaced evenly between these samples, with consecutive numbering. C) Simplified stratigraphic column of DL 20009 drill core; each of the Coleraine drill cores has similar expression in drill cores. Depth in drill core indicated.

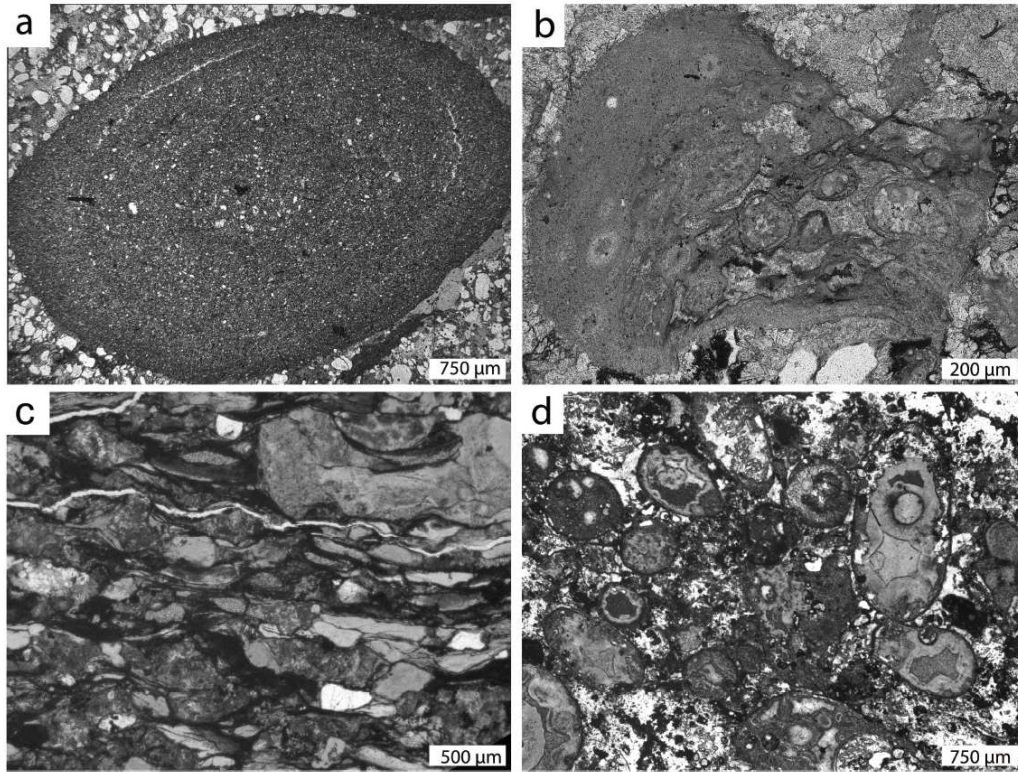


Figure 3. Thin section plane-polarized light photomicrographs; a) Accretionary lapillus from 2.0 m above the base of the Connors Creek site, showing distinct layering, a core, and quartz crystals entrained in the lapillus. b) Melt droplet from 1.4 m above the base of the Connors Creek site with irregular morphology and vesicles. c) Melt droplets from the Pine River core at 695.6 m depth. The majority of the grains in the Pine River drill core are altered melt droplets. d) Melt spherules from the Coleraine core DL 20009 at 117.2 m depth. The majority of the ejecta at the Coleraine site are melt spherules. Note the large, central vesicles that differ from those found in melt droplets at the nearer Connors Creek site.

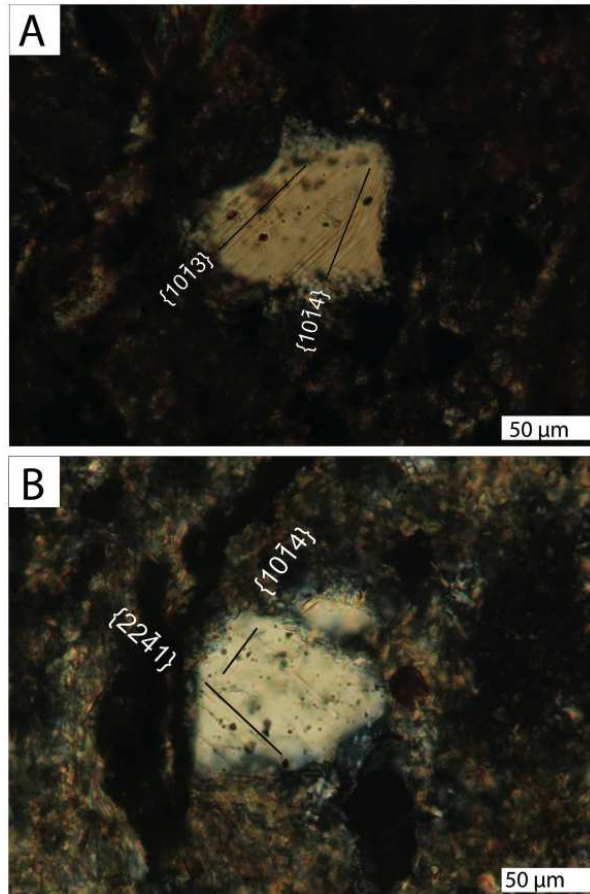


Figure 4. Planar deformation features in each of the examined sites. a) PDFs in a quartz grain from the Pine River site at 695.6 m depth. There is very little detrital quartz at this site, so that shocked grains are more readily found mixed with the glass fragments. b) PDFs in a quartz grain from the Coleraine core 20009 at 117.2 m depth. This represents the only example of shocked quartz found at this site.

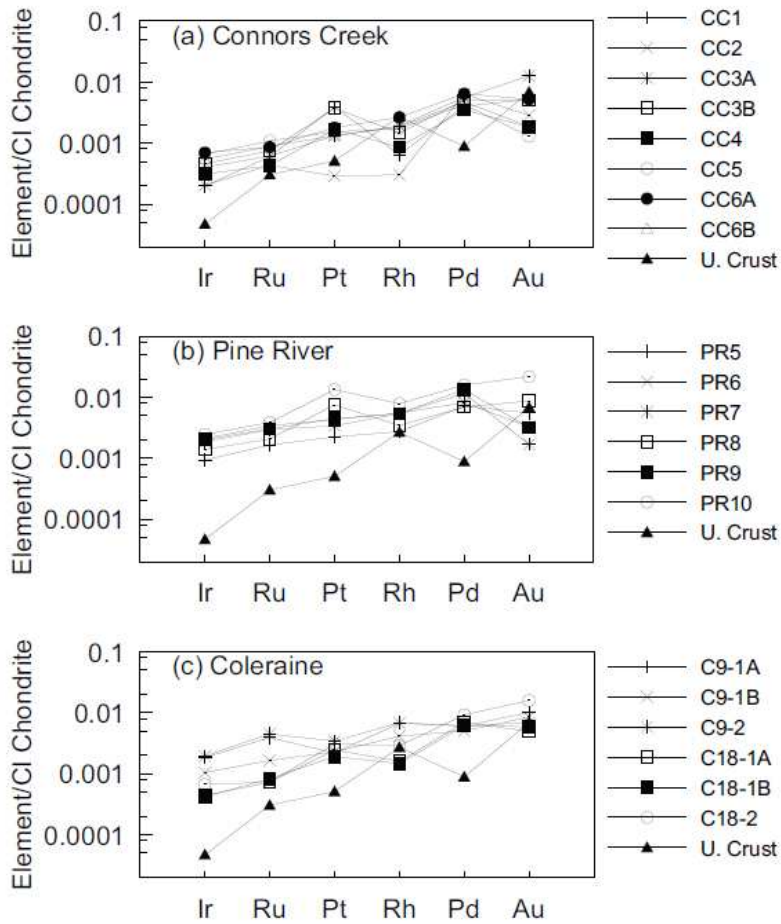


Figure 5. Chondrite-normalized platinum group element abundance patterns for samples from a) Connors Creek, b) Pine River, and c) Coleraine sites, respectively. Chondrite values from McDonough and Sun (1995).

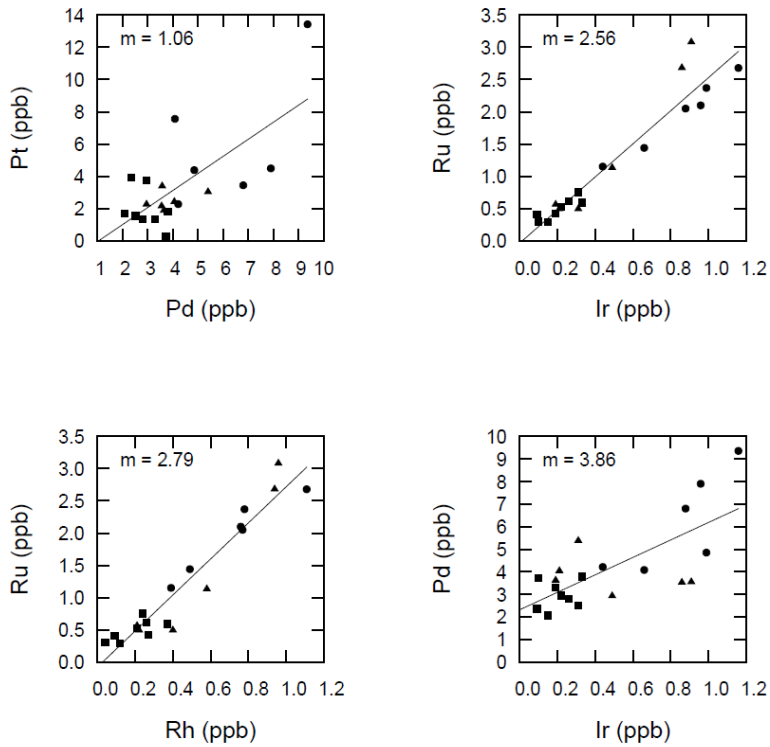
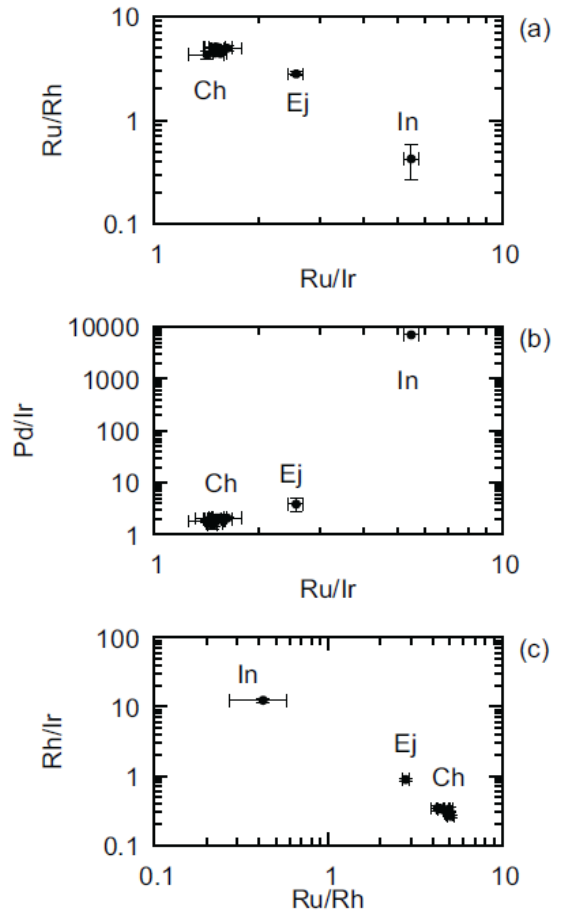


Figure 6. Platinum group element abundances in Sudbury ejecta. For all plots, squares represent samples from the Connors Creek site, circles represent samples from the Pine River drill core, and triangles represent samples from the Coleraine drill cores. The slope of a linear regression through the points is indicated for each graph ($m = \text{slope}$). Iridium, ruthenium, and rhodium abundances have a near linear relationship to one another, but Pd and Pt abundances do not follow a linear relationship. It is possible that these elements have experienced some degree of mobilization.

Figure 7. Ratios of PGEs in Sudbury ejecta at all sites measured in this study (Ej), chondrite groups (Ch), and the East Bull Lake intrusives (In). The ratios are determined from the slope of a linear regression of the measured ratios of the individual samples, and error bars represent a 95% confidence interval. As shown in Tagle and Hecht (2006), the regressed data is more reliable than individual samples for comparison of groups of data. The ratios of PGEs do not overlap with any of the chondritic groups, but this is likely because the contribution of the impactor to the ejecta is too low in any of the measured samples to positively identify the geochemical source of the impactor. It is clear that the ejecta samples are much more closely related to chondrites than to the East Bull Lake samples. Data for East Bull Lake from Djon and Barnes (2012).



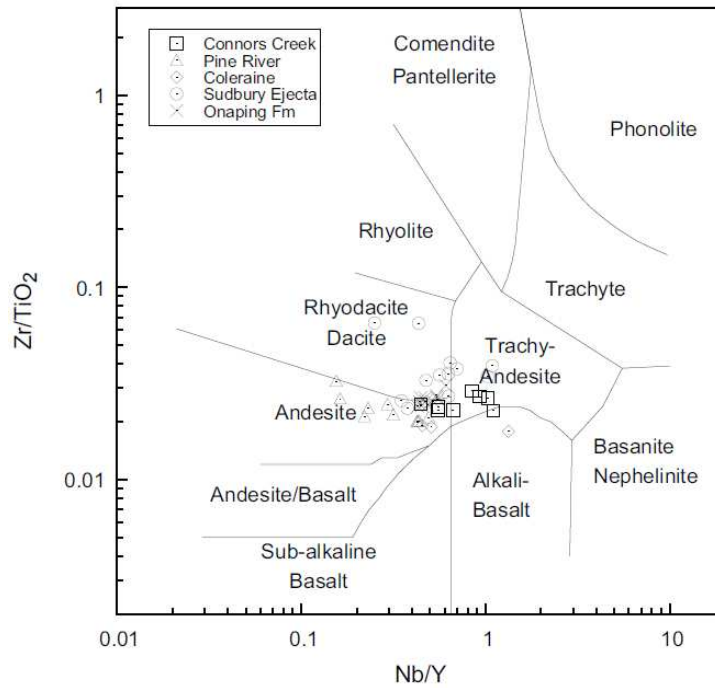


Figure 8. Compositions of samples from three investigated sites plotted in a typical volcanic rock classification (after Winchester and Floyd 1977) showing the variations in compositions of the samples from those sites, which tend towards andesitic to trachyandesitic. The same range of compositions is observed in the Onaping Formation (Ames et al. 2002). Data for “Sudbury Ejecta” from Cannon et al. (2010); data for Onaping Fm. from Ames et al. (2002).

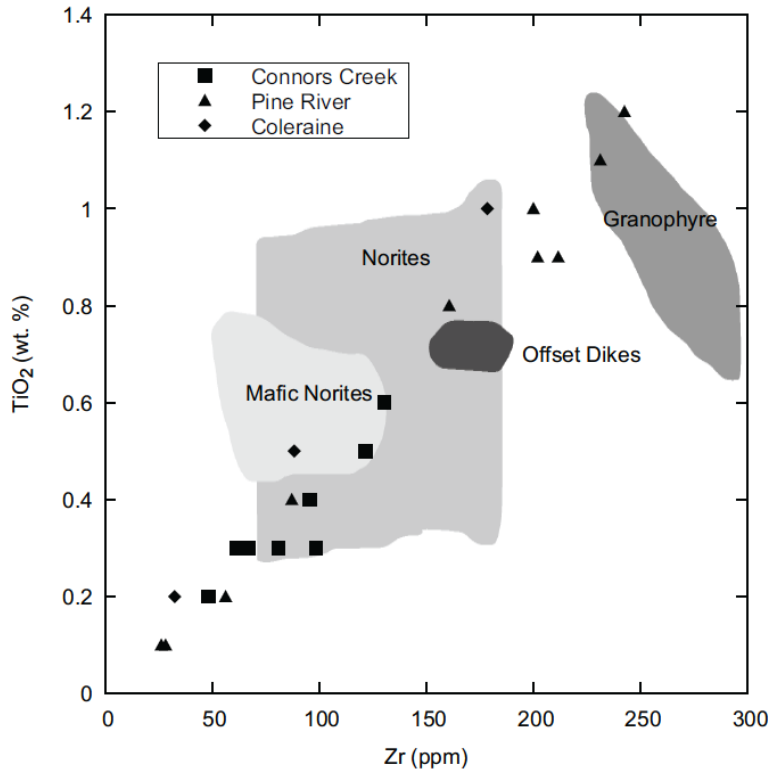


Figure 9. Plot of Zr vs. TiO₂ contents for the compositions of the ejecta at the three sites. Gray fields indicate analyses by Ames et al. (2002) from the SIC.

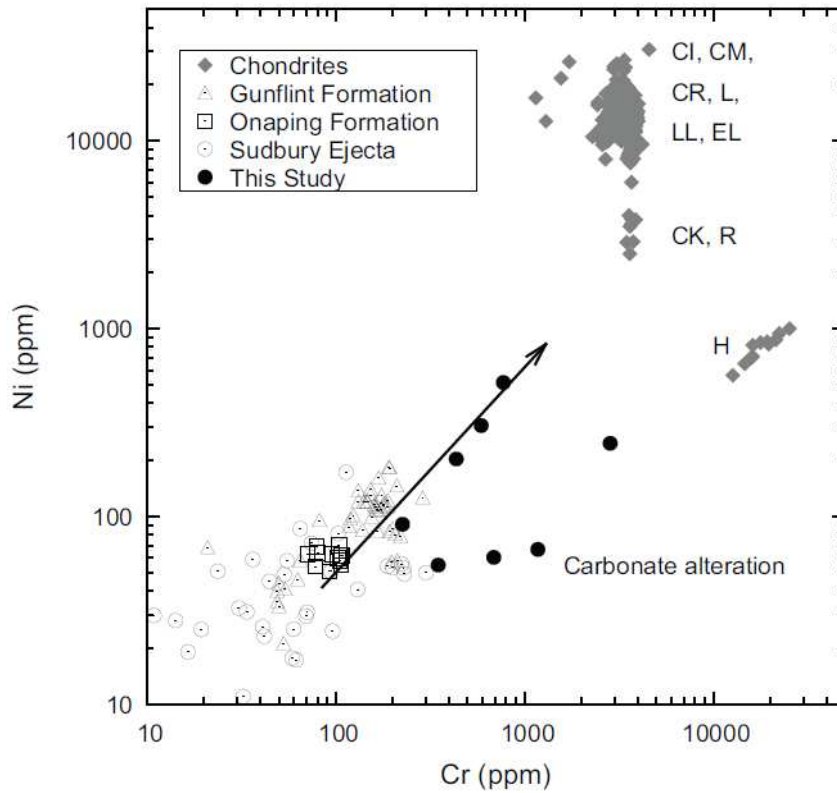


Figure 10. *Ni vs. Cr for Sudbury ejecta deposits compared to the Onaping Fm, the Gunflint Fm, and chondritic groups. The Sudbury ejecta deposits appear to contain a contribution from a carbonaceous chondrite. Data for chondrites from Tagle and Hecht (2008); Gunflint Formation from Polat et al. (2012); Onaping Formation from Ames et al. (2002); Sudbury Ejecta from Cannon et al., 2010.*

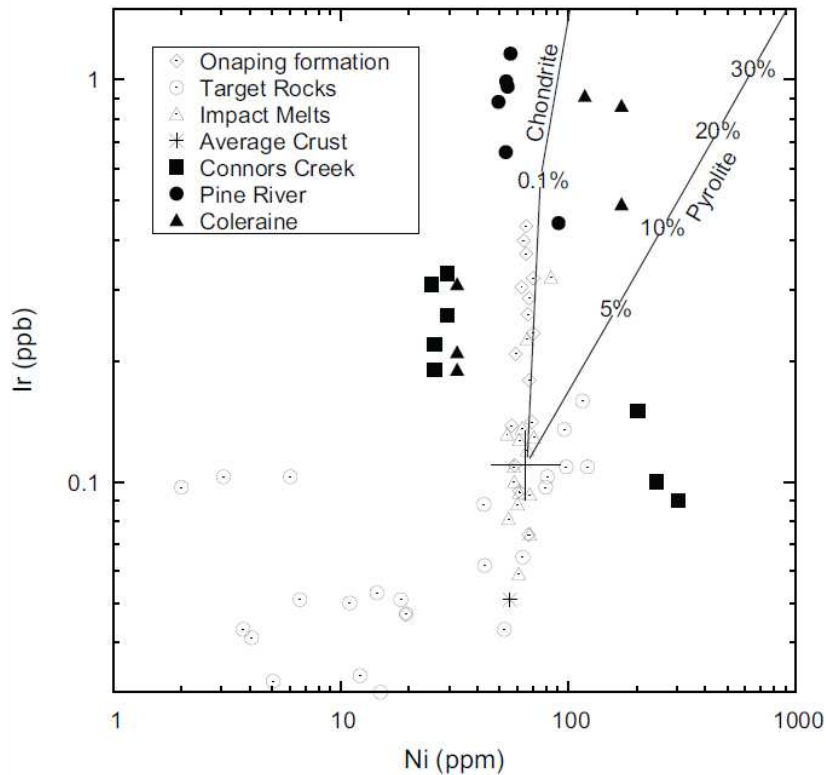


Figure 11. *Ir vs. Ni for Sudbury ejecta, the Onaping Fm, melt rocks from the Sudbury impact structure, and target rocks. Ejecta deposits follow a trend consistent with a mixture of a chondritic impactor mixing with average quartz diorite (cross symbol). The Onaping Fm. shows increasing Ir with stratigraphic height (Mungall et al. 2004), and ejecta deposits appear to have higher Ir than the Onaping Fm. The ejecta deposits have slightly depleted Ni, which may be due to carbonate alteration diluting the signal. Data from Mungall et al. (2004); crustal and chondritic values from McDonough and Sun (1995).*

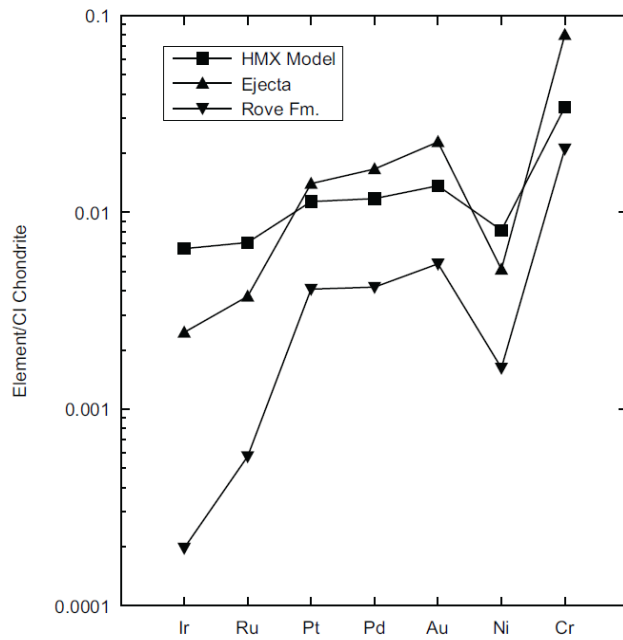


Figure 12. Modeled chondrite-normalized PGE abundances (CI values from McDonough and Sun 1995) of the Sudbury impact ejecta. Background values were taken from the Pine River drill core, and “ejecta” corresponds to the sample from Pine River drill core site that was sampled just above the accretionary lapilli layer, and in which PGEs were found to have the highest abundances.

Table 1. Geochemical data for Sudbury impact ejecta deposits

	Connors Creek								Pine River		
	CC-1A	CC-1B	CC-1C	CC-2	CC-3	CC-4	CC-5	CC-6	PR 4	PR 5	PR 6
wt. %											
SiO ₂	77.9	75.1	69.2	74.9	26.5	24.4	25.5	24.9	48.2	32.5	46.5
TiO ₂	0.34	0.45	0.57	0.36	0.21	0.29	0.25	0.34	1.20	0.41	0.80
Al ₂ O ₃	12.0	13.0	16.0	9.7	6.0	9.1	8.8	12.0	22.0	15.0	21.0
Fe ₂ O ₃	2.72	2.41	4.11	5.40	5.58	6.75	7.06	7.56	3.58	5.70	4.49
MnO	n.d.	n.d.	n.d.	n.d.	0.4	0.4	0.4	0.4	0.1	0.6	0.2
MgO	1.5	1.5	2.2	2.5	10.9	8.2	8.6	7.3	3.8	7.9	4.2
CaO	0.3	1.1	0.6	1.3	21.0	20.0	20.0	20.0	3.2	15.0	5.2
Na ₂ O	0.01	n.d.	n.d.	0.03	n.d.	0.01	n.d.	n.d.	0.16	0.01	0.14
K ₂ O	3.4	4.2	4.9	2.5	1.5	2.6	2.4	3.2	8.0	4.2	7.2
P ₂ O ₅	0.12	0.14	0.13	0.12	0.04	0.05	0.12	0.14	0.21	0.18	0.15
LOI	2.55	2.33	1.89	3.28	28.1	28.1	27.2	26.4	8.59	18.6	10.8
Total	100.8	100.2	99.6	100.1	100.3	99.9	100.3	102.2	99.1	100.1	100.7
ppm											
Sc	21.1	8.70	11.4	9.77	30.2	5.8	31.5	35.8	22.0	11.9	22.6
V	207	186	205	216	155	37	88	101	2280	1180	1450
Cr	590	58.8	70.5	2850	41.0	435	59.8	69.6	301	226	199
Co	1.22*	0.1	1.4	2.56*	2.6	10.0*	2.5	1.1	7.2	11.0*	5.7
Ni	304	17.6	30.9	245	25.8	202	25.1	29.4	50.1	90.7	53.4
Cu	22.7	25.4	19.9	23.5	9.6	6.9	7.4	5.1	12.4	26.5	7.5
As	3.26*	10.9	6.0	8.26*	6.8	16.9*	16.8	7.7	70.5	60.5*	72.8
Se	n.d.	-	-	0.26*	-	n.d.	-	-	-	n.d.	-
Br	n.d.	-	-	n.d.	-	0.2*	-	-	-	0.66*	-
Rb	83.1	87.6	103	60.2	52.1	89.6	66.1	109	418	227	362
Sr	10.5	15.4	12.4	21.8	104	154	231	158	74.6	163.0	87.0
Y	11.7	12.9	14.9	10.3	11.4	15.0	17.9	19.6	62.5	42.6	37.9
Zr	98.4	122	130	95.5	48.4	66.8	61.6	81.1	243	87.2	161
Nb	9.9	12.0	16.4	10.6	6.3	10.0	8.0	10.9	27.2	9.4	16.1
Sb	0.39*	-	-	1.16*	-	0.43*	-	-	-	0.82*	-
Cs	7.53*	-	-	5.42*	-	5.39*	-	-	-	17.0*	-
Ba	228	184	225	129	49	116	140	198	124	140	140
La	16.2*	24.5	22.8	23.6*	21.8	14.8*	19.1	26.7	42.3	29.7*	45.5
Ce	75.6*	28.1	14.2	28.8*	33.7	40.3*	23.0	52.8	68.0	61.0*	72.9
Nd	11.1*	11.9	12.2	16.5*	12.8	12.6*	17.2	26.4	46.4	19.3*	40.2
Sm	2.34*	-	-	3.17*	-	3.02*	-	-	-	4.09*	-
Eu	0.48*	-	-	0.57*	-	0.63*	-	-	-	0.75*	-
Gd	1.51*	-	-	1.71*	-	2.16*	-	-	-	2.87*	-
Tb	0.29*	-	-	0.26*	-	0.32*	-	-	-	0.45*	-
Tm	0.22*	-	-	0.21*	-	0.15*	-	-	-	0.22*	-
Yb	1.69*	-	-	0.99*	-	0.97*	-	-	-	1.42*	-
Lu	0.28*	-	-	0.16*	-	0.15*	-	-	-	0.23*	-
Hf	3.95*	-	-	2.81*	-	2.37*	-	-	-	2.13	-
Ta	0.50*	-	-	1.80*	-	0.58*	-	-	-	0.69*	-
W	3.3*	-	-	8.1*	-	1.8*	-	-	-	1.73*	-
Ir (ppb)	n.d.	-	-	n.d.	-	n.d.	-	-	-	0.92*	-
Au (ppb)	0.2*	-	-	0.3*	-	0.3*	-	-	-	0.5*	-
Th	6.0*	6.0	5.4	6.1*	2.0	3.5*	2.5	2.9	12.5	6.8*	8.0
U	2.6*	3.1	3.0	2.1*	1.9	2.1*	2.7	3.1	14.1	3.2*	7.6

n.d. = not detected

* analysis by DNAA. All other analyses by XRF.

	Pine River							Coleraine		
	PR 7	PR 8	PR 9	PR 10	PR 11A	PR 11B	PR 11C	CR 9-1	CR 9-2	CR 18-1
wt. %										
SiO ₂	50.9	51.1	51.0	51.2	23.1	24.1	19.9	53.7	48.7	28.6
TiO ₂	0.86	0.93	1.00	1.10	0.24	0.09	0.10	0.47	1.00	0.17
Al ₂ O ₃	22.0	22.0	23.0	23.0	7.4	3.5	3.7	14.0	23.0	6.7
Fe ₂ O ₃	4.58	4.14	4.58	4.14	7.85	6.95	7.23	20.3	12.2	46.5
MnO	0.1	0.1	0.1	0.1	1.0	1.1	1.1	0.7	0.1	9.2
MgO	3.3	3.4	3.2	3.1	9.0	8.7	9.4	2.9	2.4	1.1
CaO	3.4	2.5	1.9	1.8	24.0	28.0	29.0	0.3	0.1	0.9
Na ₂ O	0.16	0.20	0.19	0.21	n.d.	n.d.	n.d.	n.d.	n.d.	0.01
K ₂ O	8.2	8.1	8.4	8.3	1.3	0.2	0.1	2.2	7.5	1.7
P ₂ O ₅	0.22	0.26	0.18	0.19	0.08	0.07	0.05	0.06	0.05	0.04
LOI	6.98	6.96	6.60	6.51	25.6	27.6	30.7	5.65	5.12	7.01
Total	100.7	99.7	100.1	99.6	99.6	100.3	101.3	100.2	100.2	101.9
ppm										
Sc	19.6	22.5	20.6	20.2	35.8	36.1	38.8	18.2	21.0	18.9
V	1830	1530	1200	1030	241	55.4	63.2	76.4	153	31.9
Cr	231	229	188	223	44.6	10.9	14.2	114	173	30.7
Co	4.2	3.8	4.3	8.7	7.2	4.4	5.9	24.5	7.20*	15.7
Ni	49.4	53.2	54.2	55.8	45.1	29.7	27.9	172	118	32.5
Cu	6.6	8.0	12.1	10.3	7.3	3.5	5.3	42.5	26.0	63.3
As	48.5	65.1	57.8	75.7	56.6	27.6	24.8	19.5	25.7*	4.2
Se	-	-	-	-	-	-	-	-	n.d.	n.d.
Br	-	-	-	-	-	-	-	-	1.08*	-
Rb	443	445	448	455	63.3	7.9	2.4	82.4	294	73.4
Sr	70.6	83.1	74.7	76.3	109	110	129	28.3	28.0	13.9
Y	53.8	52.2	41.4	42.2	19.5	14.2	12.3	24.6	21.7	14.1
Zr	212	202	200	231	56.3	28.3	26.3	88.3	179	32.5
Nb	15.8	16.5	17.8	20.7	4.5	2.2	2.0	12.5	28.9	6.4
Sb	-	-	-	-	-	-	-	-	0.41*	-
Cs	-	-	-	-	-	-	-	-	0.65*	-
Ba	107	157	146	161	18.9	5.0	5.0	294	18	261
La	27.1	32.0	21.4	14.9	46.5	30.2	20.1	59.2	113*	49.0
Ce	40.8	45.1	30.3	33.9	37.7	24.4	14.8	89.4	185*	41.3
Nd	30.4	35.2	22.9	23.5	20.6	12.3	4.4	38.0	79.8*	8.5
Sm	-	-	-	-	-	-	-	-	2.79*	-
Eu	-	-	-	-	-	-	-	-	0.72*	-
Gd	-	-	-	-	-	-	-	-	2.17*	-
Tb	-	-	-	-	-	-	-	-	0.33*	-
Tm	-	-	-	-	-	-	-	-	0.15*	-
Yb	-	-	-	-	-	-	-	-	0.91*	-
Lu	-	-	-	-	-	-	-	-	0.14*	-
Hf	-	-	-	-	-	-	-	-	0.55*	-
Ta	-	-	-	-	-	-	-	-	0.15*	-
W	-	-	-	-	-	-	-	-	1.1*	-
Ir (ppb)	-	-	-	-	-	-	-	-	n.d.	-
Au (ppb)	-	-	-	-	-	-	-	-	0.4*	-
Th	10.4	11.8	10.5	14.6	3.5	0.5	0.4	3.4	8.7*	n.d.
U	8.9	8.8	7.0	6.8	1.7	2.2	1.5	5.4	14.8*	5.5

n.d. = not detected

* analysis by INAA. All other analyses by XRF.

Table 2: Platinum Group Element abundances for Sudbury impact ejecta deposits

	Connors Creek								Pine River	
	CC1C	CC2	CC3a	CC3b	CC4	CC5	CC6a	CC6b	PR5	PR6
Ir	0.09	0.10	0.19	0.22	0.15	0.31	0.33	0.26	0.44	0.99
Ru	0.41	0.30	0.42	0.52	0.29	0.75	0.59	0.61	1.15	2.37
Pt	3.91	0.29	1.32	3.75	1.69	1.53	1.79	1.32	2.27	4.38
Rh	0.09	0.04	0.27	0.21	0.12	0.24	0.37	0.26	0.39	0.78
Pd	2.35	3.72	3.29	2.95	2.07	2.51	3.79	2.80	4.21	4.85
Au	0.76	0.42	1.84	0.74	0.27	0.19	0.76	0.27	0.81	0.48

	Pine River				Coleraine					
	PR7	PR8	PR9	PR10	C9-1a	C9-1b	C9-2	C18a	C18b	C18-2
Ir	0.88	0.66	0.96	1.16	0.86	0.49	0.91	0.21	0.19	0.31
Ru	2.05	1.44	2.10	2.68	2.69	1.14	3.09	0.50	0.57	0.50
Pt	3.44	7.56	4.49	13.4	2.18	2.29	3.42	2.45	1.91	3.06
Rh	0.77	0.49	0.76	1.11	0.94	0.58	0.96	0.22	0.21	0.40
Pd	6.80	4.08	7.90	9.36	3.55	2.95	3.57	4.06	3.64	5.40
Au	0.25	1.28	0.46	3.18	1.47	1.24	0.99	0.72	0.85	2.30

All samples measured by ICP-MS after concentration by the fire assay method.

Values in ppb. Samples with lower-case letters are repeat analyses.

Table A1: Limits of detection and quantitation for PGE analysis using the X Series ICP-MS using the method outlined in the text. Also shown are typical reagent blanks for the period of study and an assessment of the accuracy of the analyses using certified reference materials WITS-1 and TDB1. All figures are in parts per billion.

	Ir	Ru	Rh	Pt	Pd	Au
Detection Limit	0.003	0.009	0.004	0.010	0.005	0.007
Quantification Limit	0.010	0.031	0.013	0.032	0.016	0.024
Reagent Blank 1	0.011	0.11	bdl	0.10	0.15	0.12
Reagent Blank 2	0.014	0.07	bdl	0.19	0.12	0.21
WITS1-1	1.46	4.29	1.13	6.99	5.31	7.82
Wits1 Recommended ($\pm 2\sigma$) ^{1,2}	1.4 \pm 0.3	3.9 \pm 0.8	1.1 \pm 0.2	5.7 \pm 1.6	5.0 \pm 1.2	4.9 \pm 2.6
Wits1 Recommended ($\pm 2\sigma$) ³	1.58	4.41	1.20	8.80	5.64	no data
TDB1-1	0.10	0.24	0.57	6.47	25.4	7.70
TDB1-2	0.06	0.22	0.43	6.00	23.4	8.68
TDB1 Certified ($\pm 1\sigma$) ⁴	0.15	0.3	0.7	5.8 \pm 1.1	22.4 \pm 1.4	6.3 \pm 1.3
TDB1 Recommended ($\pm 1\sigma$) ³	0.075	0.198	0.47	5.01	24.3	no data

Data sources: (1) Tredoux and McDonald 1996; (2) Pearson and Woodland (2000); Meisel and Moser (2004); (4) Govindaraju (1994)

5. ANIE: A MATHEMATICAL ALGORITHM FOR AUTOMATED INDEXING OF PLANAR DEFORMATION FEATURES IN QUARTZ GRAINS

Matthew S. Huber^{1*}, Ludovic Ferrière², Anna Losiak¹, and Christian Koeberl^{1,2}

¹*Department of Lithospheric Research, University of Vienna,
Althanstrasse 14, A-1090 Vienna, Austria*

²*Natural History Museum, Burgring 7, A-1010 Vienna, Austria*

**corresponding author: matthew.huber@univie.ac.at*

Submitted to: Meteoritics and Planetary Science, 12 January 2011; Accepted 22 June 2011

Abstract:

Planar deformation features (PDFs) in quartz, one of the most commonly used diagnostic indicators of shock metamorphism, are planes of amorphous material that follow crystallographic orientations, and can thus be distinguished from non-shock induced fractures in quartz. The process of indexing data for PDFs from universal-stage measurements has traditionally been performed using a manual graphical method, a time-consuming process in which errors can easily be introduced. A mathematical method and computer algorithm, which we call the Automated Numerical Index Executor (ANIE) program for indexing of PDFs, was produced and is presented here. The ANIE

program is more accurate and faster than the manual graphical determination of Miller-Bravais indices, as it allows control of the exact error used in the calculation, and removal of human error from the process.

5.1. Introduction

The presence of planar deformation features (PDFs) in quartz grains has been used as one of the most reliable indicator of shock-metamorphism for the confirmation of hypervelocity impact structures (see, e.g., French and Short, 1968; Stöffler and Langenhorst, 1994; Grieve et al., 1996; French, 1998; French and Koeberl, 2010, and references therein). PDFs are regularly spaced, thin, planar features, generally oriented parallel to rational crystallographic planes (Fig. 1), and formed in quartz grains upon shock compression greater than ~5-10 GPa (see Stöffler and Langenhorst, 1994, and references therein). Because they develop along crystallographic planes, suspected planar features can be investigated (i.e., measured and indexed) in order to determine if they correspond to known planes that accommodate shock deformation (Engelhardt and Bertsch, 1969; Stöffler and Langenhorst, 1994; Ferrière et al., 2009). PDFs with specific crystallographic orientations are known to form in quartz at different shock pressures (e.g., Hörz, 1968; Müller and Défourneaux, 1968; Huffman and Reimold, 1996), so that peak shock pressure can be estimated for a given sample based on PDF orientations measurements (e.g., Robertson and Grieve, 1977; Grieve et al., 1990; Dressler et al., 1998; Ferrière et al., 2008). The measurement of the orientations of suspected PDFs is possible using transmission electron microscopy (TEM; e.g., Goltrant et al., 1991; Trepmann and Spray, 2006), a spindle stage (e.g., Bohor et al., 1987), or the universal-stage (U-stage) on a petrographic microscope (e.g., Engelhardt and Bertsch, 1969; Langenhorst, 2002; Ferrière et al., 2009). Neverthe-

less, a note of caution is necessary: determining if some planar features are true PDFs, especially if they are altered (e.g., in the form of planar fluid inclusion trails), is not possible based on only the determination of the crystallographic orientation of these features, because deformation of quartz crystals will often (but not exclusively) follow the rational crystallographic planes even if shock metamorphism is not involved. Thus presentation of an orientation diagram alone is not sufficient to confirm the presence of true PDFs. For such questionable features, TEM work remains necessary.

The most common and least expensive method of determining PDF orientations in quartz is the U-stage microscope analysis. According to the recent study by Ferrière et al. (2009), it is also the only technique that allows large, statistically significant datasets to be readily generated. However, the manual process of converting raw measurements from the U-stage to orientations of PDFs has traditionally been done using a graphical method based on a Wulff (equal-angle) stereonet and a stereographic projection template (see, e.g., Engelhardt and Bertsch, 1969; Ferrière et al., 2009), and is rather time-consuming. It is also possible that manually determining the Miller-Bravais indices using the graphical method may introduce some additional errors to the data. Here, for the first time, the mathematical basis for indexing PDFs is presented, along with an algorithm for indexing, named Automated Numerical Index Executor (ANIE), designed for use in Microsoft Excel (version 2007 and later). In addition, mathematically indexed PDFs from three samples, BOS (a meta-greywacke from the Bosumtwi impact crater), M8 (a biotite-gneiss from the Manson impact structure), and AUS (a sandstone from the Gosses Bluff impact structure) (see Ferrière et al., 2009, for more details on these samples) are compared to results obtained by the manual method (i.e., using the stereographic projection template) in order to demonstrate the veracity of our mathematical method.

5.2. Mathematical method for determining crystallographic orientations of PDFs

Previously, indexing PDFs has involved a graphical interface, as described in e.g., Engelhardt and Bertsch (1969), Stöffler and Langenhorst (1994), and Ferrière et al. (2009). However, this method is, as mentioned above, time-consuming and somewhat imprecise, as it allows a certain “fudge factor” in the plotting of measurements on the stereonet, in the adjustment of the data, and in the actual reading of indices from the projected chart. All these inconveniences provided the motivation for a mathematical method to determine crystallographic orientations of PDFs.

The stereonet (or Wulff net) essentially represents a two dimensional projection of a three dimensional sphere. To determine PDF orientations using the stereonet, several steps must be followed. In the first step, the azimuth and inclination of the *c*-axis and poles perpendicular to planes of all PDFs in a given grain are plotted on a stereonet. Data are then adjusted by rotating the overlay by hand until the *c*-axis and a given pole lie on the same meridian (N-S great circle on the stereonet) in order to obtain the polar angle. Next, the *c*-axis is moved along the equatorial line of the stereonet to the center, and the poles perpendicular to planes of all PDFs are transformed along small circles by the same angle. Finally, the transformed data are compared to the stereographic projection template (STP) of PDFs in quartz, which displays the pole orientations of known PDF planes within a 5° envelope of measurement error. This last step is done by rotating the STP until all poles (or a maximum of them) fall into the circles of the STP (see, e.g., Engelhardt and Bertsch (1969), Langenhorst (2002), and/or Ferrière et al. (2009) for the detailed procedure). We describe here how all these

graphical steps can be performed using mathematical calculations derived from spherical trigonometry (see Fig. 2).

The first step is to calculate the great circle distance between the c-axis and the pole to PDF plane, which corresponds to the so-called polar angle. This distance is obtained from the Law of Cosines for spherical triangles, and can be calculated using the following equation:

$$\cos(90 - \Psi) = \cos(90 - z) * \cos(90 - \Lambda) + \cos(90 - z) * \cos(90 - \Lambda) * \cos(\alpha - a) \text{ [Eq. 1]}$$

where "z" is the measured c-axis inclination, "α" is the measured c-axis azimuth, "Λ" is the measured PDF inclination, "a" is the measured PDF azimuth, and "Ψ" is the polar angle of the PDF. Note that the center of the sphere would be measured at 90°, so that it is necessary for calculations to be taken as "90 minus measurement" (see Fig. 2). Therefore, the equation can be simplified as follows:

$$\sin \Psi = \sin z * \sin \Lambda + \sin z * \sin \Lambda * \cos(\alpha - a) \text{ [Eq. 2]}$$

Then, the second step is to calculate the azimuth of the PDF as it would be if the c-axis were in the middle of the sphere. This is calculated from the Law of Sines for spherical triangles using the following equation:

$$\sin \delta / \sin(90 - z) = \sin(\alpha - a) / \sin(90 - \Psi) \text{ [Eq. 3]}$$

Which simplifies to the following equation:

$$\sin \delta = \sin (\alpha - a) * \cos z / \cos \Psi \text{ [Eq. 4]}$$

where " δ " is the azimuthal angle of the PDF after correcting the c-axis to the center of the sphere. Importantly, the value of " δ " must be corrected to determine the exact azimuth of the PDF, as this equation will only result in an accurate value for half of a circle (owing to the fact that cosine is an even function). In order to find the exact value of " δ ", a determination of the proper quadrant is necessary. The value of " δ " does not need adjustment if Eq. 4 is positive and if $\sin (z) > \sin (\Psi) * \sin (\Lambda)$. The value of " δ " should be adjusted by " $\pi - \delta$ " if either Eq. 4 is negative or $\sin (z) < \sin (\Psi) * \sin (\Lambda)$. In the case where Eq. 4 is negative and $\sin (z) < \sin (\Psi) * \sin (\Lambda)$, the value of " δ " should be adjusted by " $2\pi + \delta$ " to ensure that " δ " refers to the correct quadrant and can be properly compared to other measured PDF sets in the given grain.

After the inclination " Ψ " and azimuth " δ " of all PDFs have been calculated for a given grain, the next step is to calculate the great circle distance between the two PDFs being indexed, " c "; this can be calculated using the following equation:

$$\cos c = \cos \Psi_1 * \cos \Psi_2 + \sin \Psi_1 * \sin \Psi_2 * \cos (\delta_1 - \delta_2) \text{ [Eq. 5]}$$

Once this is calculated, the angle between PDFs (denoted here as " C ") can be calculated using the law of cosines for spheres with the following equation:

$$\cos C = (\cos c - \cos \Psi_1 * \cos \Psi_2) / (\sin \Psi_1 * \sin \Psi_2) \text{ [Eq. 6]}$$

The combination of the polar angle " Ψ " and the angle between PDF sets "C" allows PDFs to be indexed. Each PDF set has a singular polar angle and occurs at a particular angle to all other PDFs (see Table S1 in the Supporting Information). Two PDF sets can be indexed by first finding the polar angles close to the determined values, then determining if the angle between the measured planes "C" is within 2 times error (i.e., within the 5° envelope of measurement error for each PDF, or 10° error) to the angle between crystallographic planes in the grain.

5.3. Description of the Automated Numerical Index Executor (ANIE) program

Based on the mathematical method described above, a computer algorithm has been written as a Microsoft Excel 2007 macro. The program, named ANIE (see Supporting Information), allows the automated indexing of up to 10 PDF sets per grain in an unlimited number of quartz grains. Data can be entered directly as obtained from U-stage measurements, including input of the full range of values determined for a particular PDF set, input as the low and high measured values for both azimuth and inclination. Data can also be input as both East and West orientations.

From the input screen, the maximum error (corresponding to the "envelope of measurement error") that is traditionally fixed at 5° (see, e.g., Ferrière et al., 2009) can be defined by the user as any value between 0 and 10° . The user also has options concerning the method of calculation. Grains with a single PDF set can either be included or excluded from the analysis, and the program can either use an average value of the U-stage measurements or the full range of measured values for in-

dexing. When PDFs fall into the region where $\{10\bar{1}3\}$ and $\{10\bar{1}4\}$ orientations overlap, the program can be set to indicate that both orientations are possible solutions.

The measurements are matched to possible crystallographic indices based on the calculated polar angle (Eq. 2) as compared to the ideal angle for each crystallographic index, plus or minus the defined error. Angles between ideal PDF sets (Eq. 5) are compared to the list of possible angles between measured planes plus or minus the defined error (Table 1) to narrow the possible orientations for each plane to a single possible Miller-Bravais index. If there are multiple indices that are possible, the Miller-Bravais index with the lowest calculated angular error (i.e., the more likely) is reported.

Such analyses take only a few seconds to complete indexing for each grain; e.g., the analysis of sample AUS, with 208 PDF sets in 71 grains, was completed in approximately 1 minute. After the U-stage measurements are indexed, the program presents the results in two forms. The cumulative data are reported along with graphs presenting the proportion of indexed PDFs and the polar angles of the PDFs. The data are also presented in a grain-by-grain list, with details on the polar angle and Miller-Bravais indices of all PDF sets. Two histograms are presented upon completion of the program (Fig. 3); one with the frequency distribution of polar angle values in bins of 5° , and one with the absolute frequency of indexed PDFs with Miller-Bravais indices (see, e.g., Grieve et al., 1996; Ferrière et al., 2009). The number of PDF sets, the number of quartz grains, as well as the percentage of unindexed planes and the error used for the indexing, are indicated directly on the upper right part of the graph.

Data can also be exported to a comma-separated value spreadsheet, which retains the original input values, the polar angle values, the Miller-Bravais indices of the PDFs, and the angular error of

the orientation for each PDF set in all grains. Graphics generated by the ANIE program can be exported directly to a Microsoft Powerpoint presentation, or they can also be copied for export to other programs.

5.4. Comparison of mathematical method and graphical method for indexing PDFs

The most recent stereographic projection template (with the pole orientations of known PDF planes; see Ferrière et al., 2009) used for the graphical method is designed to have 5° errors (i.e., "U-stage measurement errors") associated with all Miller-Bravais indices. However, additional errors can be introduced in this method from a number of factors, including the width of the line at the border of the circles (i.e., the 5° envelopes), the width of the pencil mark used when comparing the measurements to the STP by rotation, and the high likelihood that the human eye will not be able to properly discern whether measurements that are close to the border of a particular orientation are actually indexed or not. The mathematical method eliminates all of these factors of error and uncertainty. Because of that, a few minor discrepancies appear between the results obtained with graphical method versus mathematical method. Results are summarized in Table 1.

The data for three samples (AUS, BOS, and M8, all containing more than 65 grains with PDFs) have been processed mathematically using the ANIE program under four sets of conditions: (1) with a 5° error and using average values from U-stage data; (2) with a 5° error and using the full range from reported U-stage data; (3) with a 6° error and using average values from U-stage data; and (4) with a 6° error and using the full range from reported U-stage data. The reason for testing the

mathematical method with a 6° error was to account for the potential “fudge factor” introduced by the graphical method. Note that all of the PDFs were indexed by hand with the graphical method by an experienced user (see Ferrière et al., 2009, for the exact methodology and procedure). Results using ANIE with average values from U-stage data with both 5° and 6° error have a noticeable difference compared to results obtained with the graphical method. However, very similar results are found between the graphical and mathematical results for 5° error using ranges of values, and near-identical results are found when 6° error is used with ranges of values.

Sample AUS is the largest dataset indexed, with 74 grains and 208 measured PDF sets. By hand, it was found to have 10 unindexed planes, whereas when using ANIE and average values from U-stage data, with 5° and 6° error, 49 and 38 unindexed PDF sets were found, respectively. However, using the ranges of values resulted in 21 unindexed PDFs for 5° error, and 10 unindexed PDFs within 6° error. The graphically measured polar angles for AUS were similar to those found using ANIE, though with some minor discrepancies. For example, 4 PDFs were identified as being basal PDFs when plotted by hand, whereas they were unindexed using the mathematical method as the angular distance between the c-axis and the PDF set was slightly above error. The majority of differences between the graphical and mathematical method are the result of imprecision in the graphical method on the order of less than half a degree. Similar results were found for the samples BOS and M8 (Table 1).

Our comparison of results obtained with both methods allows us to identify three main categories of differences between mathematical indexing using ANIE and the graphical indexing of the data. The first one arises when there are multiple possible solutions that allow all measurements to fit within known PDF crystallographic orientations. In the manual version, the user visually esti-

mates the best fit (i.e., using eyes and "intuition"), whereas the mathematical method determines the set of Miller-Bravais indices that has the lowest error and, thus, is the most likely one. This accounts for 48% of the discrepancies. Secondly, PDF sets that are very close to a known PDF crystallographic orientation, but that fall just outside of the defined error (i.e., traditionally of 5° as in the STP presented in Ferrière et al., 2009) may be graphically counted as "indexed sets" even they are in fact unindexed PDFs. This also accounts for 48% of discrepancies. Finally, all other discrepancies between graphical versus mathematical method that do not correspond to either of these, such as errors in plotting data, account for the remaining 4% of discrepancies. The paucity of such discrepancies indicates that the mathematical method is reliably measuring the exact same features as when using the graphical method, while the commonality of the second category of discrepancies indicates that the user, in the case of the graphical method, can easily introduce some errors into the indexing process.

Thus, based on our comparison of results as obtained for the same set of U-stage data with the graphical method and the mathematical method (i.e., using ANIE), very similar results are obtained when using the range of measured values and an error of 6° . It is recommended that users of the ANIE program, or of the mathematical method described in this manuscript, state specifically which error setting is chosen for the indexing of the PDFs and whether average values or ranges of values are used for the determination of crystallographic indices.

5.5. Conclusions and recommendations

The process of indexing PDFs in quartz grains is somewhat tedious, mainly because of the time-consuming and difficult nature of plotting U-stage measurements and properly reading the Mil-

ler-Bravais indices after the data have been obtained. The development and presentation of an automated method for the determination of crystallographic orientations of PDFs removes a large part of the tedium for those who are attempting to verify the shock origin of deformation features in quartz grains and/or who are interested in the evaluation of the peak shock pressure recorded by a given sample.

Our comparison of indexing PDF sets using the mathematical method (i.e., the ANIE program) versus the "old" graphical method reveals that the best fit between the two methods is found when using 6° error and the full ranges of values (as opposed to the average value of measurements) in the ANIE program. For the 564 PDFs evaluated in the present study, a total of 46 differences were found between indexing with the mathematical method versus the graphical method, which corresponds to a difference of $\sim 8\%$. Finally, our study suggests that the graphical method, although designed with a 5° envelope of measurement error, is actually closer to 6° error in reality. However, it is recommended to users to define a 5° error when using ANIE program, as if a 6° error is used, the error envelopes of the PDFs pole traces for $\{10\bar{1}2\}$ and $\{10\bar{1}3\}$ orientations partially overlap. Anyone presenting PDF data indexed with the ANIE program or this mathematical method is asked to state clearly the error used in the calculation, as well as whether the average value of measurements or the ranges of values is used for indexing.

Acknowledgments:

This work is supported by the University of Vienna doctoral school IK-1045 and the Austrian Science Foundation (FWF), grant P21821-N19 (to CK). We express appreciation to Bevan M. French and Sam Watson for discussion and encouragement with this project. Hugues Leroux, John

G. Spray, and an anonymous reviewer are thanked for their comments and suggestions to improve the quality of the manuscript. This paper is dedicated to the memory of our late colleague and friend Jared R. Morrow (1959-2010), who was an expert in U-stage measurements of PDFs in quartz grains and who had long hoped for this program to be operating.

5.6. References

- Bohor B. F., Modreski P. J., and Foord E. E. 1987. Shocked quartz in the Cretaceous-Tertiary boundary clays: Evidence for a global distribution. *Science* 236:705–708.
- Dressler B. O., Sharpton V. L., and Schuraytz B. C. 1998. Shock metamorphism and shock barometry at a complex impact structure: State Islands, Canada. *Contributions to Mineralogy and Petrology* 130:275–287.
- Engelhardt W. v. and Bertsch W. 1969. Shock induced planar deformation structures in quartz from the Ries crater, Germany. *Contributions to Mineralogy and Petrology* 20:203–234.
- Ferrière L., Koeberl C., Ivanov B. A., and Reimold W. U. 2008. Shock metamorphism of Bosumtwi impact crater rocks, shock attenuation, and uplift formation. *Science* 322:1678–1681.
- Ferrière L., Morrow J. R., Amgaa T., and Koeberl C. 2009. Systematic study of universal-stage measurements of planar deformation features in shocked quartz: Implications for statistical significance and representation of results. *Meteoritics and Planetary Science* 44:925–940.
- French B. M. 1998. *Traces of catastrophe: A handbook of shock-metamorphic effects in terrestrial meteorite impact structures*. LPI Contribution #954. Houston, Texas: Lunar and Planetary Institute. 120 p.

- French B. M. and Koeberl C. 2010. The convincing identification of terrestrial meteorite impact structures: What works, what doesn't, and why. *Earth-Science Reviews* 98:123–170.
- French B. M. and Short N. M., editors. 1968. *Shock metamorphism of natural materials*. Baltimore: Mono Book Corporation. 644 p.
- Goltrant O., Cordier P., and Doukhan J.-C. 1991. Planar deformation features in shocked quartz; a transmission electron microscopy investigation. *Earth and Planetary Science Letters* 106:103–115.
- Goltrant O., Leroux H., Doukhan J.-C., and Cordier P. 1992. Formation mechanisms of planar deformation features in naturally shocked quartz. *Physics of the Earth and Planetary Interiors* 74:219–240.
- Grieve R. A. F., Coderre J. M., Robertson P. B., and Alexopoulos J. 1990. Microscopic planar deformation features in quartz of the Vredefort structure: Anomalous but still suggestive of an impact origin. *Tectonophysics* 171:185–200.
- Grieve R. A. F., Langenhorst F., and Stöffler D. 1996. Shock metamorphism of quartz in nature and experiment: II. Significance in geoscience. *Meteoritics and Planetary Science* 31:6–35.
- Hörz F. 1968. Statistical measurements of deformation structures and refractive indices in experimentally shock loaded quartz. In *Shock Metamorphism of Natural Materials*, edited by French B. M. and Short N. M. Baltimore: Mono Book Corp. pp. 243–253.
- Huffman A. R. and Reimold W. U. 1996. Experimental constraints on shock-induced microstructures in naturally deformed silicates. *Tectonophysics* 256:165–217.

- Langenhorst F. 2002. Shock metamorphism of some minerals: Basic introduction and microstructural observations. *Bulletin of the Czech Geological Survey* 77:265–282.
- Morrow J. R. 2007. Shock-metamorphic petrography and microRaman spectroscopy of quartz in upper impactite interval, ICDP drill core LB-07A, Bosumtwi impact crater, Ghana. *Meteoritics and Planetary Science* 42:591–609.
- Müller W. F. and Défourneaux M. 1968. Deformationsstrukturen im Quarz als Indikator für Stosswellen: Eine experimentelle Untersuchung an Quarz-Einkristallen. *Zeitschrift für Geophysik* 34:483–504.
- Robertson P. B. and Grieve R. A. F. 1977. Shock attenuation at terrestrial impact structures. In *Impact and explosion cratering*, edited by Roddy D. J., Pepin R. O., Merrill R. B. New York: Pergamon Press. pp. 687–702.
- Stöffler D. and Langenhorst F. 1994. Shock metamorphism of quartz in nature and experiment: I. Basic observation and theory. *Meteoritics and Planetary Science* 29:155–181.
- Trepmann C. A. and Spray J. G. 2006. Shock-induced crystal-plastic deformation and post-shock annealing of quartz: Microstructural evidence from crystalline target rocks of the Charlevoix impact structure, Canada. *European Journal of Mineralogy* 18:161–173.

Figures

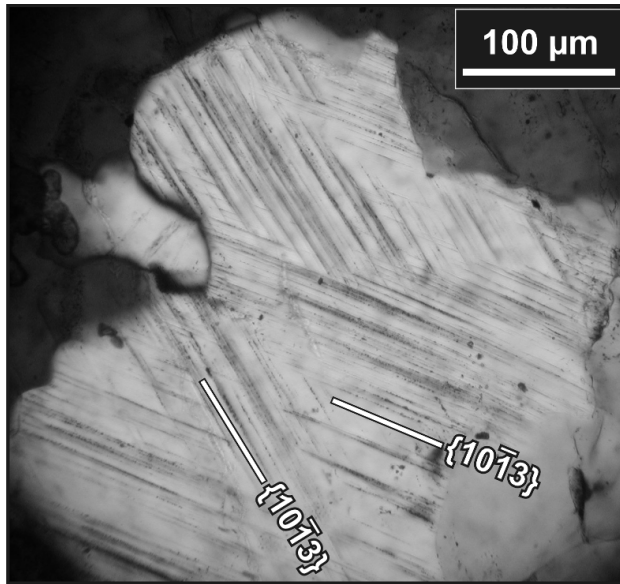


Fig. 1. Photomicrograph (crossed polars) of a quartz grain with two sets of PDFs; both PDF sets with $\omega\{10\bar{1}3\}$ -equivalent orientations (sample from the Bosumtwi impact crater).

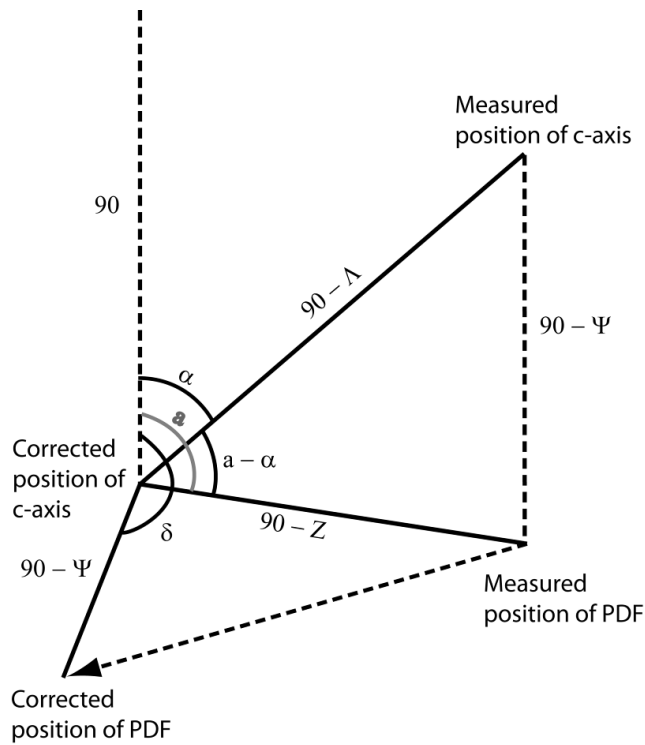


Fig. 2. Simplified representation of the process of indexing PDFs in quartz. The c-axis is measured, then moved to the center of a projected sphere; this operation is defined by a distance of " $90 - \Lambda$ " and an angle of " α ". The distance between the center of the projected sphere and the measured position of the pole to PDF plane is " $90 - z$ ", and the angle is " a ". There is a distance of " $90 - \Psi$ " between the c-axis and the pole to PDF plane, which is constant before and after correction to the center. The pole to PDF plane is moved to a new position, which has an angle of " δ ". The angle between the c-axis and the pole to PDF plane is " $a - \alpha$."

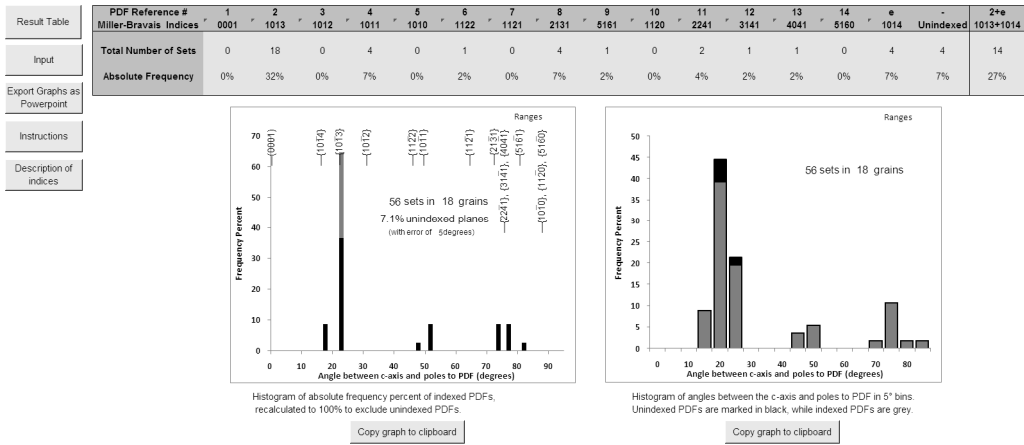


Fig. 3. Indexed PDFs data are summarized by the ANIE program as a pair of histograms, which show the absolute frequency percent of indexed PDFs and the frequency distribution of polar angle values of PDFs in 5° bins. The error used for analysis is indicated on the graph for indexed PDFs, and each graph also displays whether data are processed based on averages or ranges of values. Unindexed PDFs are marked in black on the histogram of polar angle values of PDFs.

Table 1. Comparison of the number of indexed PDF crystallographic orientations, as obtained using the graphical method and ANIE program with different settings, in quartz grains from three samples.

PDF crystallographic orientations	AUS sample (208 PDF sets in 74 grains)					BOS sample (145 PDF sets in 65 grains)					M8 sample (211 PDF sets in 71 grains)				
	Graphical method ^a	5°error averages ^b	5°error ranges ^c	6°error averages	6°error ranges	Graphical method	5°error averages	5°error ranges	6°error averages	6°error ranges	Graphical method	5°error averages	5°error ranges	6°error averages	6°error ranges
c {0001}	59	47	53	53	58	n.d.	n.d.	n.d.	n.d.	n.d.	4	4	4	4	4
{10 $\bar{1}$ 4} ^d	6	8	22	6	21	2	12	13	7	12	10	7	17	4	14
{10 $\bar{1}$ 4}://{10 $\bar{1}$ 3} ^e	44	30	23	38	35	47	28	21	36	27	77	64	52	84	71
ω {10 $\bar{1}$ 3} ^f	60	48	59	48	53	32	34	45	35	42	79	61	78	56	65
π {10 $\bar{1}$ 2}	2	2	3	2	3	28	23	28	27	29	2	2	6	2	6
r, z {10 $\bar{1}$ 1}	10	11	12	10	12	5	7	7	6	8	13	10	15	14	16
m {10 $\bar{1}$ 0}	1	1	3	1	3	1	1	1	1	1	n.d.	n.d.	n.d.	n.d.	n.d.
ξ {11 $\bar{2}$ 2}	5	1	3	1	4	4	2	3	3	2	3	3	3	2	3
s {11 $\bar{2}$ 1}	n.d.	n.d.	n.d.	1	n.d.	2	2	4	3	4	n.d.	n.d.	1	1	1
ρ {21 $\bar{3}$ 1}	3	3	4	2	4	3	2	2	3	2	3	3	8	3	8
x {51 $\bar{6}$ 1}	1	2	2	2	2	1	1	n.d.	n.d.	n.d.	1	1	1	n.d.	1
a {11 $\bar{2}$ 0}	1	1	n.d.	1	n.d.	1	n.d.	1	1	1	n.d.	n.d.	n.d.	n.d.	n.d.

$\{22\bar{4}1\}$	n.d.	1	n.d.	1	n.d.	6	5	3	5	3	10	9	6	12	6
$\{31\bar{4}1\}$	3	3	3	3	3	3	5	6	4	7	2	2	2	2	2
$t\{40\bar{4}1\}$	2	1	n.d.	1	n.d.	2	2	2	2	1	2	2	2	1	2
$k\{51\bar{6}0\}$	1	n.d.	n.d.	n.d.	n.d.	n.d.	n.d.	n.d.	n.d.	n.d.	1	1	n.d.	1	n.d.
Unindexed	10	49	21	38	10	8	21	9	12	6	5	42	16	25	12

^aPDF planes indexed with the graphical method; Data from Ferrière et al. (2009).

^bPDF planes indexed using ANIE program with a 5° envelope of measurement error and the average value of measurements for indexing.

^cPDF planes indexed using ANIE program with a 5° envelope of measurement error and the ranges of values for indexing.

^d $\{10\bar{1}4\}$ PDF orientations uniquely indexed.

^ePDF planes which plot in the overlapping zone between $\{10\bar{1}4\}$ and $\{10\bar{1}3\}$ crystallographic orientations.

^f $\{10\bar{1}3\}$ PDF orientations uniquely indexed.

n.d. = none detected.

6. RECAPITULATION

This work has explored three aspects of the impact cratering process: Two studies were made on ejecta deposits from large impact events, with one study finding a new layer of impact spherules that have previously not been described and the other study exploring the ejecta from the Sudbury impact event in petrographic and geochemical ways that have expanded the scientific understanding of the deposits particular to the Sudbury event and also for the general understanding of ejecta from large impact events, as it is only the second crater in its size range to be investigated for ejecta (the first being the Chicxulub impact event); a separate study worked to find the mathematical relationship between planar deformation features and the c-axis of quartz grains to allow them to be quantitatively indexed.

7. APPENDIX

Formatted: Normal

arXiv:1305.3631v1 [astro-ph.EP] 15 May 2013

A STATISTICAL DYNAMICAL STUDY OF METEORITE IMPACTORS: A CASE STUDY BASED ON PARAMETERS DERIVED FROM THE BOSUMTWI IMPACT EVENT

M. A. Galiazzo¹, Á. Bazzó¹, M. S. Huber², A. Losiak², R. Dvorak¹, C. Koeberl²

1. *Institute for Astrophysics of the University of Vienna*

2. *Department of Lithospheric Research, University of Vienna*

matta.galiazzo@univie.ac.at

Abstract The study of meteorite craters on Earth provides information about the dynamic evolution of bodies within the Solar System. Bosumtwi crater is a well studied, 10.5 km in diameter, ca. 1.07 Ma old impact structure located in Ghana. The impactor was ~1 km in diameter, an ordinary chondrite and struck the Earth with an angle between 30° and 45° from the horizontal. We have used a two phase backward integration to constrain the most probable parent region of the impactor. We find that the most likely source region is a high inclination object from the Middle Main Belt.

Keywords: impact craters – celestial mechanics – minor planets, asteroids

1. Introduction

When studying impact craters, it is sometimes possible to determine the properties of the impactor that produced the crater, but the source where the impactor originated in the Solar System is more difficult to determine. Recently, the Almahata Sitta fall was observed by astronomers, tracked by satellites as it entered the atmosphere, and collected soon after striking Sudan. In this case, dynamical models were combined with detailed information about the meteorite type to track the impactor back to the Inner Main Belt (Jenniskens et al., 2010). For older impacts, the same precision cannot be achieved because of the lack of detailed information on orbital parameters. However, based on the geological constraints on the dynamic nature of the impactor, a statistical model can be used to suggest the most probable region from which the impactor could have originated. The aim of this study is to statistically constrain the most probable parent region of the impactor that formed the Bosumtwi impact crater.

Bosumtwi crater: Geological background

The Bosumtwi impact crater was chosen for this study because of its relatively young age and unusually good constraints on the direction of the impactor. The Bosumtwi impact crater is a 10.5 km in diameter complex meteorite impact crater located in the Ashanti Province of southern Ghana. It is 1.07 ± 0.11 Ma old and relatively well preserved (e.g., Koeberl et al., 1997a). The Bosumtwi structure is currently filled by the closed-basin Lake Bosumtwi that is 8 km in diameter and up to 72.5 m deep. It is considered to be the largest, relatively young, confirmed impact structure on the Earth. Bosumtwi is a unique crater, since it is one of just three craters in the world that are associated with a tektite strewn field (e.g., Koeberl, 1994). Tektites are centimeter-sized pieces of natural glass formed during a hypervelocity impact event by ejection of molten target-surface material and occurring in strewn fields (e.g., Koeberl, 1994). Based on the distribution of tektites around Bosumtwi crater it is possible to constrain the direction of travel of the bolide prior to the impact. Based on the Cr isotope composition of the tektites derived from Bosumtwi, Koeberl et al. (2007b) established that the impactor that formed Bosumtwi crater was most probably an ordinary chondrite (while carbonaceous and enstatite chondrites were excluded). The properties of the impactor that formed the crater have been constrained by numerical modeling. According to Artemieva et al. (2004), the Bosumtwi structure was formed by an impactor 0.75 to 1 km in diameter, moving with a velocity higher than 15 km/s, and most probably 20 km/s. Due to association of the Bosumtwi crater with the Ivory Coast tektite strewn field, the direction of the incoming impactor was estimated to be from N-NE to S-SW and the angle of impact is thought to be between 30° and 45° (Artemieva et al., 2004).

2. Model & Methods

This study uses a statistical approach to constrain the parent region of the Bosumtwi impactor, using $a - i$ space (a and i for semi-major axis and orbital inclination, respectively) and the absolute magnitude (H_v) distribution inside the defined regions of the Solar System. First, we made a backward integration¹ from the present to the time of impact. The integration used the Radau integrator, included relativity, and all the planets plus Pluto, the Moon, Vesta, Ceres, Pallas and Juno. The integration considered the positions of the Earth between 0.96 and 1.18 Ma (1.07 ± 0.11 Ma) in order to find the possible position of the Earth during the time when the impact occurred, accounting for the error of the impact age measurement. Then, we made another backward integration using the Lie-integrator (Eggl and Dvorak, 2010) without Mercury, Pluto and the 4 asteroids, from the time of the impact to 100 Ma, simulating the orbital evolutions of 924 fictitious Bosumtwi impactors beginning at the

A statistical dynamical study of meteorite impactors: a case study based on parameters derived from the Bosumtwi impact

calculated location of the Earth. Two cases were considered for this integration:

Fixed case (FC): we started the integration at the location of the Earth (as calculated in the initial integration) exactly at 1.07 Ma. Then, 384 particles, with a gaussian distribution of impact velocities (v_i) around 20 km/s were launched with 32 different velocities. Those velocities correspond to the average value for Earth-impactors, as well as the most likely velocities indicated by numerical modeling for the Bosumtwi impactor (Artemieva et al., 2004). Velocities have a Gaussian distribution in the range of 11.2 to 40 km/s, which are the escape velocity from the Earth and cometary speed, respectively. Then, 4 impact angles were considered using random values among $\Theta = 37.5^\circ \pm 7.5^\circ$ for each velocity and 3 different directions ($\Omega_1 = 67.5 \pm 3.5^\circ$, $\Omega_2 = 78.75 \pm 3.5^\circ$ and $\Omega_3 = 56.25 \pm 3.5^\circ$ from east) for each angle. The launch position is the present latitude and longitude of the Bosumtwi crater site.

General case (GC): 540 particles were integrated using combinations of the following properties to account for the lack of knowledge of the exact position of the Earth at the time of the impact: 3 different orbital positions of the Earth, corresponding to the minimum, average and maximum aphelion (at 3 different times) in the Solar System; 3 different directions of the impactor ($\Omega_1 = 67.5 \pm 3.5^\circ$, $\Omega_2 = 78.75 \pm 3.5^\circ$ and $\Omega_3 = 56.25 \pm 3.5^\circ$ from east); and 60 different sections of the Earth along lines of longitude every 6° for each position of the Earth. For each of the 540 particles, impact angle and latitude² were distributed randomly, and v_i had a gaussian distribution like in the FC.

Once data were generated, analysis was done on two levels. First, regions were defined as in Table 1, where only the semimajor axis was considered. Then, for those particles which fell into the Main Belt, more specific constraints were necessary because of the much higher population. Assuming the impactor was an ordinary chondrite (Koeberl et al., 2007b) and from the numerical results of Artemieva et al.³ (2004), we can exclude the possibility of a cometary orbit, such as NEOs (Near-Earth objects) with orbits of $Q > 4.5$ AU (Fernández et al., 2002).

REGIONS (Table 1): At the end of the integration, the particles are examined to determine the probability that they fall into a defined region based on the semi-major axis range (called $P(a)$). The orbital properties of the particles were derived from the time intervals between close encounters where they show little variance. The average time between close encounters with planets was determined to be 284 ky.

4

MAIN BELT GROUPS (Table 2): Asteroids in the Main Belt were subdivided into 3 regions and with these 3 constraints: (1) $1.5264 < a < 5.05$ AU, $Q < 5.46$ AU (aphelion of Hilda family from Broz and Vokrouhlicky, 2008), (2) $q > 1.0017$ AU (the average semi-major axis of the Earth after 100 Myr of integration) and (3) the NEAs with $Q < 4.35$ and $q > 1.0302$.

Then, each of these 3 groups was divided into 2 subgroups: the low inclination group (*LIG*) and the high inclination group (*HIG*), the border between the two regions being $i = 17.16$ (Novaković et al., 2011). The regions with the highest densities of particles were then determined. For these the Tisserand parameter with respect to Jupiter: $T_j = \frac{a_j}{a} + 2\sqrt{\frac{a_j}{a}(1-e^2)} \cos i$, where a_j is the semi-major axis of Jupiter, a , e and i are the actions of the osculatory elements of the asteroid. It was calculated to test whether or not the properties correspond to known families in the Main Belt.

Absolute magnitude and spectroscopy

Ordinary chondrites, thought to be responsible for the Bosumtwi impact, are associated with the taxonomical S-group: S, L, A, K, R, Q and intermediate types Sl, Sa, Sk, Sr, Sq (Bus & Binzel, 2002).

Surveys have also revealed that the NEA population is dominated by objects belonging to the taxonomic classes *S* and *Q* (25% as Q-type and 40% as S-type, Bus et al., 2004). When corrected for observational biases, about 40% of the NEA population belong to one of these two taxonomic classes. In the case of Mars crossers, 65% belong to the S class (de León et al., 2010). To compute the absolute magnitude of our impactor, we used the equation of Fowler and Chillemi (1992): $H_v = -5 \log(\frac{D_p^{1/2}}{1329})$. Using the average albedo for the S-group asteroids, 0.197 (Pravec et al. 2012), and considering the likely size range of the Bosumtwi impactor, its absolute magnitude ranged from 17.4 to 18.0 mag. The absolute magnitude of the impactor can be used to calculate the probability (called $P(H_V)$) that the impactor originated from a particular region based on the likelihood of objects of similar absolute magnitude originating in a particular region, i.e., from the IMB, $11.21 < H_{vIMB} < 27.60$. The spectral properties of ordinary chondrites exclude the possibility that this object come from a family such as Vesta or Hungaria, but it favours the Flora, Anadne, Nysa, Maria, Eunomia, Mersia, Walsonia, Coelestina, Hellona, Agnia, Gefion and Koronis groups (Cellino et al., 2002) Barcelona and Hansa for the *HIG* (Novaković, et al., 2011).

A statistical dynamical study of meteorite impactors: a case study based on parameters derived from the Bosumtwi impac

3. Results and discussion

The final backward integration of 100 My shows that particles which survived the integration tend to converge on the Main Belt (Figure 1), and that only a negligible number of them is found in cometary orbits with an initial aphelion greater than Jupiter's one, with a $v_i > 27$ km/s; then a very negligible part in hyperbolic orbits with a $v_i > 33$ km/s. This suggests that the impactor most likely originated in the Main Belt.

REGIONS: The results are listed in Table 1, where $P(H_v)$ shows that on the basis of the absolute magnitude, the object most likely originated from the Main Belt, with a 37% probability of originating from the IMB and a 29% probability of originating in the MMB. The integration performed in this work shows that the majority of backwards integrated particles fall into the IMB and MMB, with $\sim 10\%$ of objects in the FC falling into each of these. The GC, however, resulted in the majority of objects originating from the MMB, again with $\sim 10\%$ of objects, and only $\sim 4\%$ of objects originating from the IMB.

Table 1. Regions are defined by the a that corresponds to strong perturbative Mean Motion Resonance (2.06 AU for $J_4 : 1$ and 3.28 for $J_2 : 1$), apart for the inner border of the (IMB) equal to the aphelion of Mars. The borders of the Jupiter Trojans (TRO) as in Tsiganis et al. (2005) and for the TNOs, the standard definition is used. *MMB*, *OMB*, *CEN* stand respectively for Middle Main Belt, Outer Main Belt and Centaurs. *Orb.* stands for semi-major axis borders of the region. For the lower border of the IMB (*), we take the minimum a for the innermost group of asteroids (see Galiazzo et. al. 2012). The "♣" means that H_v are biased for the absence of a small bodies survey, so no significative computation is possible. $P_{FC}(a)$ and $P_{GC}(a)$ stands respectively for probability to find the origin in the region through the a in the FC and in the GC.

Reg.	Orb.	$P(H_v)$	$P_{FC}(a)$	$P_{GC}(a)$
IMB	$1.78^* \leq a \leq 2.06$	0.3737	0.0924	0.0404
MMB	$2.06 < a < 3.28$	0.2870	0.1036	0.1030
OMB	$3.28 < a < 5.05$	0.0232	0.0112	0.0121
TRO	$5.05 < a < 5.35$	♣	0.0056	0.0000
CEN	$5.35 < a < 30.00$	♣	0.056	0.0646
TNO	$a > 30.00$	♣	0.0112	0.0020

MAIN BELT: Results are given in Table 2, subdivided in 2 rows. In the upper row we have the *LIG* and the lower one, the *HIG*: $P(a, i)$ is the probab-

6

Table 2. MBAs group have the same subdivision per semi-major axis, as in Table 1, apart for the IMB: $1.53 < a < 2.06$ where the lower limit is the average apseion of Mars in 100 Myr from the impact time). "Low"= Low inclined orbit ($i < 17.16$) and "High"= High inclined orbit. $P_F(a, i)$ and $P_G(a, i)$ stands respectively for probability to find the origin in the region defined by semi-major axis, and inclination too, in the FC and in the GC.

Reg. Low	$P_F(H_+)$	$P_F(a, i)$	$P_G(a, i)$
Reg. High	$P_F(H_-)$	$P_F(a, i)$	$P_G(a, i)$
IMB Low	0.234	0.006	0.000
IMB High	0.420	0.006	0.018
MMB Low	0.307	0.000	0.010
MMB High	0.113	0.020	0.022
OMB Low	0.023	0.003	0.000
OMB High	0.019	0.000	0.004

ity to find the asteroid at high or low inclinations in the regions defined via semi-major axis, G and F stands respectively for GC and FC.

- FC: The most probable source region of the Bosumtwi impactor based on the fixed case integration falls within the Main Belt at high inclination, with the most likely group being the MMB at high inclination, with 2% of the population falling into this group. The objects have highly inclined orbits (up to $\sim 75^\circ$), and the most populated zone at $2.42 \pm 0.03 < T_j < 2.84 \pm 0.25$.
- GC: The most probable source region of the Bosumtwi impactor based on the general case is from the MMB with high inclination: $i > 36.9$ (Fig. 2) and $2.42 \pm 0.05 < T_j < 2.79 \pm 0.09$. However, low inclination MMB is also possible, together with high inclination IMB.

A statistical dynamical study of meteorite impactors: a case study based on parameters derived from the Bosumtwi impact

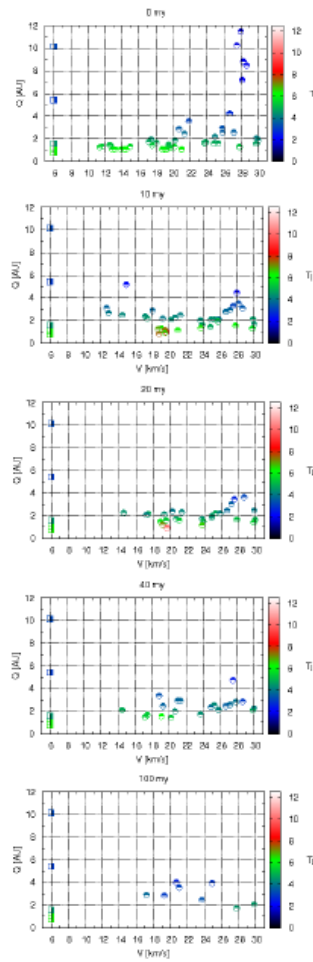


Figure 1. Evolution of a sample, through the different ranges of admitted velocities, of fictitious asteroids (impactors) over the total integration time. In colours the T_j , x-axis is the impact velocity (km/s) and the y-axis is the aphelion (AU). On the left, at a fictitious velocity of 6 km/s we have the planets as reference, from top to the bottom: Saturn, Jupiter, Mars, Earth, and Venus. The T_j shows that the particles tend to achieve the values of the MBAs (plot at 100 my).

8

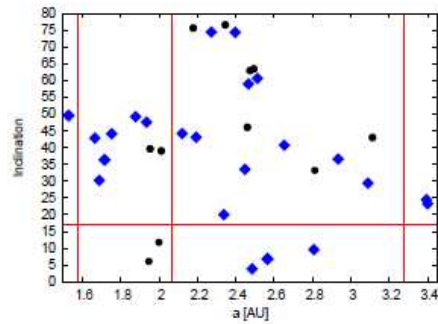


Figure 2. $a - i$ space. Vertical lines define the border of the regions in semi-major axis, as in Table 1, and the horizontal line discriminate *HIG* and *LIG*. Diamonds for *GC* and circles for *FC*.

4. Conclusions

The Bosumtwi impactor probably originated in the MMB at orbital inclinations greater than 35° with a possible initial T_j equal to 2.63 ± 0.25 . These values are based only on our numerical integrations (the highest values⁴ in $P_G(a, i)$ and $P_G(a)$ found in the *GC*, see Table 1 and 2 and Figure 2.) and not considering the spectroscopical type too, because we do not have yet any significant number of measure in this zone of the Main Belt (Cellino et al, 2002). Also this zone is still not well studied and so we could not identify a particular family as the most likely source. Asteroids with similar orbital parameters to the modeled Bosumtwi impactor are: 2002 MO₃, 2009 XF₈, 2002 SU and 2010 RR₃₀. There could be a cluster of asteroids at very high inclined orbits as shown by these results, something that we are planning to study after this work. This method should be improved to find more consistent probabilities (i.e. with more fictitious particles and larger integration times) and it can potentially be applied to other old impact craters with well constrained impactor properties, and even to impacts on other planets.

A statistical dynamical study of meteorite impactors: a case study based on parameters derived from the Bosumtwi impact

Notes

1. Due to the fact that a backward integration could be distorted by chaotic motion in close encounters, we have looked for a measure that is as simple as possible and is expressed in terms of orbital elements, since these are familiar indices of orbit differences. Because there should be preferential orbits in the regions far from the Earth, we can use a statistical approach. We stopped the integration for a particular body whenever the asteroids overcome an eccentricity equal to 0.985 or have had a close encounter with a planet less than $\sim 10^{-8}$ AU.
2. varying $\pm 1.3^\circ$ (Neron deSurgy & Laskar, 1995) from the present one, to account for the variance of the obliquity.
3. see also their Table 2 where the fit between the diameter of the crater and the impact velocity is in agreement with impact velocities typical of asteroids.
4. Because of close encounters, some integrations were stopped before 100 My, so less orbits and their evolution in the Main belt, see Fig. 1. These ones are the missing percentage from the results, a part still happen to be as NEAs, a part reach our maximum tolerance value for eccentricity (0.95) and another small fraction has again impacts during the backward integration.

References

- Artemieva, N., Karp, T., Milkereit, B.: 2004, *GGG* 5, 11016
- Broz, M.; Vokrouhlicky, D.: 2008, *MNRAS* 390, 715
- Bus, S. J., Binzel, R. P., Volquardsen, E. L., Berghuis, J. L.: 2004, *BAAAS* 36, 1140
- Bus, S. J., Binzel, R. P.: 2002, *Icarus* 158, 146
- Cellino, A., Bus, S. J. and Doressoundiram, A. and Lazzaro, D.: 2002, *Asteroids III*, 633
- de Léon, J., Licandro, J. and 3 coauthors: 2010, *A&A* 517, A23
- Dvorak, R., Pilat-Lohinger, E., Schwarz, R., Freistetter, F.: 2004, *A&A* 426, L37
- Eggi, S., Dvorak, R.: 2010, *LNP* 790, 431
- Fernández, J. A., Gallardo, T., Brunini, A.: 2002, *Icarus* 159, 358
- Fowler, B., Chillemi, B.: 1992, *MNRAS* 423, 3074
- Galiazzo M. A., Bazzo, A., Dvorak R.: 2012, *PSS*
- Koerberl, C.: 1994, *GSA Special Paper* 293, 133
- Koerberl, C., Bottomley, R., Glass, B. P., Storzer, D.: 1997a, *GCA* 61, 1745
- Koerberl, C.; Milkereit, B., Overpeck, J. T., and 9 coauthors: 2007a, *MPS* 42, 483
- Koerberl, C., Shkolnyukov, A., Lugmair, G. W., Guenther W.: 2007b, *EPSL* 256, 534
- Jenniskens, P., Vaubaillon, J., Binzel, R. P. and 13 coauthors: 2010, *Met. Plan. Sc.* 45, 1590
- Neron de Surgy, O., Laskar, J.: 1995, *BAAAS* 27, 1172
- Novaković, B., Cellino, A., Knežević, Z.: 2011, *Icar.* 216, 69
- Pravec, P., Harris, A. W., Kusnirák, P., Galád, A. and Hornoch, K.: 2012, *Icarus* 221, 365
- Tsiganis, K., Varvoglis, H. and Dvorak, R.: 2005, *CeMDA* 71

8. CURRICULUM VITAE

Matthew Huber

Department of Lithospheric Research

University of Vienna

Althanstrasse 14

A-1090 Vienna, Austria

+43 680-501-2455

matthew.huber@univie.ac.at

Education

2013	Postgraduate: University of Vienna Ph.D. Geoscience (Planetology) Advisor: Christian Koeberl Thesis: Petrographic and geochemical analysis of distal ejecta from large Proterozoic impacts	GPA: 3.83 (Equivalent)
May, 2010	Postgraduate: Louisiana State University M.S. Geology (Geochemistry) Advisor: Gary Byerly Thesis: Volcanological and petrogenetic characteristics of komatiites of the 3.3 Ga Saw Mill Complex, Weltevreden Formation, Barberton Greenstone Belt, South Africa.	GPA: 3.5
May, 2007	Undergraduate: University of Tennessee at Martin B.S. Geoscience Senior Thesis: Mineral and sediment infill of the root bulb Camerocrinus of the Ross Fm. (Devonian), Hardin County, Tennessee.	GPA: 3.7

Peer Reviewed Publications

Huber, M., Ferrière, L., Losiak, A., and Koeberl, C., 2011. ANIE: A mathematical algorithm for automated indexing of planar deformation features in quartz grains. *Meteoritics and Planetary Science*, 46, 1418-1424.

Galiazzo M.A., Bazso A., Huber M.S., Losiak A., Dvorak R., Koeberl C. 2013. A statistical dynamical study of meteorite impactors: a case study based on parameters derived from the Bosumtwi impact event. Accepted to *Astronomische Nachrichten*.

Kring D. A., Balcerski J., Blair D.M., Chojnacki M., Donohue P.H., Drummond S.A., Garber J.M., Hopkins M., Huber M.S., Jaret S.J., Losiak A., Maier A., Mitchell J., Ong L., Ostrach L.R., O'Sullivan K.M., Potter R.W.K., Robbins S., Shankar B., Shea E.K., Singer K.N., Sori M., Sturm S., Willmes M., Zanetti M., Wittmann A. Fold Hinge in Overturned Coconino Sandstone and its Structural Displacement During the Formation of Barringer Meteorite Crater (a.k.a Meteor Crater). Submitted to *Meteoritics and Planetary Science*.

Huber, M., Crne, A., Lepland, A., McDonald, I., Melezhik, V., Koeberl, C., and the FAR DEEP Science Team. Probable Vredefort ejecta from Karelia, Russia: A key to understanding Precambrian impacts. Submitted to *Geology*.

Huber, M., Hecht, L., and Koeberl, C. Geochemistry of impact ejecta from the Sudbury impact: Insights into large impacts. Submitted to *Meteoritics and Planetary Science*

Publications in preparation

Huber, M., and Plado, J. Misuse of evidence in identifying possible impact structures: Case study of the Suavjärvi structure. In preparation for *Meteoritics and Planetary Science*.

Huber, M., and Koeberl, C. Accretionary lapilli formed from the Sudbury impact. In preparation for *Meteoritics and Planetary Science*.

Huber, M., and Byerly, G. Komatiites of the Saw Mill Complex, Weltevreden Formation, Barberton Greenstone Belt. In preparation for *South African Journal of Geology*.

Other Publication

Huber, M., and Crane, D., 2009. Examination of reservoir formational processes of the Eocene Gatchell Sandstone. Internal document for Chevron Corp. 12 pp.

Geology Experience

2012 Lunar and Planetary Institute Sudbury Field Camp Sudbury, Canada

2011	Network on Impact Research Ries Field Camp	Nördlingen, Germany
2010	Collaboration with FAR-DEEP ICDP drilling project	Trondheim, Norway
2010	Lunar and Planetary Institute Meteor Crater Field Camp	Meteor Crater, AZ
2010	Field analysis of impact ejecta in Orosirian terrains of the Canadian Shield in Michigan and Ontario	Marquette, MI and Thunder Bay, ON
2009	Laboratory technician	Baton Rouge, LA
	Prepare rocks for chemical analysis	
	Prepare powders and thin sections	
	Separate zircons using magnetic separation and heavy liquids	
2009	Asset Development Team Intern for Chevron	Bakersfield, CA
	Developed VBA macros to aid in analysis of core data	
	Used Stratworks and Geolog to evaluate reservoir properties	
	Adapted data to develop new reservoir formation model	
2007-2009	Teaching Assistantship at Louisiana State University	Baton Rouge, LA
	Classes: Physical Geology	
	Historical Geology	
	Physical Geology Lab	
	Igneous and Metamorphic Petrology	
2008	Geological mapping of Weltevreden Formation, Barberton Greenstone Belt, South Africa	Barberton, SA
2005-2010	Geology presentations for the North MS Gem and Mineral Society, UT Martin Geoclub, and LSU geology club	
2007	Geologic mapping of Grenvillian Orogenic belt in Piseco Lake Shear Zone	Hamilton, NY
2006	Geology of Belize: Field studies of Bolide impacts through time with an emphasis on the Chicxulub impact crater.	Central Belize
2006	Field Methods in Volcanology course from the Center for the Study of Active Volcanoes	Hilo, Hawaii

Conference Contributions

- Huber, M. S., King Jr., D. T., Petruny, L. W., and Koeberl, C. 2013. **Revisiting Kilmichael (Mississippi), a possible impact structure.** 44th Lunar and Planetary Science Conference, Abstract #2250.
- Huber, M., and Koeberl, C., 2012. **Accretionary lapilli from the Sudbury impact: observations from five sources.** GSA Annual Meeting, Abstract #210692.
- Huber, M., and Koeberl, C. 2012. **Distribution of meteoritic material in Sudbury impact ejecta.** 75th Annual Meeting of the Meteoritical Society Cairns, Australia, Abstract #5136.
- Huber, M., Crne, A., Lepland, A., McDonald, I., Melezhik, V., Koeberl, C., and the FAR DEEP Science Team, 2012. **Chemical analysis of ballistic impact spherules from the Zaonega Formation, Karelia, Russia, and implications for Vredefort origin.** Lunar and Planetary Science XVIII, Abstract #1970.
- Huber, M., and Koeberl, C., 2011. **Variation of fallout ejecta with distance from the Sudbury crater.** Geological Society of America *Abstracts with Programs*, 43, 305.
- Huber, M., and Koeberl, C., 2011. **Components of distal Sudbury ejecta.** *Meteoritics and Planetary Science*, 46, A104.
- Kring, D.A., Balcerski, J., Blair, D., Chojnacki, M., Donohue, P., Drummond, S., Garber, J., Hopkins, M., Huber, M., Jaret, S., Losiak, A., Maier, A., Mitchell, J., Ong, L., Ostrach, L., O'Sullivan, K., Potter, R. W. K., Robbins, S., Shankar, B., Shea, E., Singer, K., Sori, M., Sturm, S., Willmes, M., Zanetti, M., Wittmann, A., 2011. **Fold hinge in Overtuned Cononino Sandstone and its structural displacement during the formation of Barringer Meteorite Crater (a.k.a Meteor Crater).** Lunar and Planetary Science XVII, Abstract #1740.
- Kring, D.A., Balcerski, J., Blair, D., Chojnacki, M., Donohue, P., Drummond, S., Garber, J., Hopkins, M., Huber, M., Jaret, S., Losiak, A., Maier, A., Mitchell, J., Ong, L., Ostrach, L., O'Sullivan, K., Potter, R. W. K., Robbins, S., Shankar, B., Shea, E., Singer, K., Sori, M., Sturm, S., Willmes, M., Zanetti, M., Wittmann, A., 2011. **Asymmetrical distribution of impact ejected lithologies at Barringer Meteorite Crater (a.k.a Meteor Crater).** Lunar and Planetary Science XVII, Abstract #1746.
- Huber, M., Crne, A., Lepland, A., Melezhik, V., Koeberl, C., and the FAR DEEP Science Team, 2011. **Possible occurrence of distal impact ejecta from the Vredefort impact event in drill cores from the Onega Basin, Russia.** Lunar and Planetary Science XVII, Abstract #1487.

- Huber, M., Ferrière, L., Losiak, A., and Koeberl, C. 2011. **ANIE: A mathematical algorithm for automated indexing of planar deformation features in shocked quartz**. Lunar and Planetary Science XVII, Abstract #1200.
- Losiak, A., Wojciechowski, J., Ferrière, L., Huber, M., and Koeberl, C. 2011. **A web-based program for indexing planar deformation features in quartz**. Lunar and Planetary Science XVII, Abstract #1286.
- Huber, M. and Gibson, M., 2007. **Preliminary interpretation of paragenesis of mineral and sediment infill in Scyphocrinites loboliths from the lower Devonian Ross formation of Western Tennessee**. Geological Society of America *Abstracts with Programs*, 39, 35.

Technical Skills

- Optical microscope and universal stage
- Openworks Suite experience (Chevron)
- Geolog experience (Chevron)
- Microsoft Excel VBA programming
- Scanning Electron Microscope
- Electron Microprobe
- X-ray diffractometer
- X-ray fluorescence
- μ -X-ray fluorescence
- Infra-red spectrometry
- Raman spectrometry

Professional Organizations

2010-present	Meteoritical Society
2007-present	American Geophysical Union
2007-present	American Association of Petroleum Geologists
2006-present	American Association for the Advancement of Science
2004-present	GSE (UT Martin chapter president 2006-2007)
2003-present	Geological Society of America

Awards

2012	Wiley-Blackwell Award for outstanding presentations by students
2012	Planetary Studies Foundation travel grant
2011	Barringer Family Fund Award
2011	LPI Career Development Award
2007	Outstanding Geoscience Student Award
2003-2007	University Scholars Academic Scholarship
2006	McCutchen Geology Award
2003-2006	North Mississippi Gem and Mineral Society Scholarship

Other Experience and Activities

Employment

2008-2010	Grader for Office of Independent Learning, LSU
2004-2007	Resident Manager of the Baptist Student Center, Martin, TN.

Non-professional Organizations

2011-present	Vienna chess club
2006-present	PADI (SCUBA Diving).
2003-present	United States Chess Federation.
1995-present	North Mississippi Gem and Mineral Society, Memphis Archaeological and Geological Society.

Community Service

2012	Guest lectures on geology at Mississippi Delta Community College
2009	Education outreach for Baton Rouge elementary students.
2008	Hurricane Gustav evacuation center care giving.
2006	Hardin Co., TN geological presentation for elementary students.